ANSI/ASME
PTC 19.23-1980

F-29-01

PART 23
Guidance Manual for Model Testing

INSTRUMENTS AND APPARATUS

Supplement to ASME PERFORMANCE TEST CODES

THE AMERICAN SOCIETY OF MECHANICAL ENGINEERS
United Engineering Center
345 East 47th Street New York, N.Y. 10017

PART 23
Guidance Manual for Model Testing

ANSI/ASME PTC 19.23-1980

INSTRUMENTS AND APPARATUS

THE AMERICAN SOCIETY OF MECHANICAL ENGINEERS
United Engineering Center
345 East 47th Street New York, N.Y. 10017

Date of Issuance: April 15, 1980

FOREWORD

In 1971 the PTC Supervisory Committee, then called the PTC Standing Committee, recognized that the high cost of prototype testing had resulted in increased interest in the use of models to confirm or extend performance data. The Supervisory Committee suggested that a group of specialists in several areas of Model Testing undertake to study the larger aspects and implications of Model Testing. The result of this suggestion was the formation in March 1972 of PTC 37 on Model Testing. The Committee was later designated PTC 19.23.

This Committee was charged with the responsibility of surveying the varied fields of PTC activity in which the techniques, opportunities for, and the limitations of, Model Testing may be useful. The initial concept was to develop a Performance Test Code. After further deliberations, it was agreed, with the permission of the PTC Supervisory Committee, based upon the complexities of the subject matter and the uniqueness of its application, to prepare an Instruments and Apparatus Supplement on Code Applications of Model Experiments, (Guidance Manual for Model Testing). This document was submitted on various occasions to the PTC Supervisory Committee and interested parties for review and comment. Comments received as a result of this review were duly noted and many of them were incorporated in the document. This I & A Supplement represents the first effort to prepare a manual on the techniques and methods of Model Testing and it is intended that it would eventually be utilized by all the Performance Test Code Committees.

This I & A Supplement was approved by the PTC Supervisory Committee on May 10, 1979, and was approved by ANSI as an American National Standard on January 14, 1980.

This document is dedicated to Professor J. H. Potter, Bond Professor of Stevens Institute of Technology, who was instrumental in the development of this report.

PERSONNEL OF PERFORMANCE TEST CODE COMMITTEE NO. 19.23

ON MODEL TESTING

C. A. Meyer, *Chairman*
Professor J. H. Potter, *Past Chairman**

Brown, D. H., Environmental Systems Engineer, General Electric Company, P. O. Box 43-5-345, Schenectady, New York 12301

Burton, C. L., Section Manager, R & PD Kreisinger Development Lab., Steam Generator Development & Testing, Combustion Engineering, Incorporated, 1000 Prospect Hill Road, Windsor, Connecticut 06095 (Deceased)

Fisher, R. K., Supervisor, Hydraulic Labs., Allis-Chalmers, York Plant, Hydro-Turbine Division, P. O. Box 712, York, Pennsylvania 17405

Karassik, I., Consulting Engineer, 476 Walton Road, Maplewood, New Jersey 07040

Langhaar, H. L., Professor, Theoretical and Applied Mechanics, University of Illinois, Urbana, Illinois 61801 (Retired)

Meyer, C. A., Professor, Engineering Center, Widener College, Chester, Pennsylvania 19013.

Neale, L. C., Professor, Charles T. Main, Incorporated, Southeast Tower, Prudential Center, Boston, Massachusetts 02199

*Potter, J. H., Professor, Department of Mechanical Engineering, Stevens Institute of Technology, Castle Point Station, Hoboken, New Jersey 07030 (Deceased)

Rolsma, B., Senior Engineer, Design Thermodynamics, Medium Steam Turbine Department (E & M), Building 264 G2, General Electric Company, 1100 Western Avenue, Lynn, Massachusetts 01910

Yorgiadis, S., Partner, Sheppard T. Powell Associates, 31 Light Street, Baltimore, Maryland 21202

Personnel of Performance Test Codes Supervisory Committee

J. H. Fernandes, *Chairman*
C. B. Scharp, *Vice Chairman*

D. W. Anacki
R. P. Benedict
K. C. Cotton
W. A. Crandall
R. C. Dannettel
J. S. Davis
V. F. Estcourt
W. L. Garvin
A. S. Grimes
K. G. Grothues
R. Jorgensen
E. L. Knoedler
W. C. Krutzsch, Jr.
C. A. Larson
A. Lechner
P. Leung
F. H. Light
S. W. Lovejoy
W. G. McLean
J. W. Murdock
L. C. Neale
R. J. Peyton
W. A. Pollock
J. F. Sebald
J. C. Westcott

CONTENTS

AN AMERICAN NATIONAL STANDARD

ASME Performance Test Codes Supplement on Instruments and Apparatus Part 23

GUIDANCE MANUAL FOR MODEL TESTING

SECTION 1

0 GENERAL

0.1 Objective

To prepare a compendium of techniques and methods for model testing. This general procedure is to serve as a guide for the design and application of models by those concerned with the extension or supplementation of prototype tests of equipment and apparatus coming under the aegis of the ASME Performance Test Codes Committee. Where there are test codes in existence covering specific equipment, the guiding principles, instruments and methods of measurement from such codes shall be used with only such modifications as become necessary by virtue of the fact that a model is being tested instead of a prototype. Where models of components, systems, etc. are involved, and no test codes covering these are in existence, guiding principles and methods of measurement may be requested from this Committee (PTC 19.23).

0.2 Intended Use of This Document

Although PTC 19.23 has been concerned with the preparation of a guidance manual, it is appropriate to ask what background should be required of the user. It has been tacitly assumed that the practitioner should have some prior knowledge of model theory, such as might be obtained in an upperclass college course in fluid mechanics of heat transfer. Certainly he should have been introduced to the concepts of dimensional homogeneity and dynamic similarity.

It is important to recognize that model testing is a very broad and complex field with its own specialties, and that working engineers cannot expect to do effective work on the basis of a single document. What has been assembled, then, is a review of the basic theory coupled with some illustrative examples. It is hoped that the user will be stimulated to further study and professional growth. Particular care has been taken to indicate the limitations and pitfalls of model testing.

0.3 Definition of a Model

A model is a device, machine, structure or system which can be used to predict the behavior of an actual and similar device, machine, structure or system which is called the prototype. A physical model may be smaller than, the same size as, or larger than the prototype. Initially, the Committee will consider only physical models for those prototypes covered by the Performance Test Codes Committee.

0.4 General Philosophy

A model, when built before the prototype, is an engineering design tool that may overcome economic or practical limitations of prototype testing. It could permit imposing operational conditions that may not be attainable in the testing of a prototype. It may also be used to indicate potential remedial changes to a prototype which is not performing as predicted or desired. Wherever possible, relationships between the performance of model and prototype should be determined, or confirmed experimentally.

Models shall be physically similar to the prototype and must experience the same physical phenomena as the prototype, as detailed subsequently in this document. Analogs are not included in Performance Test Code modeling at this time. Of most immediate importance to the engineer is the ability to use a model of a prototype to predict the performance of equipment covered by Performance Test Codes such as centrifugal pumps, fans, compressors, hydraulic turbines and steam turbines.

Certain systems being considered do not lend themselves to complete system modeling, (such as steam generators, steam and gas turbines and steam condensing equipment). Others such as hydraulic turbines and pumps are frequently modeled to determine and even prove prototype performance. Where complete system modeling is not effective, various approaches are available such as the selective modeling of components and an interpretive ability to relate the component model results. With this approach, modeling can be used as a design guide or used to determine the remedial action that might be required if the equipment is not performing as expected. The ability to interpret modeling results is strongly dependent on an understanding of dimensional analysis such as developed in the next section.

A treatment of the theoretical background of model testing is given in Section 3. Examples illustrating modeling applications are given in Section 2. The remaining sections are devoted to definition and application.

1 DIMENSIONS

Certain fundamental entities are identified as dimensions. Some common dimensions are cited below:

(M) mass
(L) length
(T) time
(θ) temperature
(Q) electric charge

TABLE 1

Quantity	U.S. Customary Units	S.I. (Metric Units)	Conversion Factor (*)
Length	inch	meter	2.54 E–02
	foot	meter	3.048 E–01
Area	square inch	square meter	6.451 600 E–04
	square foot	square meter	9.290 304 E–02
Volume	cubic inch	cubic meter	1.638 706 E–05
	cubic foot	cubic meter	2.831 685 E–02
Velocity	foot/min	meter/sec	5.08 E–03
	foot/sec	meter/sec	3.048 E–01
Mass	pound mass	kilogram	4.535 924 E–01
Acceleration	ft per sec^2	meter per sec^2	3.048 E–01
Force	pound force	newton	4.448 222 E+00
Torque	(pound force) (ft)	newton-meter	1.355 818 E+00
Pressure (stress)	(lbf/sq in)	pascal	6.894 757 E+03
	(lbf/sq ft)	pascal	4.788 026 E+01
Energy, work	BTU (IT)	joule	1.055 056 E+03
Power	horsepower	watt	7.456 999 E+02

(*) Note: Conversion factors are expressed as a number greater than one but less than ten, followed by E (for exponent) and a sign showing whether the decimal should be moved to the left (–) or to the right (+), and the power of ten to which the change is made.

As an example, the conversion factor from inches to meters is 2.54 E–02, or inches multiplied by 0.0254 is meters.

Furthermore, many useful quantities may be expressed in terms of the above dimensions and may be considered as dimensions themselves. Some examples of these derived dimensions are:

($1/T$) frequency
(F) force, ML/T^2
(E) energy, ML^2/T^2
(P) power, ML^2/T^3
(p) pressure, or stress, ML/T^2L^2
(V) velocity, L/T
(A) acceleration, L/T^2
(ρ) density, M/L^3
(μ) absolute viscosity, M/LT

It can be demonstrated (1) that the selection of a fundamental set of dimensions is arbitrary, e.g., *MLT, FLT, FMLT* are in common use.

2 UNITS

Dimensions must be assigned magnitudes according to a consistent system of units. The Council of the ASME has gone on record as favoring the introduction of the S.I. (Metric) Units, aware of the fact that the changeover may require a protracted time to achieve. See Reference 9 for an extensive coverage of S.I. (Metric) units.

Some commonly used quantities are listed in Table 1, citing U.S. Customary and S.I. (Metric) Units with appropriate conversion factors.

3 DIMENSIONLESS GROUPS

Certain groupings of dimensions yield dimensionless numbers. These are found to be useful tools in many areas of engineering science, especially in fluid flow, heat transfer and mass transfer. Some of the better known dimensionless groups are cited below. More than 150 such groups are identified in the Appendix.

The use of dimensional analysis and dimensionless groupings (numbers) can greatly simplify a problem and the modeling of a problem. For example, in studying the force (F)* on a body in a moving fluid, one would expect the force to depend on the fluid velocity (V) and density (ρ) and viscosity (υ) and on the size (L) or area (A) if the body.

There are five (5) variables, which would require nine (9) curve sheets to plot the data, if we tested three values of each variable.

Using dimensional analysis, we find that there are only two real (dimensionless) variables:

*The force may be any force such as the lift or the drag of an airfoil or the fluid shear on a surface.

TABLE 2

Name	Symbol	Definition
Reynolds number	N_{Re}	$LV\rho/\mu$ or LV/υ
Froude number	N_{Fr}	$V/\sqrt{gL}$ or V^2/gL
Euler number	N_{Eu}	$p/\rho V^2$
Mach number	N_{Ma}	V/a
Prandtl number	N_{Pr}	$c_p\mu/k$
Nusselt number	N_{Nu}	hL/k
Weber number	N_{We}	$L\rho V^2/\sigma$

Where:

L = An arbitrarily chosen dimension used to measure the relative size of a model or prototype. The diameter of a pipe or the chord of an airfoil cross section are examples (often called a characteristic length).
V = velocity
a = sonic velocity
ρ = density
μ = dynamic viscosity
υ = kinematic viscosity
g = acceleration of gravity
p = pressure
A = An arbitrarily chosen area* used to measure the size of a model or prototype, often in place of L^2
k = thermal conductivity
c_p = specific heat at constant pressure
h = film coefficient of heat transfer
σ = surface tension

*For airfoils it is the custom to use the chord length of the airfoil as the reference (characteristic) length in the Reynolds number and to use the plan area of the wing in the lift and drag (force) coefficients. For non-lifting bodies, such as rivets or steps or spheres, the frontal area is used in the drag coefficient.

$$\text{Force coefficient} = \left(\frac{F}{\rho\frac{V^2}{2}A}\right) = \text{a function of}\left(\frac{VL\rho}{\mu}\right)$$

(dimensionless force) = a function of (dimensionless viscosity)

The test results can now be plotted as a single curve on a single curve sheet. The 2 in the force coefficient has been arbitrarily added since ($\rho V^2/2$) = q is the well known velocity pressure.

4 SIMILITUDE (SIMILARITY)

The previous list of dimensionless numbers presents historically useful engineering concepts. Before these concepts are used in modeling, considerations of similitude must be considered. Among these are geometric, kinematic and dynamic similitude. In the case of fluid mechanics consideration of specific similitude vary from one modeling problem to another. Geometric and kinematic similitude must be considered before dynamic similitude such as N_{Re}, N_{Fr} can be applied.

4.1 *Geometric similarity* requires that the model (larger, equal to, or smaller than the prototype) must be a geometrically accurate reproduction of the prototype. That is $(X, Y, Z)_{\text{prototype}} = K(x, y, z)_{\text{model}}$ where X, Y, Z . . . .(1) are the coordinates and K is the size scale factor.

The surface finish and clearances to be used in fabricating the model are derived from an evaluation of their effects on the phenomenon being evaluated.

Under certain conditions, such as in modeling of rivers, it may be desirable to create a distorted geometric model, i.e., one in which the vertical and horizontal scale factors are not equal. Scaling down the length of a river to fit into the laboratory, will lead to very small depths in the model, unless the model is distorted.

Kinematic similarity requires that the motion of the fluid, in the system being studied, is the same in both the model and prototype. For this to be true, then the velocity ratios

$$\frac{V_{X,Y,Z}}{V_{x,y,z}} = \text{constant} \tag{2}$$

must exist. Also, the acceleration ratios

$$\frac{A_{X,Y,Z}}{A_{x,y,z}} = \text{constant} \tag{3}$$

must exist.

4.2 *Dynamic similarity* requires that the forces acting on the corresponding masses between the prototype and the model,

$$\frac{(F/m)_{X,Y,Z}}{(F/m)_{x,y,z}} = \text{constant} \tag{4}$$

must be related. The Reynolds number N_{Re}, or the Froude number N_{Fr} are examples from fluid mechanics.

The idea of dynamic similitude is derived from the consideration that the dimensionless numbers are typically ratios of transport functions and/or other specific properties of the system being modeled. Typically (10)

N_{Re} = Inertia forces/Viscous forces
N_{Fr} = Inertia forces/Gravity forces
N_{Eu} = Pressure forces/Inertia forces
N_{We} = Inertia forces/Surface tension forces
N_{Ma} = Local velocity/Acoustical velocity
N_{Nu} = Convective heat transfer/Conductive heat transfer

The above dynamic dimensionless numbers should not be considered to be exclusive in themselves. There are cases where experimental data is correlated better by ratios of dimensionless numbers such as:

$$N_{Kn} \text{ (Knudsen no.)} = N_{Re}/N_{Ma} \tag{5}$$

$$N_{St} \text{ (Stanton no.)} = N_{Nu}/N_{Pr} \tag{6}$$

$$N_{Pe} \text{ (Peclet no.)} = N_{Re}\,N_{Pr} \tag{7}$$

The classical case in heat transfer is

$$N_{Nu} = C\,N_{Re}{}^{a}\,N_{Pr}{}^{b} \tag{7}$$

where a, b, and C are experimentally derived empirical constants. Even in this case, the data is correlated only within a band of ±15 percent and is also dependent on whether the fluid is being heated or cooled.

This poor correlation is evidently due to the fact that turbulence levels and velocity distributions have not been the same in the different tests. Subsequent sections of this presentation will cite examples of the typical application and interpretation of dimensionless numbers. Section 2 will provide examples of the application of these techniques to real problems, taken from current industrial practice.

5 SOME MODELING EXAMPLES USING DIMENSIONLESS NUMBERS

Much time, effort and expense may be saved through a knowledgeable application of modeling using similitude and dimensionless numbers. Some selected examples are presented here to point out the advantages of using dimensional analysis, especially for the testing of models.

5.1 The Pendulum

The simple pendulum affords an excellent example for demonstrating the principles of model testing. A dimensional analysis shows that the period (t) of a pendulum multiplied by the square root of the ratio of the acceleration of gravity (g) divided by its length is a function of the amplitude (θ) of its swing and is independent of its mass (m).

$$(t\sqrt{g/L}) = \text{function of } (\theta) \tag{8}$$

Any one of the pendulums shown in Fig. 1 (a) could be used as a test model for any of the others, for the analysis of this system shows:

$$t\sqrt{(g/L)} = 2\pi\left[1 + \tfrac{1}{4}\sin^2\left(\frac{\theta}{2}\right) + \frac{9}{64}\sin^4\left(\frac{\theta}{2}\right)\cdots\right] \tag{9}$$

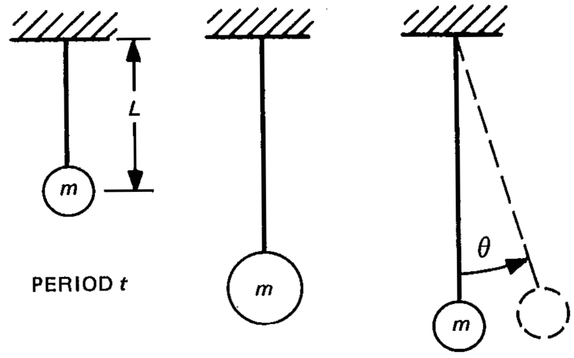

FIG. 1 (a)

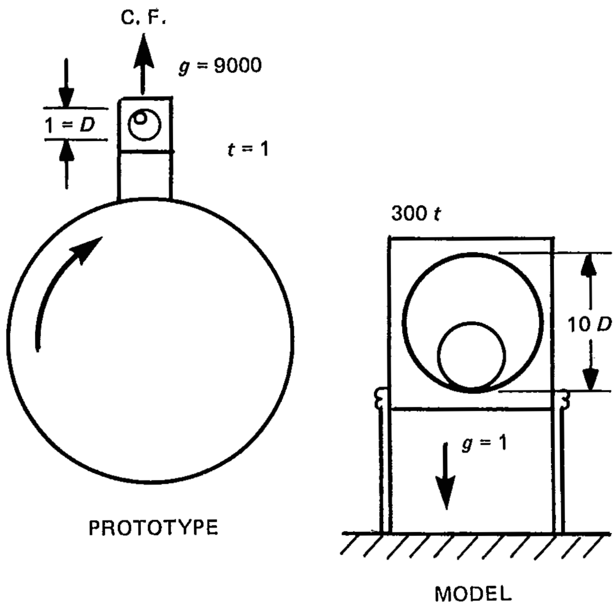

$$(t\sqrt{g/D}) = \bar{1} \times \sqrt{\frac{9000}{1}} = 300\sqrt{\frac{1}{10}}$$

FIG. 1 (b)

For small amplitudes (θ), all pendulums, short or long, fast or slow, will give the same value (2π) for the dimensionless period. This is only true, however, if the damping effect of the air and support is negligibly small. When air damping is to be taken into consideration, a dimensionless number must be introduced which will include a measure of the viscosity of the air. Reynolds number $\left(\frac{L^2}{t\upsilon}\right)$ or $\frac{L}{\mu}\sqrt{\rho p}$ could be used.

5.2 A Vibration Dynamic Damper

The modeling principle above was applied in a device for the testing of a vibration damper for turbine blades. To test such a damper in a rotating rig would have been difficult and costly, as there were no instruments available to measure the vibration during rotation. The model test technique shown in Fig. 1 (b), consisted of a cylindrical rod located in a cylindrical hole of slightly larger diameter. The rod, acted upon by centrifugal force, performed as a pendulum. The damper was tested in a stationary arrangement, at one g instead of 9000 g, at ten times the size, and at a period 300 times as long, as would be the case in the rotating prototype. However, the value of $t\sqrt{\frac{g}{L}}$ was the same in model and prototype.

5.3 Incompressible Flow Turbine Blade Cascade Study

Modeling can lead to substantial savings in the aerodynamic testing of turbomachinery, especially when the effects of Mach number are small. When such items as viscosity and fluid density are the same, the power of this type of machinery varies as the product of the velocity cubed (V^3), times the square of the size (L^2). Then:

$$\text{Power } (P) \propto \text{Flow} \times \text{Kinetic energy } (V^2/2g) \propto VA \times V^2 \propto V^3 L^2 \qquad (10)$$

and the Reynolds number varies as the product of the velocity (V) and the size (L).

$$N_{Re} \propto VL \qquad P \propto N_{Re}^3/(L) \qquad (11)$$

Thus the power for the same Reynolds number varies inversely with the size (L). (See Fig. 2.)

Hence, a turbine or a cascade ten times larger, with 1/10 the velocity, will require 1/10 the air power to test it provided, the Reynolds numbers are the same. Large low speed turbines or large low velocity cascades, require less air or steam power, can be constructed more accurately, and are affected less by the presence of instrument probes. The above reasoning can be applied to all fluid compressors, pumps and turbines.

5.4 Compressible Flow Turbine Study

If the effects of Mach number are important, and the prototype Reynolds number is large enough to cause the flow to be turbulent, or the flow is turbulent for other reasons, one could reduce the Reynolds number by reducing the model size while maintaining the prototype Mach number and still achieve flow similarity. With this model the power varies as the square of the model size. A half size model (turbine or compressor Fig. 3) will have one quarter of the prototype power and twice the rotational speed. This approach causes difficulties of manufacturing half size blades, surface finish and instrument size.

An alternative to the above method is to reduce the pressure level while maintaining full size. This reduces the

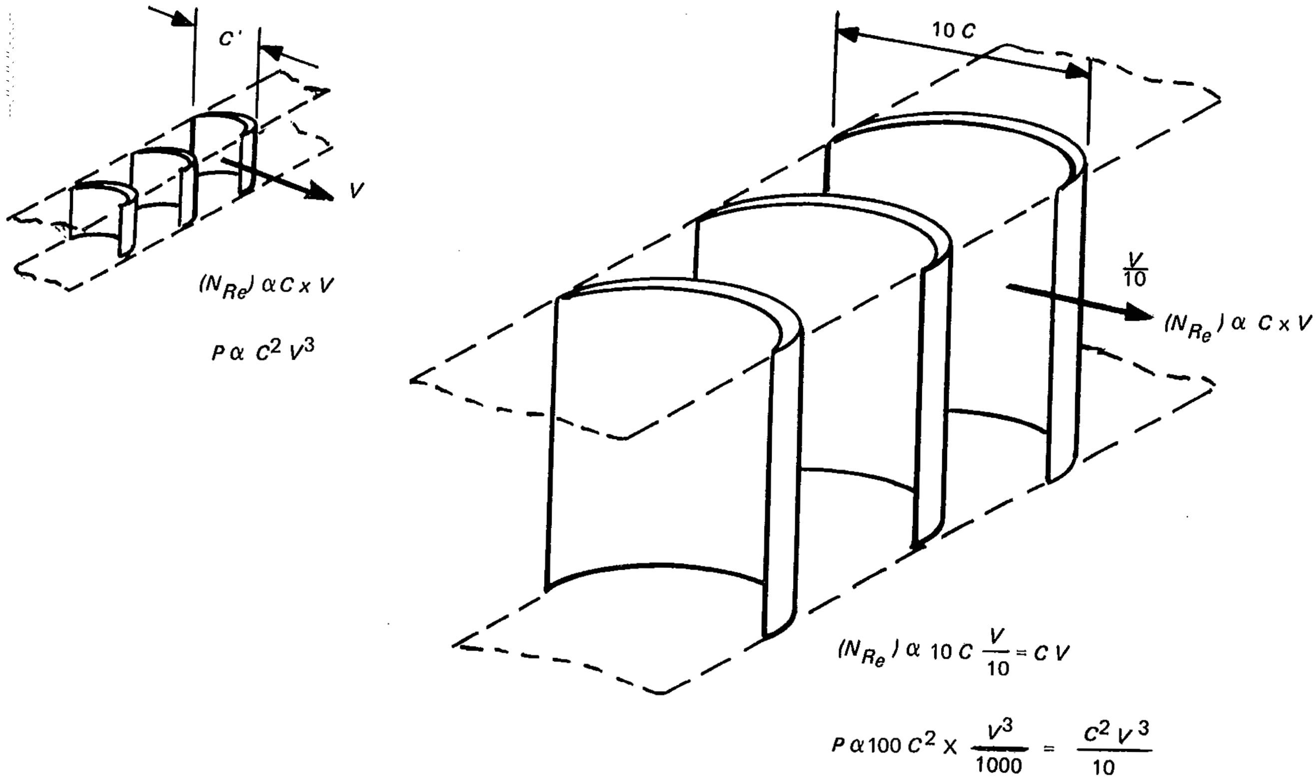

FIG. 2

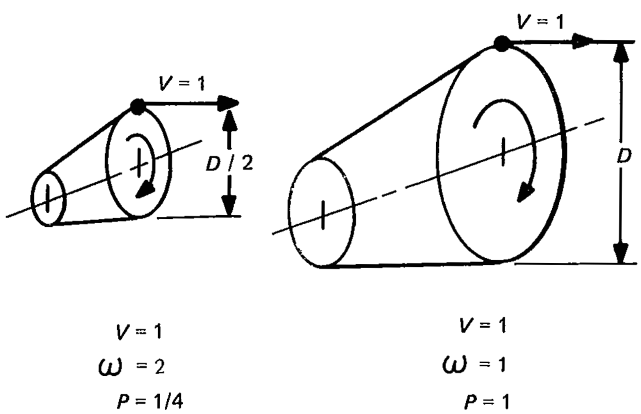

FIG. 3

Reynolds number, maintains the Mach number, and reduces the mass flow and power required, in proportion to the pressure. This method avoids the complications and tooling needed to manufacture a scale model.

The above examples indicate the latitude that is available when designing models while maintaining predetermined dimensionless numbers.

No mention of surface roughness has been made in Sections 5.3 and 5.4. In general, the roughness of the model must be exactly similar to the prototype. If however, the flow is laminar, the effects of roughness have been found to be very small, as for example in boundary layer or in pipe flows. If the flow is turbulent, one can either:

(1) Match the roughness of the model and the prototype.

or

(2) Induce turbulent flow on the model at the calculated transition point by means of artificial roughness such as nails or airfoils (as is done when testing model boats).

or

(3) Make use of the fact that roughness, smaller than a certain amount, have no effect on the flow and the model is considered aerodynamically smooth. This roughness is smaller than the thickness of the laminar sublayer which is under the turbulent boundary layer. The Reynolds number, based on the roughness size, must be less than 100.

The modeling of two phase flows as occurs when moist steam flows through turbines or piping is difficult to accomplish. In a turbine the unsteady shedding of droplets off the upstream blades and the centrifuging of the moisture off the rotating blades evidently requires a rotating test to obtain similarity between model and prototype.

In the case of piping where liquid collects in horizontal runs, additional dimensional numbers based on liquid density, gravity, surface tension and viscosity must be introduced.

5.5 Flow Induced Turbulence

The general characterization of flow turbulence by the Reynolds number

$$N_{Re} = \frac{DV}{\upsilon} \tag{12}$$

can be misleading. The following are several examples of how the Reynolds number criteria is used to describe or evaluate various phenomena.

5.5.1 Flow Over a Flat Plate

The development of a flow field over a flat plate is illustrated by Fig. 4[2]*. Here, a flat plate with a sharp leading edge is located parallel to the fluid velocity vectors. The viscous effects first form a laminar boundary layer where the viscous drag is a function of stress on the plate $\tau = \mu A\ (dv/dy)$.

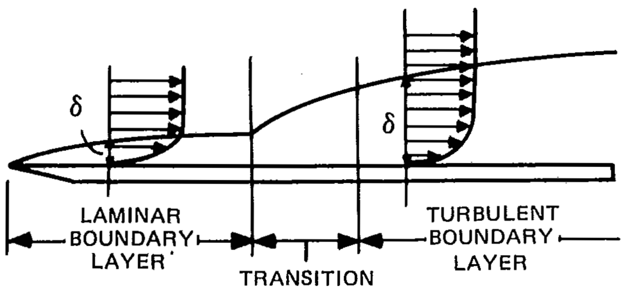

FIG. 4

When the velocity gradient (dv/dy) exceeds the shear stress capability of the fluid, the flow becomes turbulent. The momentum transfer of V_1 into V_2, Fig. 5[3], again adds to the viscous drag of the system. The results are characterized by the relationship:

$$N_{Re} = x\ V\rho/\mu \tag{14}$$

where x is the distance downstream from the leading edge of the flat plate. Hence, there is a dimension x, where fully developed turbulent boundary layer flow is established. The boundary layer thickness is shown in Fig. 4 as δ.

5.5.2 Pipe Flow

Historically, the Reynolds number turbulence concept has been useful in calculating the pressure drop of fully developed pipe flow. Typically, the Moody[1] diagram, Fig. 6, relates the friction factor f to N_{Re} and the relative roughness ϵ/D, where ϵ is the median height of the source of roughness on the inside diameter of the pipe D. The Moody diagram is only applicable for flow conditions at least 20 diameters downstream from the pipe inlet or from a turbulence inducing device. This permits the full hydraulic development of the boundary layer as noted in Fig. 4.

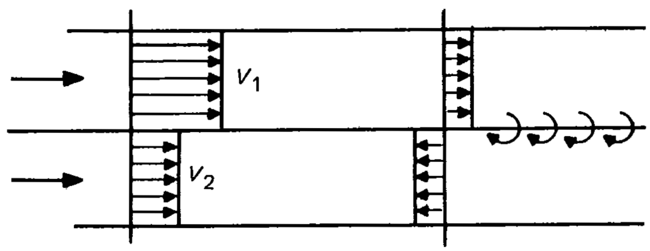

FIG. 5

5.5.3 Flow Past a Sphere

The analysis and experimental data on the sphere afford further insights into the proper interpretation of dimensionless numbers. The plot of drag coefficient of a sphere, Fig. 7, has a characteristic cusp at a Reynolds number of about 3×10^5. The location of this cusp has been found to depend on the surface roughness of the sphere and also on the free stream turbulence, both of which influence the flow separation point and therefore the drag of the sphere. Without this empirical knowledge one might assume the drag coefficient is a function of the Reynolds and Mach numbers and ignore the effects of surface roughness and turbulence. Therefore, turbulence and surface roughness must be considered also to get model to full scale correlation.

5.5.4 Flow in Pipe Bends

The preceding discussion of turbulence was based only on the viscous properties and the resultant boundary layer of the fluid stream. Other turbulence-producing agents are encountered in real fluid flow systems. Figure 8 indicates the creation of secondary flow systems when a fluid traverses a pipe bend[4]. Here the centrifugal forces due to turning create a pressure gradient of $(p_1 - p_2)/d$. The lower momentum boundary layer on the wall of the pipe permits the pressure gradient to initiate a secondary flow on the wall from p_1 to p_2. This secondary flow adds to the pressure drop of the system by increasing the velocity gradient at the pipe wall. Additional fluid energy is converted to heat by the viscous dissipation of the free stream turbulence of the vortices.

*Numbers in brackets identify references in Item 7 of Section 1.

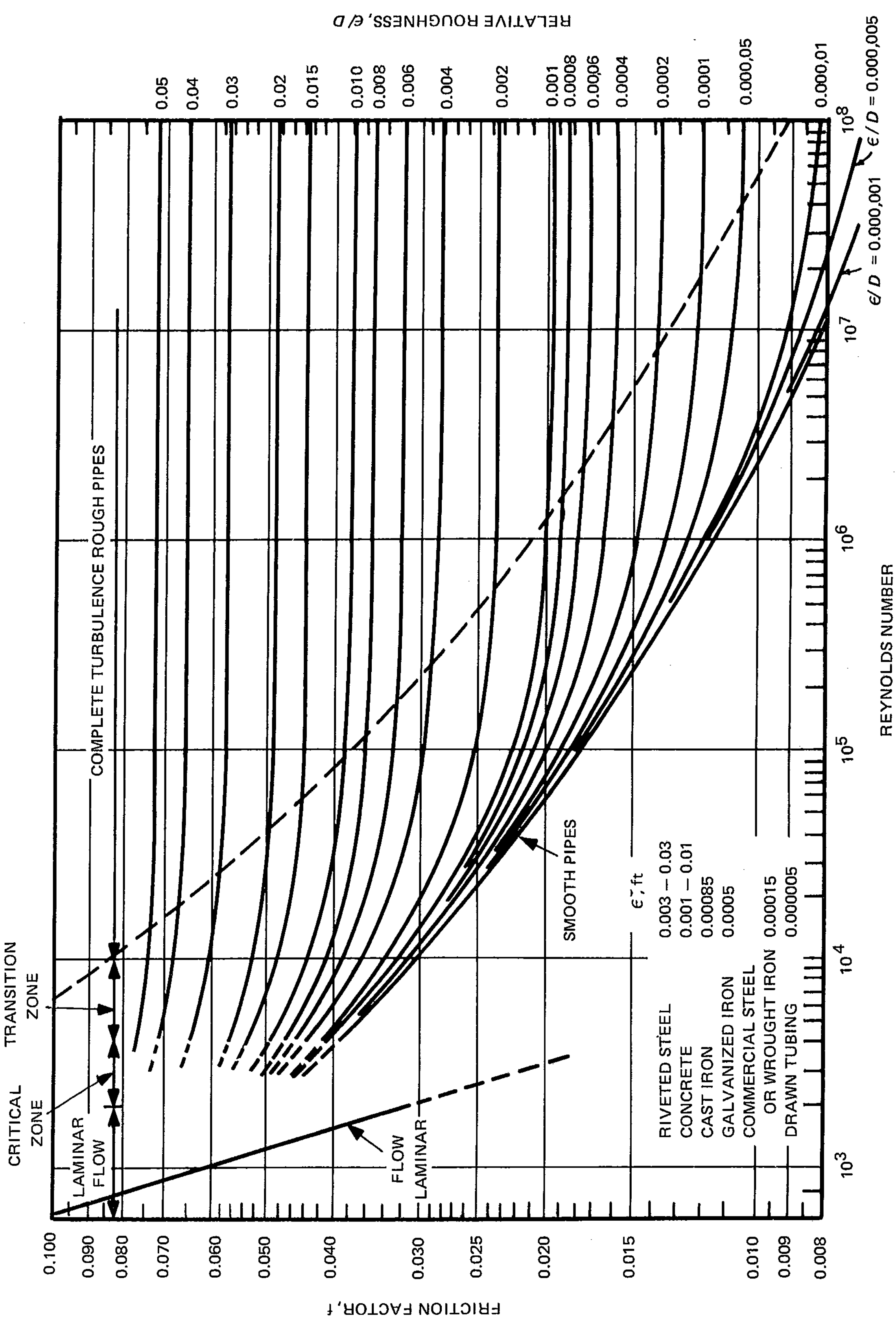
RELATIVE ROUGHNESS, ε/D
FRICTION FACTOR, f
REYNOLDS NUMBER
COMPLETE TURBULENCE ROUGH PIPES
TRANSITION ZONE
CRITICAL ZONE
LAMINAR FLOW
SMOOTH PIPES
ε, ft
RIVETED STEEL 0.003 – 0.03
CONCRETE 0.001 – 0.01
CAST IRON 0.00085
GALVANIZED IRON 0.0005
COMMERCIAL STEEL OR WROUGHT IRON 0.00015
DRAWN TUBING 0.000005
ε/D = 0.000,005
ε/D = 0.000,001

FIG. 6

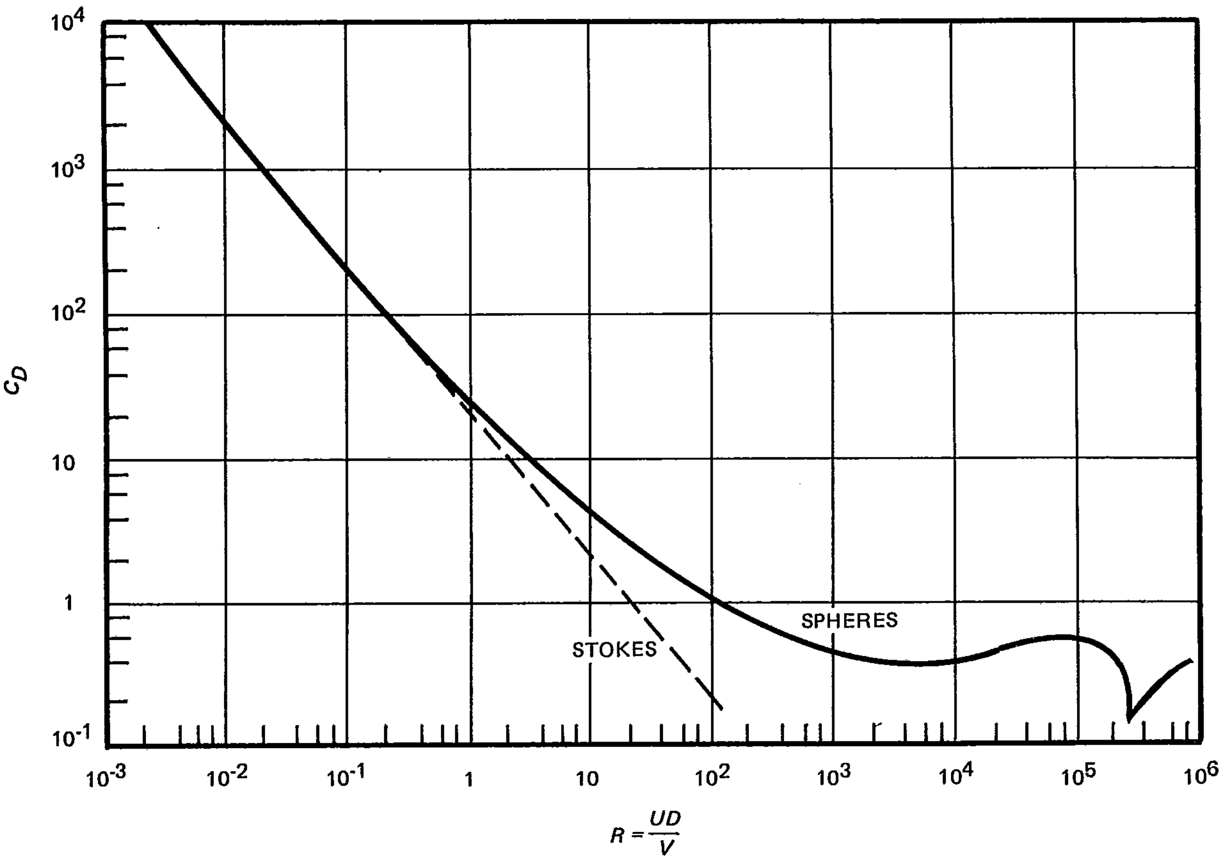

FIG. 7

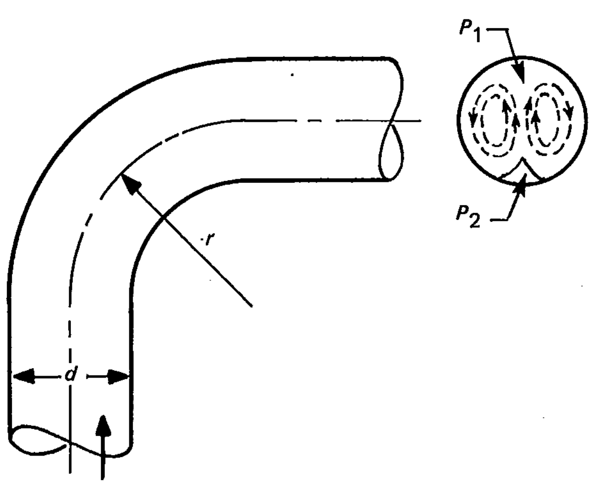

FIG. 8

5.5.5 Flow Through Regions of Rapid Expansion/Contraction

Changes in cross-sectional area may also create turbulence which will be reflected in pressure drop, as shown in Fig. 9.

Here, it is seen that sudden changes in pipe flow area create pressure drop coefficients equivalent to some 10 to 100 pipe diameter lengths based on the Moody friction factor. In explanation, it can be shown that the pressure drop is principally due to momentum interchange caused by mixing and hence is independent of Reynolds number.

5.6 Characteristic Length

Reynolds number, $N_{Re} = \frac{x\rho V}{\mu}$, is used to correlate different types of flow. In the case of a flat plate, x is the distance downstream from first contact of the fluid on the surface. In the case of a perforated plate x can be the hole diameter. These are different, but arbitrary selections of the characteristic length x to be used as a measure of the size of the device. The user of the Reynolds Number concept is cautioned to make sure that the characteristic length (x) is known and consistent throughout a given work and among authors.

5.7 Additional Considerations

Because turbulence can be produced by many means, a system of turbulence quantification other than Reynolds

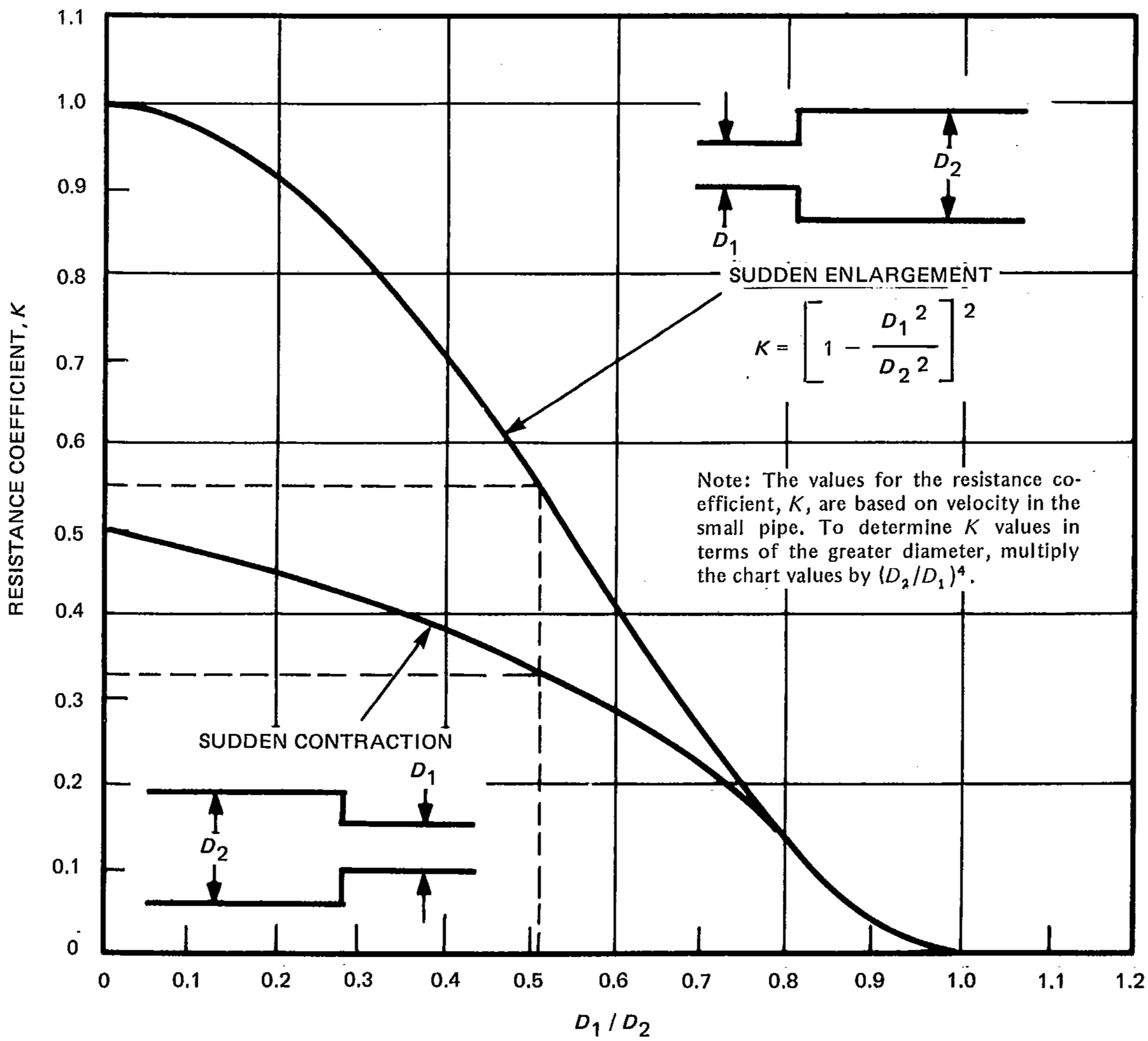

FIG. 9

number is needed. Figure 10[5] shows the mean stream velocity, U, with the Root Mean Squared turbulent components of velocity $\bar{u}$, $\bar{v}$, and $\bar{w}$. A statistical analysis of these flow elements is then used to quantify turbulence in terms of intensity, frequency, and scale.

Based on this analysis, one should expect that the efficiency of a major item of equipment, such as a turbine or a kinetic compressor, is not fully dependent on Reynolds or Mach number alone, but also on the upstream turbulence which is not homogeneous, but consists, in the case of turbomachinery, of a succession of hub and tip lifting vortices interspersed with blade trailing edge wakes.

These application examples discussed in this section illustrate that the criteria are not size, larger or smaller, nor speed, faster or slower, but rather the proportion among significant physical entities that are expressible as dimensionless numbers. Model testing can save expense or enhance ease of measurement, provided that the critical physical effects are reproduced. An additional benefit is the succinct presentation of experimental results and design data when expressed in terms of the significant dimensionless groups. For example, to test three (3) values each of five (5) independent variables, requires 243 tests and requires 27 curve sheets to plot the results. Whereas the five variables can be reduced to two (2) nondimensional variables which will require only nine tests and the results can be plotted on one curve sheet.

6 REFERRED QUANTITIES

Referred quantities have been devised to avoid some of the inconveniences associated with dimensionless numbers but at the expense of a loss of generality.

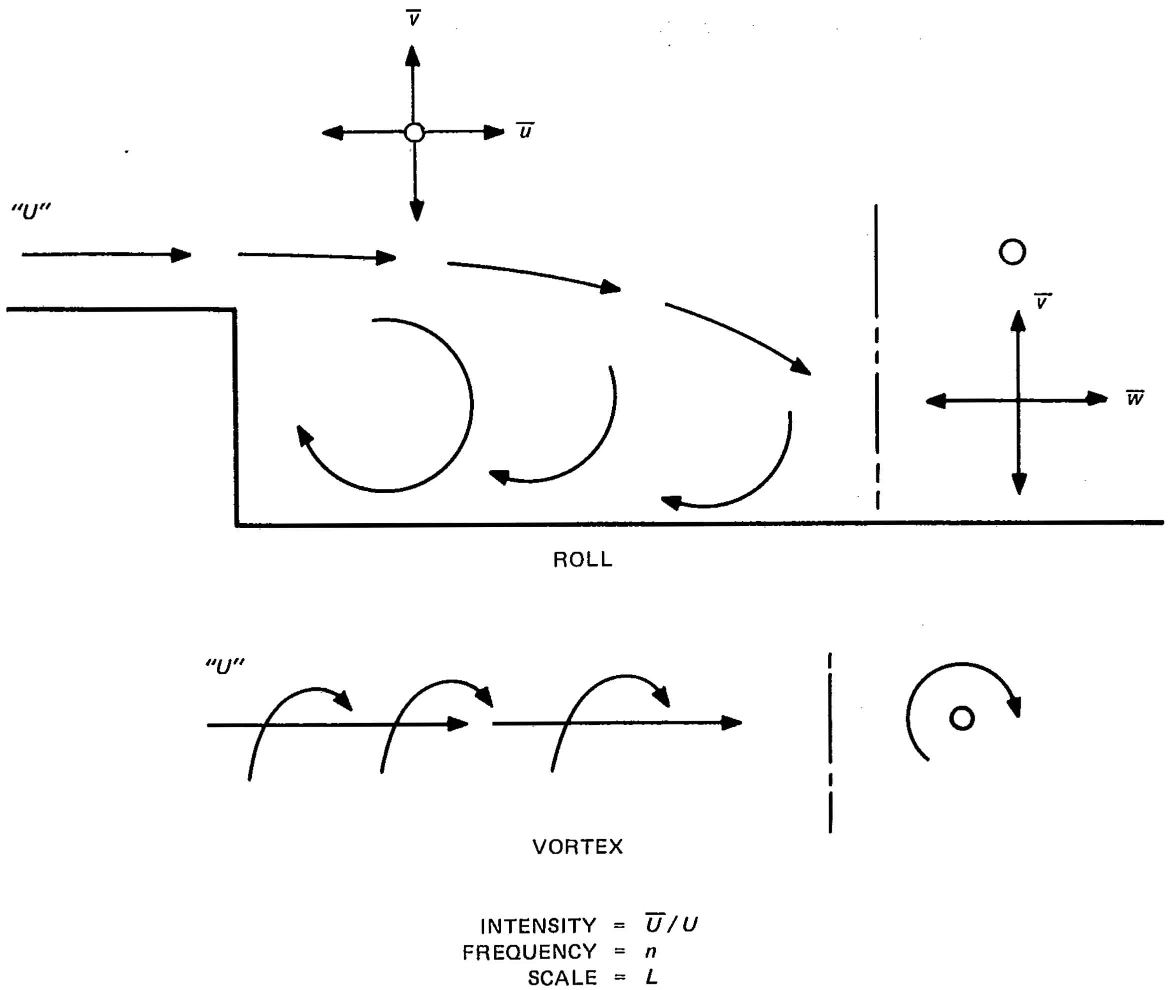

FIG. 10 CLASSIFICATION OF TURBULENT FLOW

Consider a compressor, for which

w = mass flow, lbm per sec
a_{t_1} = inlet sonic velocity, ft per sec
A = cross-sectional area, sq in.
p_{t_1} = total inlet pressure, psi
g = Acceleration of gravity, ft per sec^2

A dimensionless mass flow rate may be computed from

$$\frac{W\,(a_{t_1})}{A(p_{t_1})\,(g)} \tag{17}$$

In a specific example, equation (17) is evaluated

$$\frac{W a_{t_1}}{A\, p_{t_1} g} = \frac{100(\text{lbm/sec}) \times 1100(\text{ft/sec})}{4 \times 144\ (\text{in.}^2) \times 14.7(\text{lbf/in.}^2) \times 32.17(\text{ft/sec}^2)} = 0.40$$

The magnitude 0.40 is the dimensionless mass flow rate. It is the mass flow rate (W/g) slugs per unit area (A), per unit inlet total pressure (p_{t_1}), corrected for inlet sonic velocity (a_{t_1}).

This dimensionless number is converted to a referred quantity by first ignoring the reference size (A) and referring the flow to standard sea level inlet pressure (p_0) and temperature (T_0) conditions, assuming the sonic velocity to vary as $\sqrt{T}$.

$$\left(\frac{(W a_{t_1})}{A\, p_{t_1}\, g}\right) = 0.40 \qquad \frac{W\,(T_{t_1}/T_0)}{(p_{t_1}/p_0)} = 100(\text{lbm/sec})$$

Dimensionless Flow   Referred Flow   (18)

Thus the referred quantity adjusts the flow to standard inlet conditions but not for compressor size. Other referred quantities are developed in Table 3, Section 3.

7 REFERENCES FOR SECTION 1

[1] "Friction Factors for Pipe Flow," L. F. Moody, Tr. ASME, v.66, 1944, pg. 671.

[2] "Elements of Fluid Mechanics," J. K. Vennard, McGraw-Hill, New York, 1940, pg. 116.

[3] Ibid. pg. 118.

[4] "Technical Paper No. 410," Crane Company.

[5] "Average Velocity in a Duct," ASTM-D-3154, 1974; Part 26, Appendix, pg. 655.

[6] "Centrifugal Pumps & Blowers," A. H. Church, John Wiley & Sons, Inc., New York, 1944, pg. 64.

[7] "Turbomachinery Design Described by Similarity Considerations," G. F. Wislicenus, NASA Publication SP-304, 1974, pp. 7-39.

[8] "Theory of Turbomachines," G. T. Csanady, McGraw-Hill, New York, 1964.

[9] "ASME Orientation and Guide for Use of Metric Units," 7th Edition, 1976.

[10] "Fluid Mechanics and Its Application," J. W. Murdock, P.E., Houghton Mifflin Co., Boston 1976, pg. 204.

[11] "Model Tests of Two Types of Vibration Damper," C. A. Meyer, H. B. Saldin, trans. ASME A59, 1942.

SECTION 2

In this section a group of real problems are solved, either in whole or in part, by model testing.

INDEX OF EXAMPLE PROBLEMS

Figures are designated as follows: For instance, Ex.5-2 represents Example 5, Figure 2.

EXAMPLE 1 – OVERSIZED TURBINE STAGE FLOW MODEL

Certain aerodynamic effects in turbine stage flow defy rigorous analysis or theoretical appraisal. Their proper understanding requires a model where the physical phenomena can be directly observed and measured. The aerodynamic effects which appeared to be the major probable sources of losses in efficiency, and for which no clear understanding exists, were:

(1) The time varying nature of the flow in turbine stages caused by the interaction between the stationary nozzles and the moving buckets.

(2) Effects due to the interaction of the nozzle end vortex with bucket end wall flow.

(3) Radial forces on the nozzle and bucket boundary layers due to radial pressure gradients and the centrifugal forces in the rotating bucket.

(4) Intra-stage three-dimensional effects due to radial aerodynamic forces induced by the warped nozzles and buckets.

Studies in several of these areas were carried out, but it soon became apparent that economy of effort required the identification of the sources of the most significant losses, so that work could then stress these most promising areas. Consideration of the problem areas indicated that it would be very desirable to expand both the physical and time scales involved. Such scaling would permit rather detailed investigations of boundary layer and main-flow behavior using simple, well-proven instruments, and, with the time-scale expansion, would also permit relatively easy visual and photographic studies of all aspects of the flow. Such a time and size expansion would also entail a low enough speed to permit an observer to ride on the rotating wheel of a test facility, and thus directly study the relative flow through the moving buckets.

Establishment of Design Parameters

Obviously, it would be difficult to operate a large-scale visualizer with any appreciable pressure drop across the stage. Fortunately, the turbine stages being investigated have a pressure ratio across the buckets so near to unity that no serious distortion of the flow picture is introduced by testing under incompressible-flow conditions. The factors governing the design of the model were:

(1) Maintenance of the correct ratio between the flow velocity and the wheel speed.

(2) Operation at the same Reynolds number as the prototype stages to permit direct comparison of results.

(3) Consideration of size and speeds such that observers could obtain useful results without undue discomfort.

Preliminary experiments with large airfoil mockups indicated that the air velocity relative to the bucket should be no higher than 10 ft/sec for visual studies with smoke. This figure, plus the necessity of maintaining the proper velocity ratios, established the design bucket tangential speed of 11 ft/sec and the flow velocity at the nozzle throat of about 20 ft/sec.

To obtain these velocities at the same Reynolds Number as exists on the actual turbine, the model stage is 25 times the size of the prototype. Table 1-1 shows the operating conditions and some pertinent dimensions of the facility.

The axis of the model turbine stage is vertical with air flow downward through the stationary nozzles and then downward through the turbine buckets. Example 1-1 shows the buckets and an observer riding on the ring shaped car (like a merry-go-round) that rotates on a circular track.

Because of the low velocities and pressure differentials at which the model operates, it would have been very difficult to eliminate all troublesome air infiltration and thermal convective effects if the structure were directly exposed to the weather. Accordingly, it was enclosed in a 90-ft-diameter air-supported fabric radome which completely eliminates wind effects and provides weather protection.

Due to the low air flow velocity the power generated in the model turbine stage is insignificant. An electric motor drive of the ring that bears the moving buckets and the moving observer synchronizes the pitchline velocity to the air flow velocity.

The air flow is induced by a 14-ft-diameter propeller-type fan. It was necessary to suppress the general whirl and many smaller disturbances leaving the fan. An arrangement of flow-smoothing screens was developed using a 1/50th size scale model with water as the fluid and dye tracers.

TABLE 1-1

Dimensions of Test Stage	
Diameter (pitch line)	49 ft-4 in.
Radial height of buckets	53¾ in.
Nozzle partitions	
Number	50
Axial width	48-1/8 in.
Pitch	37.15 in.
Exit area	166.4 ft^2
Buckets	
Number	95
Axial width	25 in.
Pitch	19.6 in.
Overall Structure	
Height	45 ft-4 in.
Diameter	72 ft
Radome	90 ft diameter X 55 ft high
Operating Conditions for Visualization	
Air flow	174,000 cfm
Wheel speed	4.3 rpm (11 fps at pitch line)
Stage pressure drop	0.09 in. H_2O
Nozzle-passing frequency (moving observer)	3.6/sec

Observing Flow Behavior

The moving buckets in Ex. 1-1 are bounded by transparent plastic end plates. Penetrations of the plastic permit the moving observer to insert measurement probes and smoke probes.

An excellent picture of flow conditions in the boundary layer is obtained by wiping the bucket surface with a swab soaked in a mixture of titanium tetrachloride and anhydrous alcohol. During the few seconds required for the liquid film to evaporate, a dense smoke is liberated directly into the boundary layer. For exploratory studies, the observer uses a long-handled applicator to apply the chemicals to any region of interest. Since the moist swag "smokes" continuously it is a convenient probe for investigating flow in the main stream also. When more detailed studies are

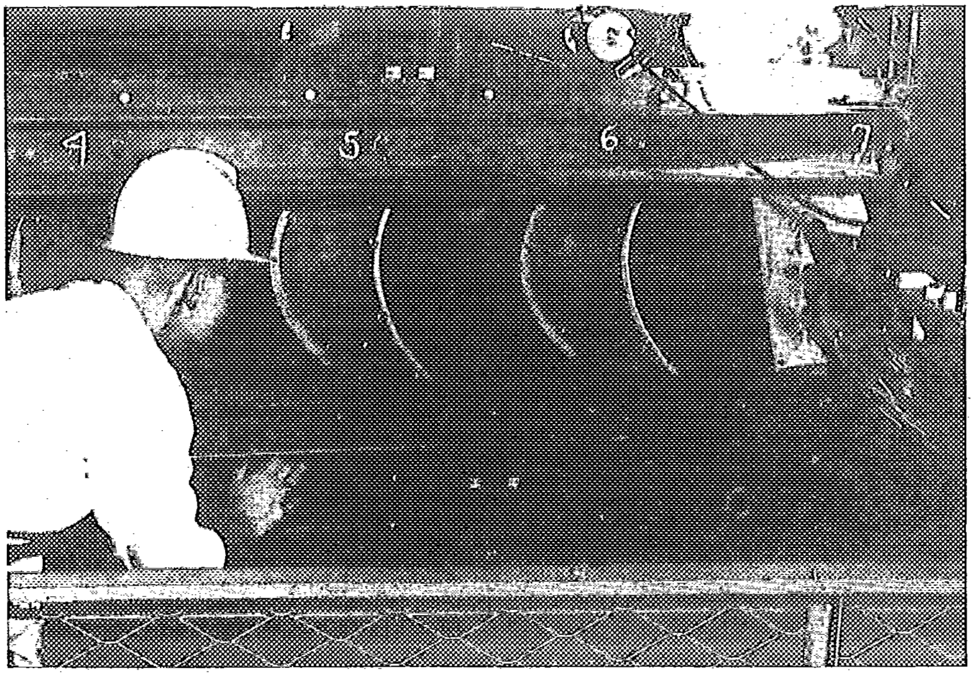

EX. 1-1 MOVING BUCKETS AND OBSERVER ON GENERAL ELECTRIC 25/1 SCALE TURBINE STAGE

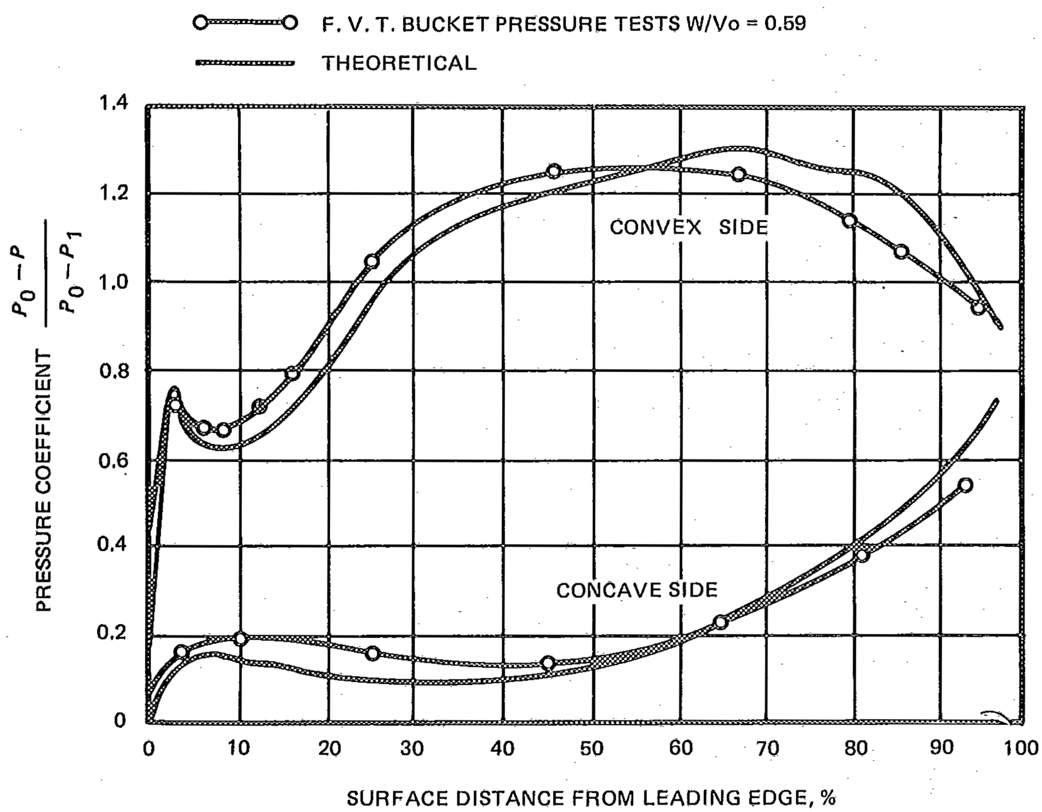

EX. 1-2 COMPARISON OF THEORETICAL AND MEASURED PRESSURE DISTRIBUTIONS ON ROTATING BUCKET

needed, smoke may be liberated from fixed probes, rakes, or ports in the surfaces.

The smoke generated on the bucket surface is rapidly diffused into the turbulent boundary layer by the turbulent eddies, and thus tends to outline the extent of the boundary layer thickness at this point. In motion pictures of this region taken at high framing rates, the presence of individual eddies in the boundary layer can be detected. The smoke generated outboard along the trailing edge is seen to pass smoothly into the bucket wake with no backward flow along the bucket surface, thus indicating that there is no flow separation from the convex bucket surface.

The facility is well adapted for detailed quantitive measurements of the various flow parameters, and such work is being carried out. Example 1-2 illustrates one type of result which has been obtained. In this case, the pressure distribution on the bucket surface was measured, and in the graph the time average pressures at one radial position are compared to the values calculated for that section as a two-dimensional cascade. The quantity plotted is the pressure coefficient

$$c_p = \frac{p_0 - p}{p_0 - p_1}$$

where:

p_0 = total pressure
p_1 = static pressure at the discharge
p = local static pressure on the bucket surface

This pressure coefficient varies as the square of the local velocity, being zero at the stagnation point and unity at the downstream condition.

The correspondence between the measured and calculated pressures is quite good, with the principal differences occurring near the trailing edge of the bucket. These differences are believed to be mainly due to the accumulated three-dimensional flow effects near the discharge side of the bucket, and also to boundary layer growth on the bucket surface.

Much interesting flow visualization data has been obtained using this facility. Motion pictures have been used for this documentation. Complex flows near the surfaces are observed with definite secondary flow effects. Cyclical patterns at the frequency of nozzle passing are readily observed.

Conclusion

The understanding of turbine stage efficiency started with steady-flow concepts of simple pitch-line vector diagrams and has advanced to sophisticated concepts for accounting for radial equilibrium and radial velocity components of the turbine flow. Further efficiency refinements are dependent on specific understanding of loss mechanisms. The large-scale turbine stage model provides the means for the direct observation of non-steady flows and other fine flow details by observers riding with the moving buckets.

ACKNOWLEDGMENT

This article was based entirely on ASME Paper 65 WA/PWR-2 by J. E. Fowler and J. J. Parry, "A Facility For Flow Visualization in a Large-Scale Turbine Stage."

EXAMPLE 2 — PUMP INTAKE VORTEX STUDIES

The most serious problem encountered in suction intakes is that of a persistent and large-scale vortex at the pump suction. The design specific speed of a wet-pit pump is dependent upon straight-through flow into the suction bell, and if this pattern is disturbed the capacity and head at maximum efficiency will be affected. If the water at the suction rotates in a direction opposed to that of the pump rotation, the pump will increase with a proportional increase in power required to produce this condition. Since the pump head is dependent upon the sum of the angular momentum at the suction and that produced by the impeller, it is apparent that a negative angular momentum of the flow at the suction, as a result of counter-rotation produced by the intake structure, will increase the pump output. Conversely, if the rotation of the water is in the same direction as the pump rotation, the pump output will decrease with a reduction in power, and may not satisfy the anticipated conditions. The formation of a large-scale vortex is usually associated with an intake design that causes a change in direction of the flow before it enters the pump suction.

It has been learned from field experience and through model studies, that if the change in direction of the water is not too severe, a baffle placed between the suction-bell rim and the back wall in line with the incoming flow, as shown in Ex. 2-1, will assure satisfactory operation. The baffle should be placed as close to the suction bell as possible and extend to the surface of the water in an open

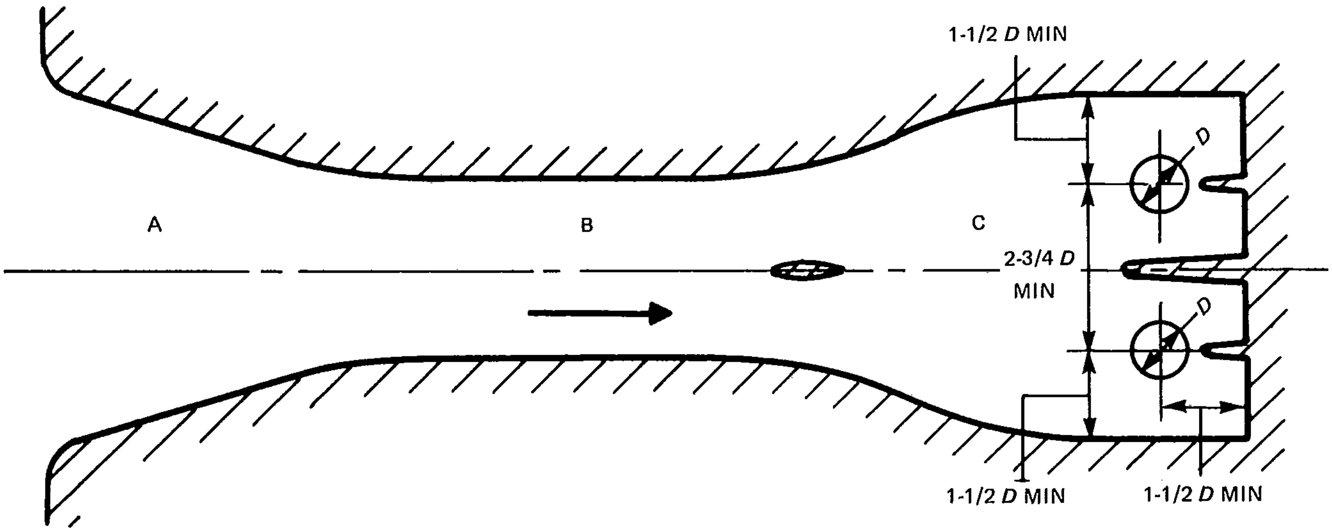

EX. 2-1 TYPICAL PUMP INSTALLATION AND INTAKE DESIGN

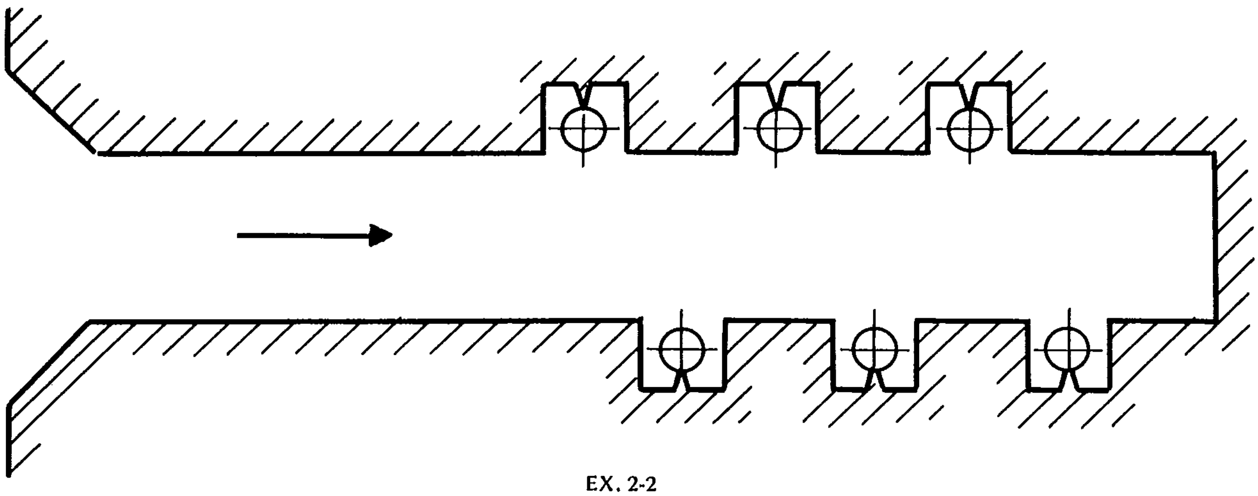

EX. 2-2

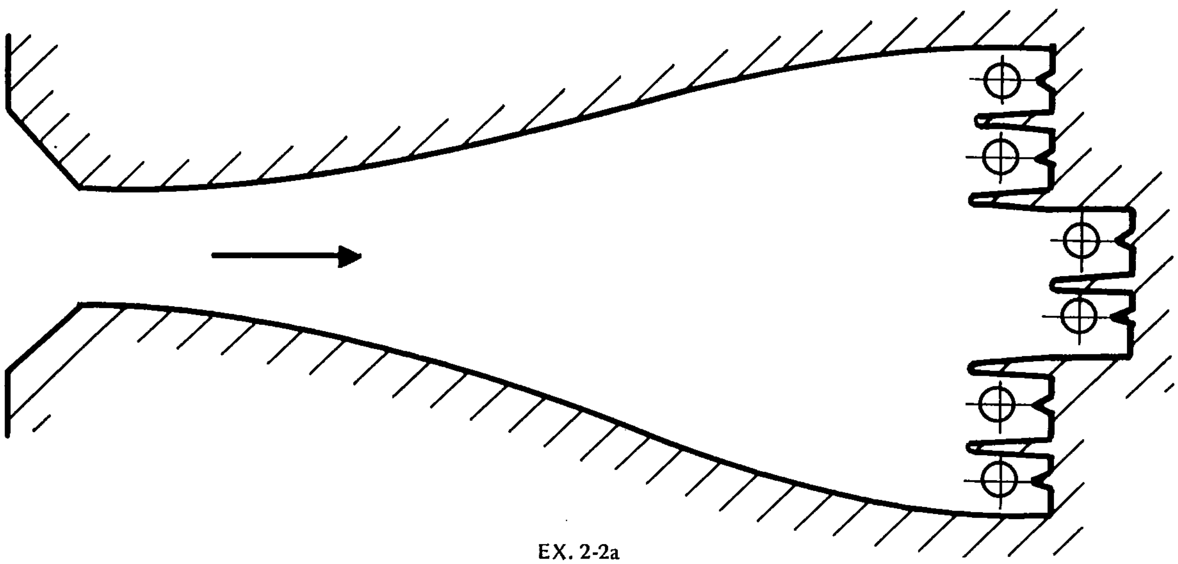

EX. 2-2a

channel or to the roof of the tunnel in a closed system.

In a multiple-unit installation of identical pumps a number of the pumps may operate satisfactorily, but the remaining units may overpump or underpump in an apparently haphazard fashion. Upon investigation, however, it will be evident that because of the location of the various units the suction conditions are not duplicated and overpumping and underpumping occurs depending upon the magnitude and direction of the swirls. It is thus apparent that identical pumps cannot be considered as duplicates unless the suction-flow conditions to each are also duplicated.

Larger and more complex installations involving a number of pumps generally operate at higher tunnel velocities. Shown in Ex. 2-2 is a typical installation of this type in which the pumps are placed in individual wells out of the main stream flow. To illustrate, if each of the six pumps shown has a design capacity of 25,000 gpm, the tunnel flow at the first well is 150,000 gpm at tunnel velocity of 6 fps. The velocity head represented by this velocity tends to maintain straight flow through the tunnel and the flow into the wells will be proportional to the difference in the pressure in the tunnel and the level in the well. The level in the well is determined by the drawdown of the pump and will increase until a sufficient differential exists to divert the required capacity into the well. The reduction in level, however, will manifest itself to the detriment of the pump in at least three forms:

(a) The suction head available at the impeller is reduced, and if less than that required by the pump, cavitation will occur.

(b) That portion of the flow which is diverted into the well still retains a component of its forward velocity and produces a severe swirl that cannot be controlled effectively by baffling.

(c) The reduction in level will increase the total pumping head by increasing the static head between the suction and discharge levels. This is an example of uncontrolled flow at high velocities and can be improved only by providing a means to utilize a portion of the energy of the tunnel flow and guiding the flow evenly to the impeller. The usual practice is to provide a scoop or contracting elbow located in such a manner that as much flow is diverted as required by each pump and yet does not restrict the flow to the downstream units.

Formed suctions have proved to be very effective with high-velocity flows and, when it is realized that a flow of 150,000 gpm at a velocity of 6 fps represents 21 hp, it is apparent that every effort should be made to utilize this power with a minimum of loss. The formed intake structure, however, will increase the cost of the installation materially and the engineer must decide whether or not the sacrifice in pump performance warrants the additional construction cost.

The most effective method for the study of these problems is by model tests of the intake structure where controlled conditions can be maintained and alterations made at little cost. Model studies, however, are not infallible, and considerable skill and judgment must be exercised in their design, operation, and interpretation of results. Such models have been designed, built, and tested and the results when applied to the prototype have proved effective. A model of the complete intake structure, from the inlet to the pump suction, is seldom necessary and the usual practice is to model that portion where the most severe conditions occur and to select as large a scale as is practicable.

Models of intake structures fall into two general classifications, models of open-channel intakes and models of closed conduits or tunnel intakes. The surface conditions in an open channel follow Froude's law which states that the surface disturbance can be described by Froude's number. It is further recognized that to produce comparable conditions in two geometrically similar structures of different size, Froude's number must be held constant. Now if L_m is a linear dimension of the model and L is the corresponding linear dimension of the prototype, the scale factor is L_m/L. Further the Froude number of the model is

$$F_{rm} = \frac{V_m}{\sqrt{L_m g}}$$

and of the prototype is

$$F_r = \frac{V}{\sqrt{Lg}} \; *$$

and it follows that with constant Froude number

$$V_m = V\sqrt{\frac{L_m}{L}}$$

Modeling of the pump suction to maintain geometric similarity requires that the suction bells and the flow pattern in the model and the prototype be similar. The ratio of the model and the prototype velocities, however, need not be related to the scale factor to maintain geometric similarity.

It would appear that a model designed for constant Froude number, i.e.,

$$V_m = V\sqrt{\frac{L_m}{L}}$$

*If the water depth (h) is used in place of (L), the wave velocity $(V_w) = \sqrt{hg}$ and the Froude number is the ratio of velocity $F_r = (V/V_w)$. The Froude number is unity when the head is 2/3 the initial head.

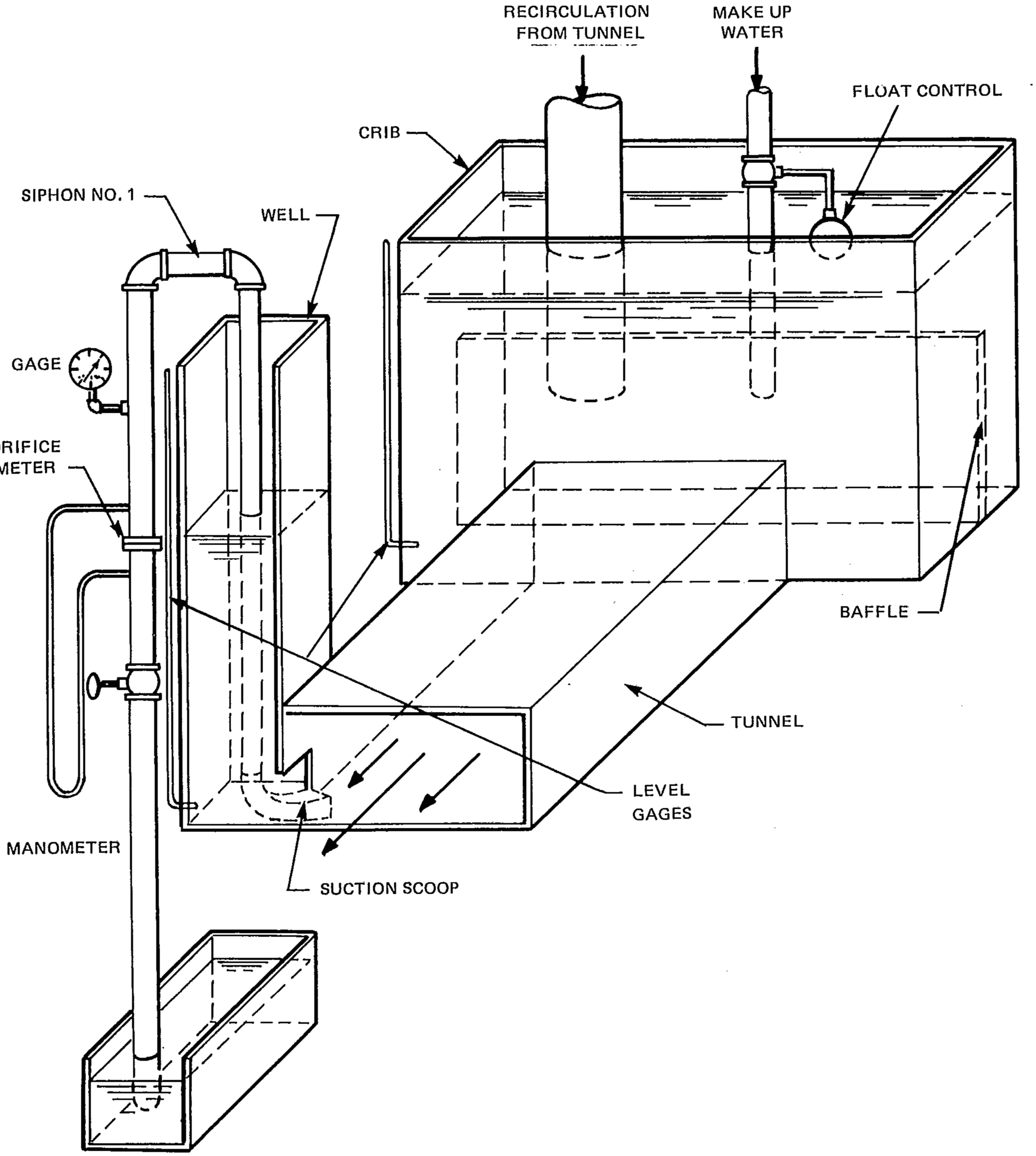

EX. 2-3 MODEL SUCTION TUNNEL

will satisfy the model relations for both the surface flow conditions and the pump suction. This assumption is reasonable if the model scale is not too small and the prototype velocities sufficiently high.

As the model scale decreases, the model flow velocities become very low as compared to the prototype and the results are unreliable. Satisfactory results have been obtained, however, if the model is designed with the same flow velocities as in the prototype. With velocities higher than required for a constant Froude number the eddies and turbulence in the model will be more severe than in the prototype and it is reasonable to assume that if these adverse flow conditions can be corrected in the model, the same measures will be effective when applied to the prototype.

A 1/16-scale model was used to study the effectiveness of suction scoops in an installation with varying tunnel velocities. The model was built with the same velocities as in the prototype. To attain the desired velocities past the first well, a true model would have included additional pumps, but modeling of the first two wells only was considered sufficient to obtain the essential information. The model consisted of a crib which served as a reservoir to maintain a constant static head on the tunnel comparable to the actual river level. The No. 1 well was placed a sufficient distance from the junction of the tunnel and the crib so that the inlet conditions into the tunnel would not affect the readings at the first well. The desired tunnel velocities were obtained by an auxiliary pump which took its suction from the end of the tunnel and recirculated the water back to the crib. By throttling the discharge of this pump it was thus possible to vary the tunnel velocities over a wide range. It is very convenient in this type of model to use siphons with modeled inlets to duplicate the pumps.

Example 2-3 shows the modeled scoop in place in the No. 1 well and the orifice meter in the down leg of the siphon to measure the flow rates. The siphon head required to produce the flow rate through the suction bell and siphon system. The flow removed by the siphons was replaced by make-up water in the crib to maintain a constant level throughout the tests. Table 2-1 gives the pertinent specifications of the prototype and the corresponding model values.

To obtain a comparison of the relative merits of the suction bell and the scoop suction, the change in capacity and siphon head with each suction design at a constant valve setting of the siphon was obtained. It is apparent that the greater the turbulence and losses into the well, the lower will be the capacity of the siphon and the greater will be the required siphon head. It follows that all losses in the siphons themselves must be isolated and this was done by plotting the static levels in the wells against the siphon flows with tunnel velocities equal only to those caused by the siphon flow. This plots, as shown in Ex. 2-4, with the suction-bell inlet, and in Ex. 2-5 with the suction scoop inlet. Using these curves as a calibration for each, any deviation in capacity at constant siphon heads will indicate the effectiveness of the suction design.

TABLE 2-1 PROTOTYPE AND MODEL DATA

	Prototype	Model
Tunnel cross section	8 ft X 15 ft	6 in. X 11¼ in.
Well opening	8 ft X 8½ ft	6 in. X 6-3/8 in.
Well size	9½ ft X 8¼ ft	7¼ in. X 6-3/8 in.
Pump capacity—each	34500 gpm	135 gpm
Suction-bell diameter	44 in.	2¾ in.
Scoop inlet	2 ft X 4 ft	1½ in. X 3 in.
Static head on tunnel	15 in.	3¾ ft

Examination of Ex. 2-4 with the bell suction shows a marked decrease in capacity for pumps Nos. 1 and 2 up to about 3½ fps tunnel velocity, and then with a further increase in tunnel velocity, the curves approximately parallel the calibration curve up to the velocities of 9 to 10 fps when the deviation begins to increase. Throughout the range of velocities tested, with the exception of the low tunnel velocities, there is little difference in performance between the Nos. 1 and 2 pumps.

Example 2-6 shows the loss in capacity plotted on a percentage basis against tunnel velocity. The single curve shown is an average of the loss in capacity of the Nos. 1 and 2 pumps. It must be remembered in the application of these curves to the prototype that the percentage loss in capacity reflects losses into the well only, and gives no indication of the magnitude or direction of the swirl in the well and its effect upon the pump performance.

Visual examination during these tests revealed severe swirling in both wells even though a baffle had been installed between the suction bell and the back of the well. Readings of the drawdown in each well were taken and the feet drawdown is plotted against tunnel velocity in Ex. 2-7. The curve applies for both the Nos. 1 and 2 wells as very little difference was noted between the two. The velocity head in the tunnel also is plotted on the same scale and the difference between the velocity head and the drawdown represents the head loss incurred with a 90-deg turn of the water into the well. It can be seen from this curve that a drawdown of 1½ ft at a tunnel velocity of 7.8 fps, which would be of the same order of magnitude in the prototype, would be quite serious with a low-head pump as it would increase the pumping head and decrease the available submergence by the same amount.

In contrast of these curves is that in Ex. 2-5 where the same test was run with the suction scoop in place. It will

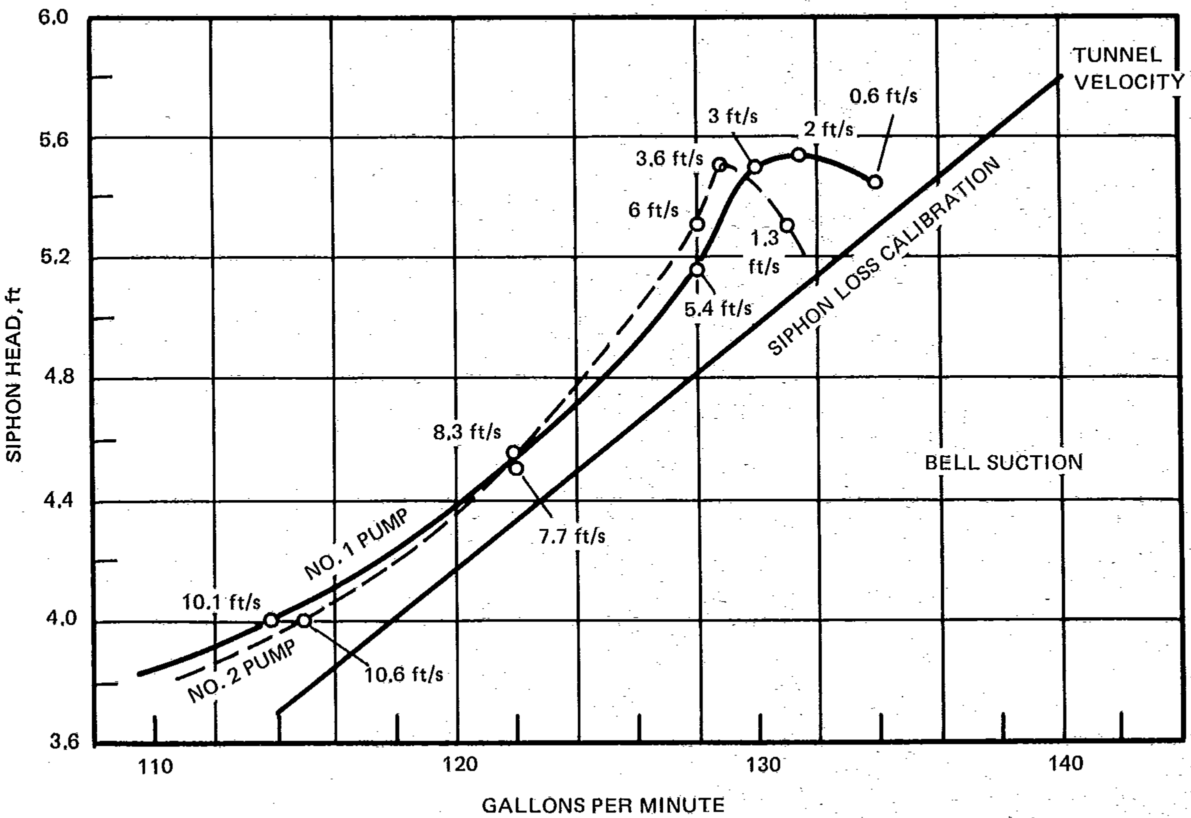

EX. 2-4 SIPHON LOSS WITH BELL SUCTION

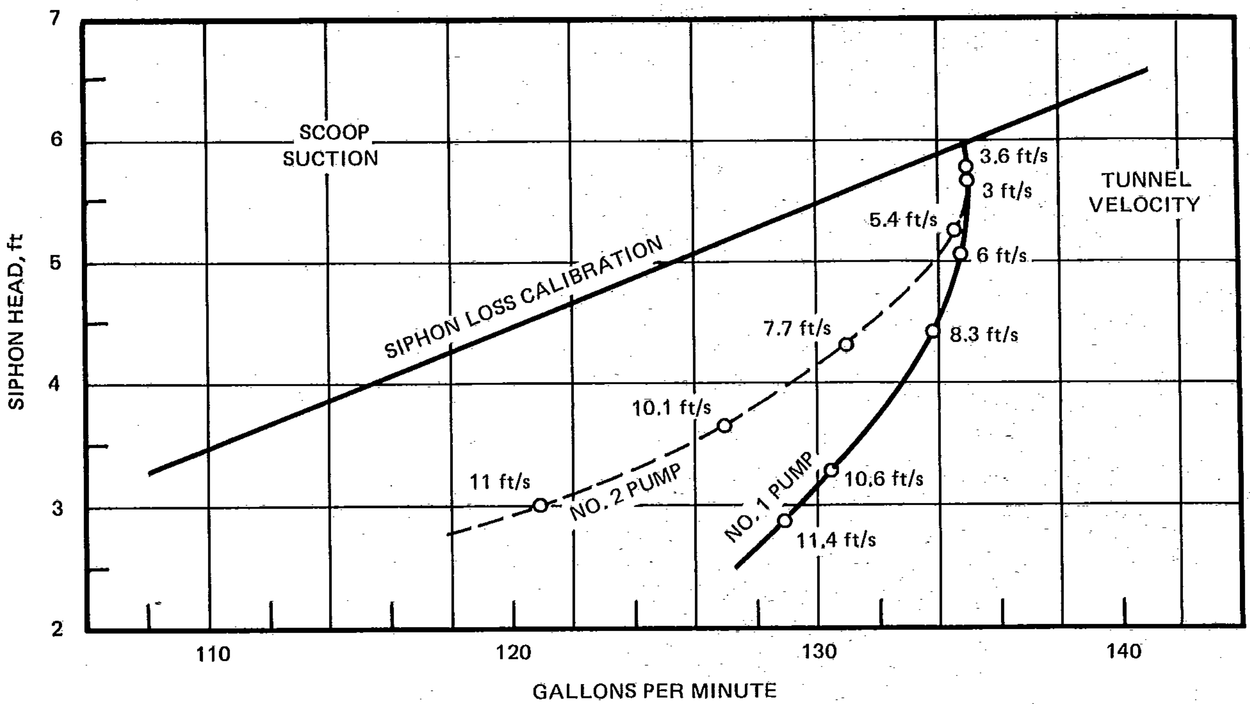

EX.2-5 SIPHON LOSS WITH SCOOP SUCTION

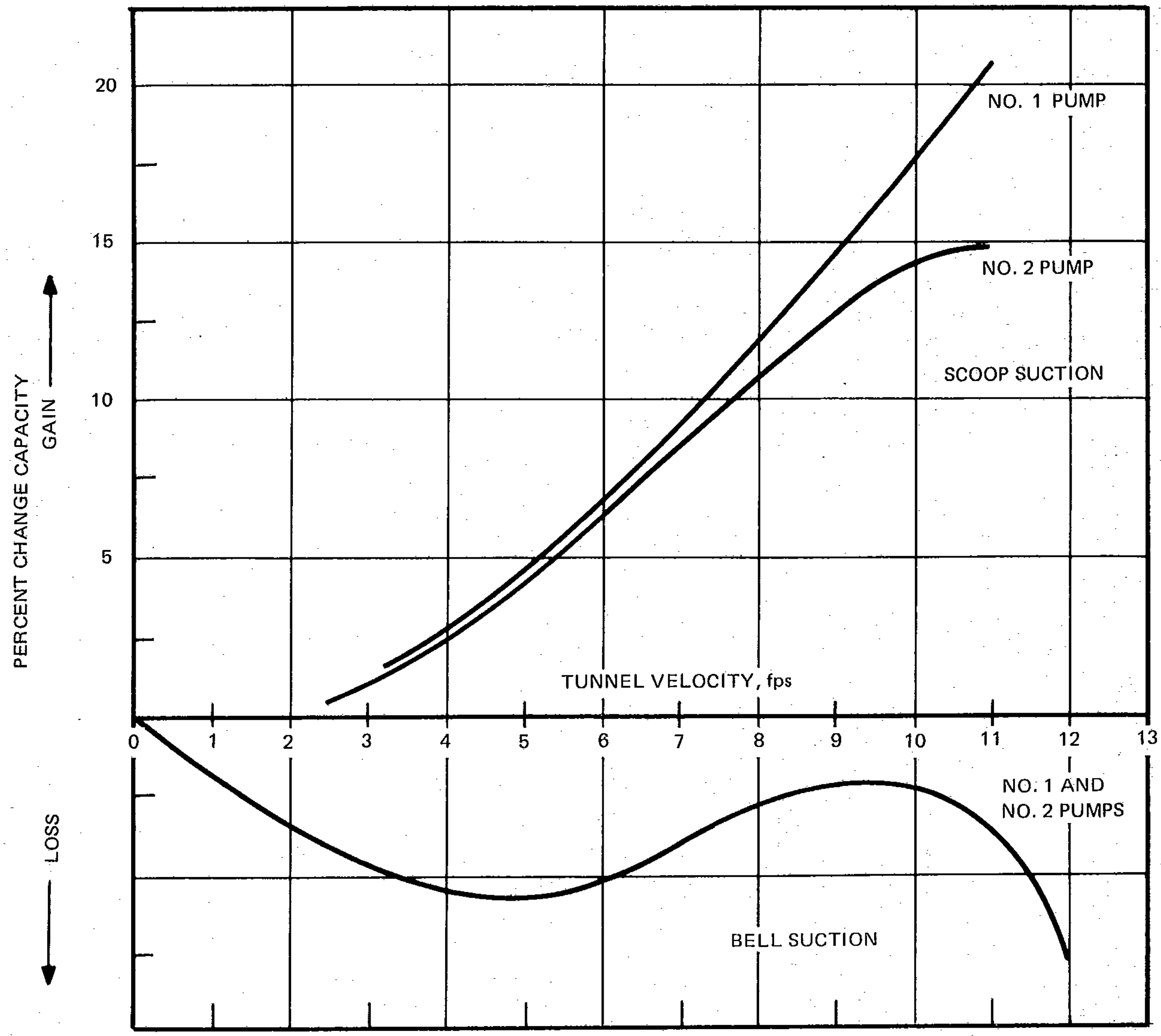

EX. 2-6 COMPARISON OF LOSSES WITH SCOOP SUCTION AND BELL SUCTION

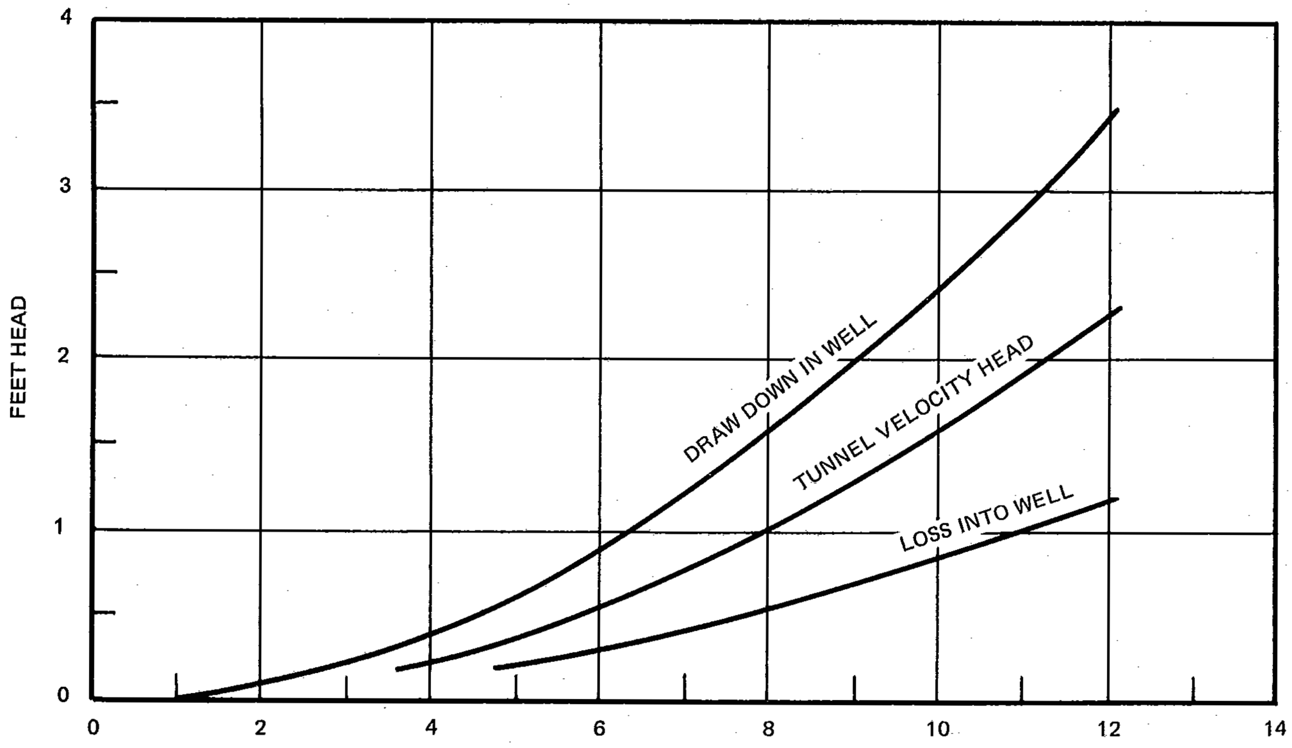

EX. 2-7 DRAWDOWN AND HEAD-LOSS CURVES

be noted that there is a gain in capacity as the tunnel velocity is increased with an appreciable spread between the Nos. 1 and 2 pumps.

Example 2-6 shows this increase as a percentage rise in capacity plotted against tunnel velocity. It is apparent from these curves that much is to be gained by the use of the suction scoop which utilizes a portion of the impact velocity of the tunnel flow over the suction-bell design and, with performance data of this nature, the problem then resolves itself into the cost study of the increase in tunnel construction to reduce velocities, if the suction bell is to be used, as against the cost of the scoop construction which will operate satisfactorily with the high tunnel velocities.

Evidently the tests show that the source of vortices is the moment of momentum of the flow at inlet to the pump. Any flow whose moment is about the center of the pump must result in a vortex of equal momentum. A design similar to Ex. 2-2a should fulfill this requirement.

EXAMPLE 3 – HYDRAULIC TURBINE TESTS

Model testing of hydraulic turbines is a well established method for design research and development. The results of model testing are used to predict and/or verify the performance of prototype units.[1] All the major manufacturers of hydraulic turbines have their own laboratories for model performance and cavitation tests. In these laboratories the turbine efficiency, power, flow and cavitation characteristics are determined. The model testing is done for development and improvement of existing designs and for contract acceptance.

For accurate prediction of performance of a prototype turbine based upon a model, complete homology is necessary. This includes modeling of the inlet casing and the draft tube discharge. The model must be carefully built with fine attention to the degree of dimensional accuracy between the model and prototype. When good correlation

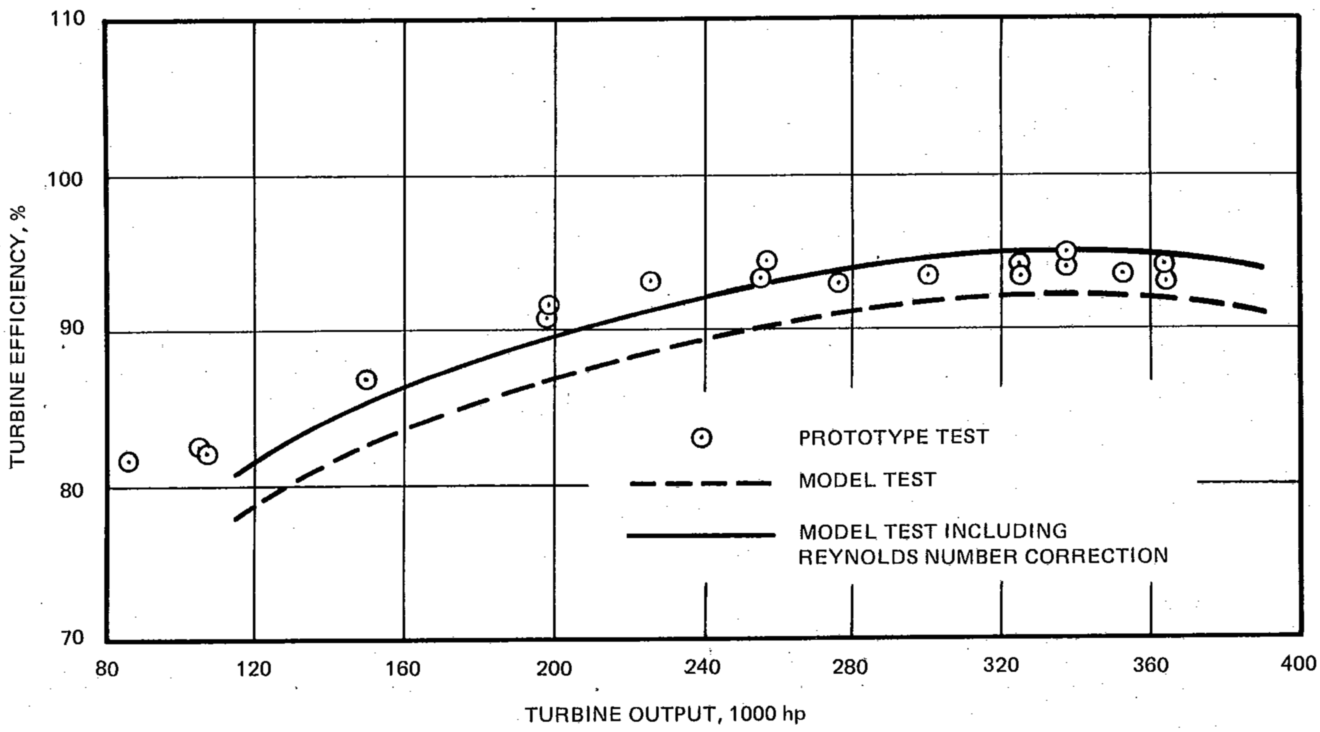
110
100
90
80
70
TURBINE EFFICIENCY, %
80
120
160
200
240
280
320
360
400
TURBINE OUTPUT, 1000 hp
PROTOTYPE TEST
MODEL TEST
MODEL TEST INCLUDING
REYNOLDS NUMBER CORRECTION

EX. 3-1

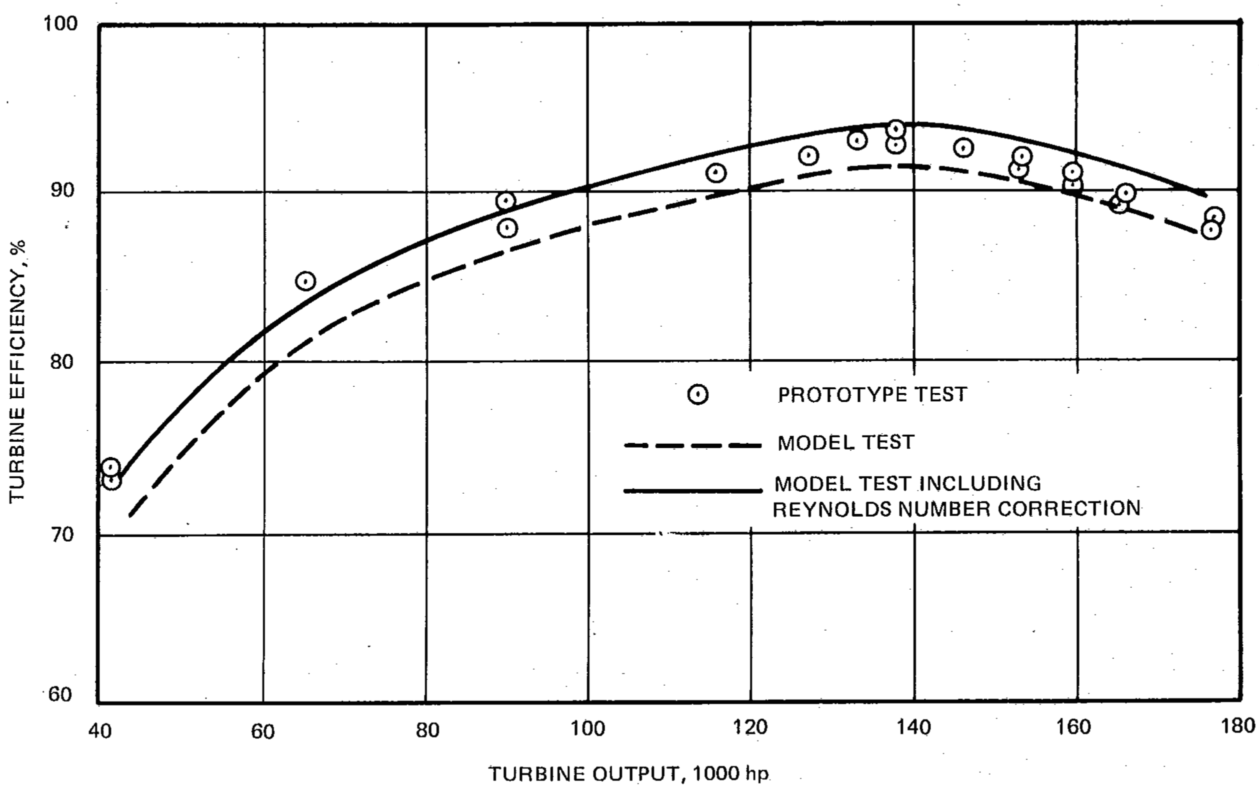
100
90
80
70
60
TURBINE EFFICIENCY, %
40
60
80
100
120
140
160
180
TURBINE OUTPUT, 1000 hp
PROTOTYPE TEST
MODEL TEST
MODEL TEST INCLUDING
REYNOLDS NUMBER CORRECTION

EX.3-2

between model dimensions and prototype dimensions are obtained accurate predictions of prototype performance based upon model results is possible. However, these predictions must take into account the effect of Reynolds number in scaling from model to prototype size. The Reynolds number effects are taken into account by applying a correction to the model results based on formulas derived by Moody, Hutton, and others.[2] Furthermore, tests on models must be done in a Reynolds number regime where the flow can be considered super critical.* Tests on models which are too small or are tested with flow velocities that are low or where the possibility of subcritical Reynolds number exists yield results which are erroneous. Each manufacturer has evolved generalized dimensions for his models which yield test results which can be satisfactorily scaled to prototype size. Models are constructed to be as small as possible in physical size to minimize the cost of the testing while still being large enough to be in the super critical flow regime.

Examples 3-1 and 3-2 illustrate the correlation between tests done on prototype turbines and the expected performance derived from model test results. In both cases good correlation is obtained between model based prediction and actual prototype measurements. The power levels are satisfactorily predicted from the model tests. The efficiency levels obtained on the model are lower than the efficiencies measured on the prototype, but when the effect of Reynolds number is taken into account the model efficiency is increased and a better estimate of prototype efficiencies is obtained.

In addition to determining the steady state performance of the prototype, model testing is used to obtain the hydraulic characteristics of the turbomachine when operating in a transient condition. The data is obtained on the model in a quasi-static manner and then is used to predict transient prototype performance through the use of computer modeling. Furthermore, pressures, stresses, and vibration are measured on models to be able to understand how design can be built which will have smooth operating characteristics.

*Critical, as used here, refers to the critical Reynolds number where the flow changes from laminar to turbulent, rather than from subsonic to supersonic as used elsewhere.

REFERENCES

[1] Symposium on Laboratory Testing of Hydraulic Turbine Models in Relation to Field Performance – Transaction of the ASME for October 1958.

[2] International Electrotechnical Commission – Publication 193 International Code for Model Acceptance Tests of Hydraulic Turbines.

EXAMPLE 4 – BUTTERFLY VALVE TESTS

The design of butterfly valves, for example in cross-over pipes in low pressure steam turbines, requires a knowledge of the flow and the torque on the valve shaft as a function of the valve shaft angular position and the pressure drop across the valve. In case of emergency, the valve must be closed quickly to prevent the turbine from running away. The size of the operating piston and its supply pressure will, of course, depend on the inertia and aerodynamic torque of the valve and the required closing time and the flow through the valve during closing.

Dimensional Analysis

The independent variables are:

$(\Delta p/p_1)$ = The pressure drop across the valve, measured in terms of the inlet pressure (p_1) which is used as a standard dimension to replace *M, L,* or *t*.

α = The angle setting of the valve shaft, from the open position, which is already dimensionless.

The dependent variables are:

$K = \Delta p/(\rho V^2/2)$ = The total pressure drop across the valve, measured in terms of the velocity pressure ahead of the valve, taken as a standard dimension itself to replace either *M, L,* or *t*.

C_D = (Flow/Ideal flow) = The discharge coefficient, which is the flow measured using an ASME Standard Nozzle, given as a fraction of an ideal flow which is used as a standard dimension itself to replace *M, L* or *t*.

THE CALCULATION OF THE LOSS COEFFICIENT (K) USING THE THRUST FACILITY

Operation

(1) An arbitrary thrust is selected by placing a weight on the scale which opposes the nozzle thrust and holds nozzle against a stop toward the left.
(2) A blower, supplying air at "O" is increased in speed until it develops sufficient pressure and nozzle thrust to lift the nozzle off its stop, toward the right where it hits another stop. The greater the loss of the specimen, the greater the supply pressure must be to lift the selected weight.
(3) The difference between the total pressure required to lift the weight when the specimen is in the nozzle and when the nozzle is empty is used to calculate the incremental loss coefficient.

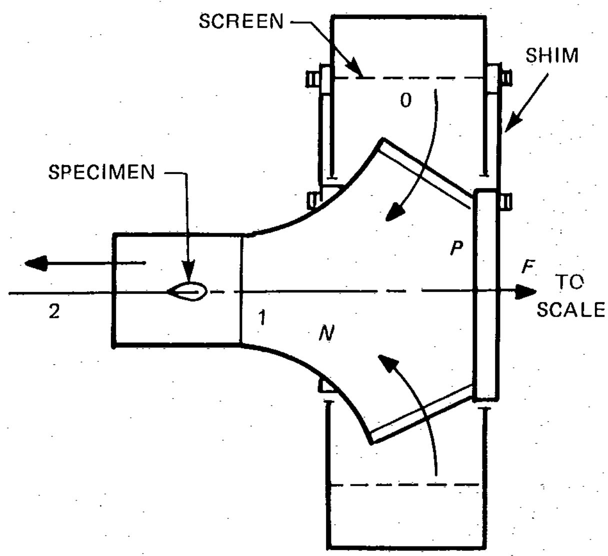

$$p_{t_0} - p_{t_2} = K\,\rho_2 V_2^2/2 \text{ (definition of the loss coefficient)}$$

$$p_{t_2} = p_{s_2} + \rho_2 V_2^2/2 \text{ (definition of the total pressure } p_{t_2}\text{)}$$

Adding

$$p_{t_0} = p_{s_2} + (1+K)\,\rho_2 V_2^2/2 = p_{s_2} + (1+K)\,(F/2A)$$

$$p_{t_{0r}} = p_{s_{2r}} + (1+K_r)\,\rho_2 V_2^2/2 = p_{s_{2r}} + (1+K_r)\,(F/2A)$$

Subtracting, Holding (F/A) Constant

$$\frac{(p_{t_0} - p_{s_2}) - (p_{t_{0r}} - p_{s_{2r}})}{(F/2A)} = (K - K_r)$$

or

$$\boxed{\frac{(_{t_0}\Delta p_{s_2})}{(F/2A)} - \frac{(_{t_0}\Delta p_{s_2})_r}{(F/2A)} = (K - K_r)}$$

If p_{s_2} is atmospheric pressure, $(p_{t_0} - p_{s_2}) = {}_{t_0}\Delta p_{s_2}$ is the inlet total *gage* pressure.

EX. 4-1

$\tau = (T/A\,\Delta p\,D)$ = The torque coefficient (= dimensionless torque) is the torque, measured in terms of the product of valve area, pressure drop and diameter; taken as a dimension itself in place of M, L or t.

The above analysis assumes incompressible turbulent flow since the valve is downstream of turning vane elbows and other valves and has a small pressure drop across it at full flow. If this were not the case we would have to include the Reynolds number (dimensionless viscosity) and the Mach number (V/a) in the independent variable list above. For reasonably low Mach numbers, the quantity $(\gamma) = -(\partial p/p)/(\partial v/v)$, a measure of compressibility, can be used in place of Mach number.

Tests

Tests were run using the facility shown on Ex. 4-1, which consists of a nozzle N which is connected to a circular pressure balancing plate (P). When high pressure fluid is supplied at (O), the nozzle and its pressure balancing plate are forced to the right, due to the nozzle thrust. A lever system and a dead weight scale are arranged to hold the nozzle against a set of stops toward the left.

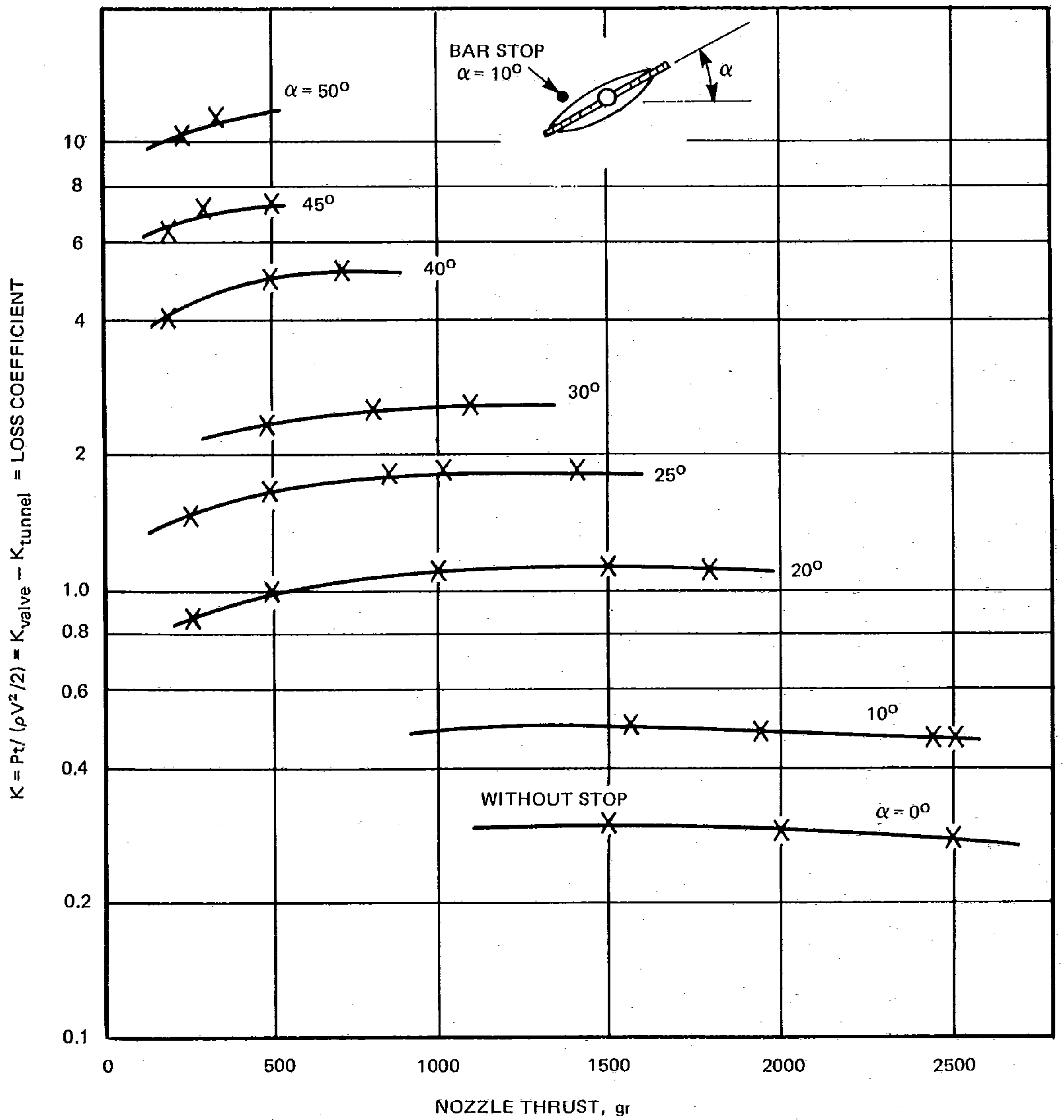

EX. 4-2 LOSS COEFFICIENTS OF BUTTERFLY VALVE FOR VARIOUS CLOSING ANGLES (α) AND NOZZLE THRUSTS

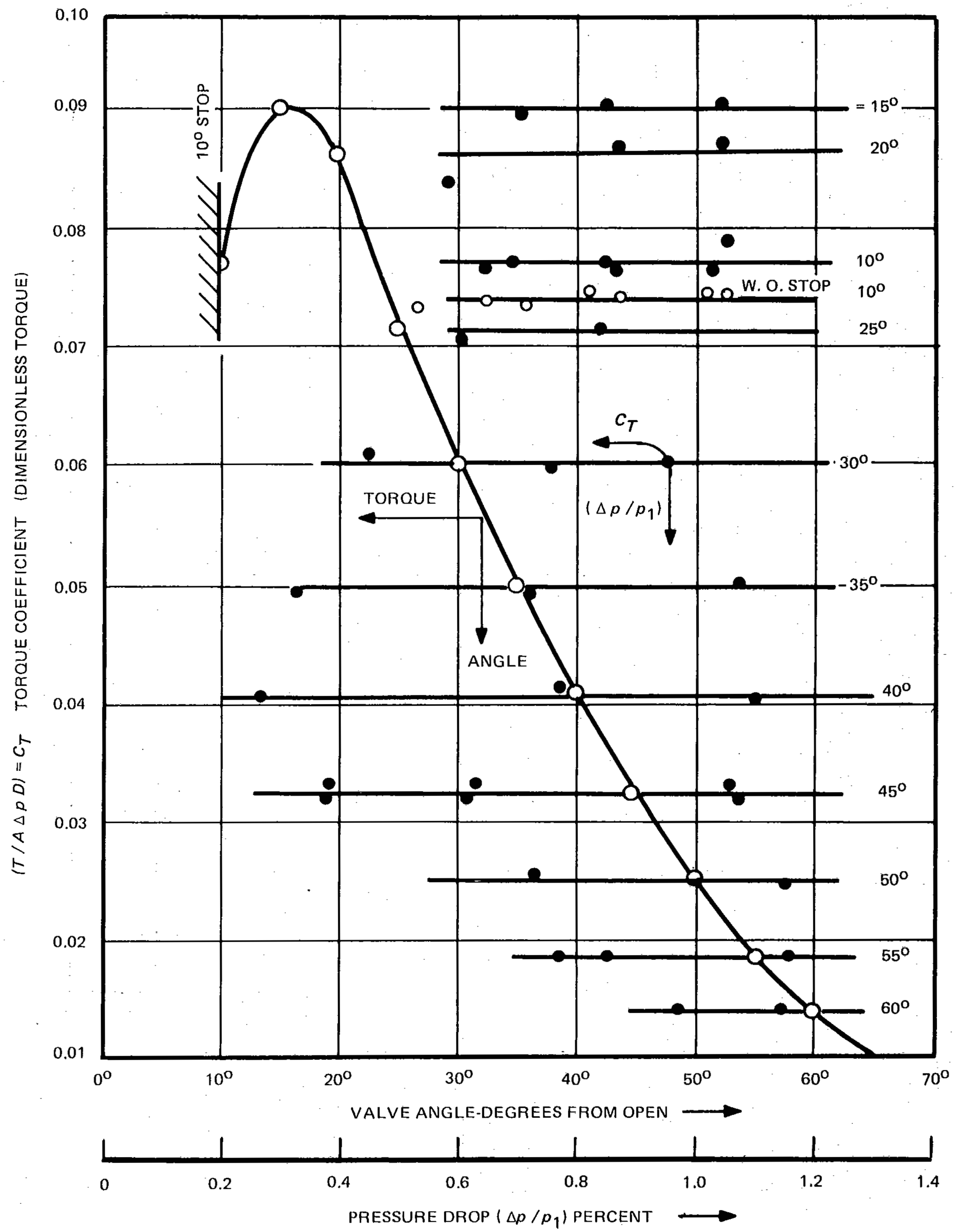

EX. 4-3 TORQUE OF BUTTERFLY VALVE FOR VARIOUS ANGLES AND PRESSURE DROPS

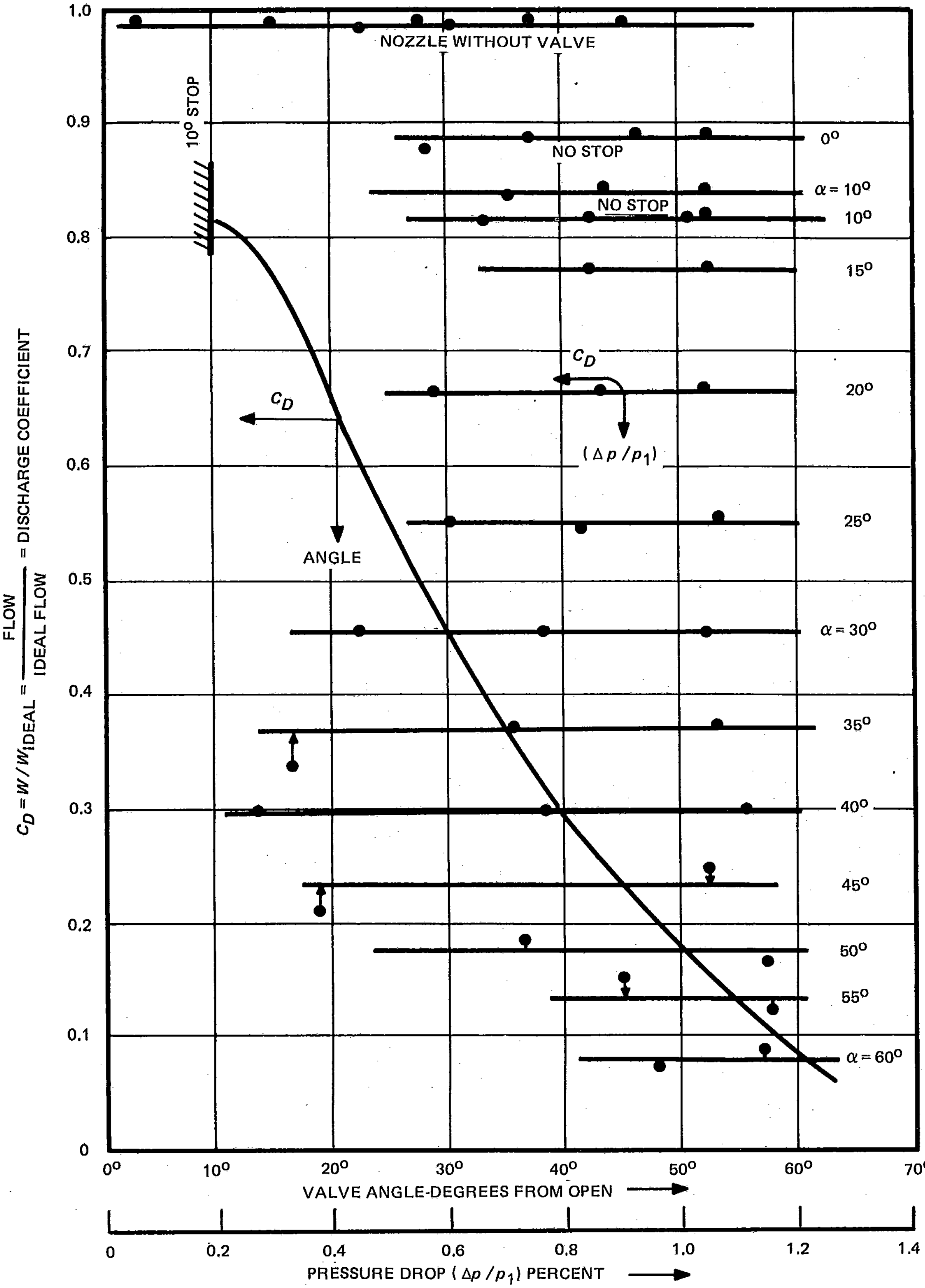

EX. 4-4 DISCHARGE COEFFICIENT FOR VARIOUS ANGLES AND PRESSURE DROPS

The nozzle and its balancing plate are hung from flexible shims attached to the air supply drum. A tare reading of the thrust is found by blocking off the nozzle and supplying the air at high pressure at (*O*). At 100 psi one can move the nozzle and its balancing plate with a light push of the finger.

The analysis, shown in Ex. 4-1, tests how much supply pressure is required to lift a given weight on the scale and move the nozzle off its stops. Tests of the nozzle alone and also with the valve installed give the incremental loss of the valve. No traversing is required, unless you want to know the details of the flow. The drag of a human hair can be measured by placing it across the end of the nozzle.

A similar system was used to measure the torque of the valve. A dead weight on a lever arm was arranged to hold the shaft against a stop. The air supply was increased until the valve was able to lift the weight. A light circuit was used to indicate when the weight was lifted.

Test Results

The loss coefficients of the tunnel alone and with the valve installed, for different angle settings and with and without the bar stop are shown in Ex. 4-2.

The tested torque coefficients are shown in Ex. 4-2 for various angle settings and pressure drops ($\Delta p/p_1$). A cross plot shows the variation of torque for one percent pressure drop.

The discharge coefficient is shown in Ex. 4-4. The flow was measured using the standard nozzle which is built into the thrust facility and measures only the flow which generates thrust and does not include the leakage around the nozzle and its pressure balancing plate.

REFERENCE

C. A. Meyer, R. D. Swope – Widener College Report TR 75-3, April 7, 1975.

EXAMPLE 5 – ELECTROSTATIC PRECIPITATOR, GAS FLOW DISTRIBUTION

This section describes some model and field gas flow studies of the inlet and outlet flues of an electrostatic precipitator installation. This precipitator was designed to produce 99.6 percent (.004 loss) dust collection efficiency. The actual measured collection efficiency was measured at 98.8 percent (.012 loss) to 99.1 percent (.009 loss). The reduced performance was attributed to poor gas flow as it passed through the precipitator.

Example 5-1 is a side elevation of the precipitator complex. Gas leaves two Ljungstrom air preheaters and is divided between the two precipitators of the double deck installation. During initial operation, flue gas flow traverse were conducted to determine the gross division of gas between the two precipitators. Detailed velocity traverses were also conducted in the vertical outlet flue leaving the upper precipitator and at the inlets to the I.D. fans. The gas volume flow passing through the lower precipitator was determined by subtracting the measured gas flow leaving the upper precipitator from the measured gas flow entering the induced draft fan inlets. These tests showed that approximately 54.6 percent of the gas was going through the lower precipitator. Based on this result, the perforated plate shown in Ex. 5-1 was installed to distribute more gas to the upper precipitator.

The velocity traverses conducted at the inlet to the I.D. fans also revealed a lateral imbalance of gas flow across the precipitators. Example 5-2 shows the north I.D. fan was receiving 9 percent more flow than the south but, more importantly, the inboard leg of each fan received more flow than the outboard legs.

Finally, dust samples were taken at the inlet to each I.D. fan to check for system performance and it was found that 88 percent of the total dust going up the stack, as measured at each fan inlet, occurred at Sample Port No. 1 as noted in Ex. 5-3.

Based on these results and supplemental visual off-line inspections, it was obvious that gas flow problems in this unit were a major contributing factor to its deteriorated performance. It was concluded that a three-dimensional air model study would have to be conducted to evaluate the various options available to remedy the situation. It was also decided that a complete field velocity traverse of the inlet to both the upper and lower precipitators should be conducted. This information would then be used to check the "as built" model results to ensure an accurate presentation of the problem.

The field tests were performed using cold air at approximately 60 percent of design velocity. This provided a Reynolds number approximately equal to that which would be seen under actual full load operation. Example 5-4 presents an example of a typical field velocity profile in the lower precipitator. Once these velocity profiles had been obtained across the width of the precipitators they were reduced to numerical form. These velocity data

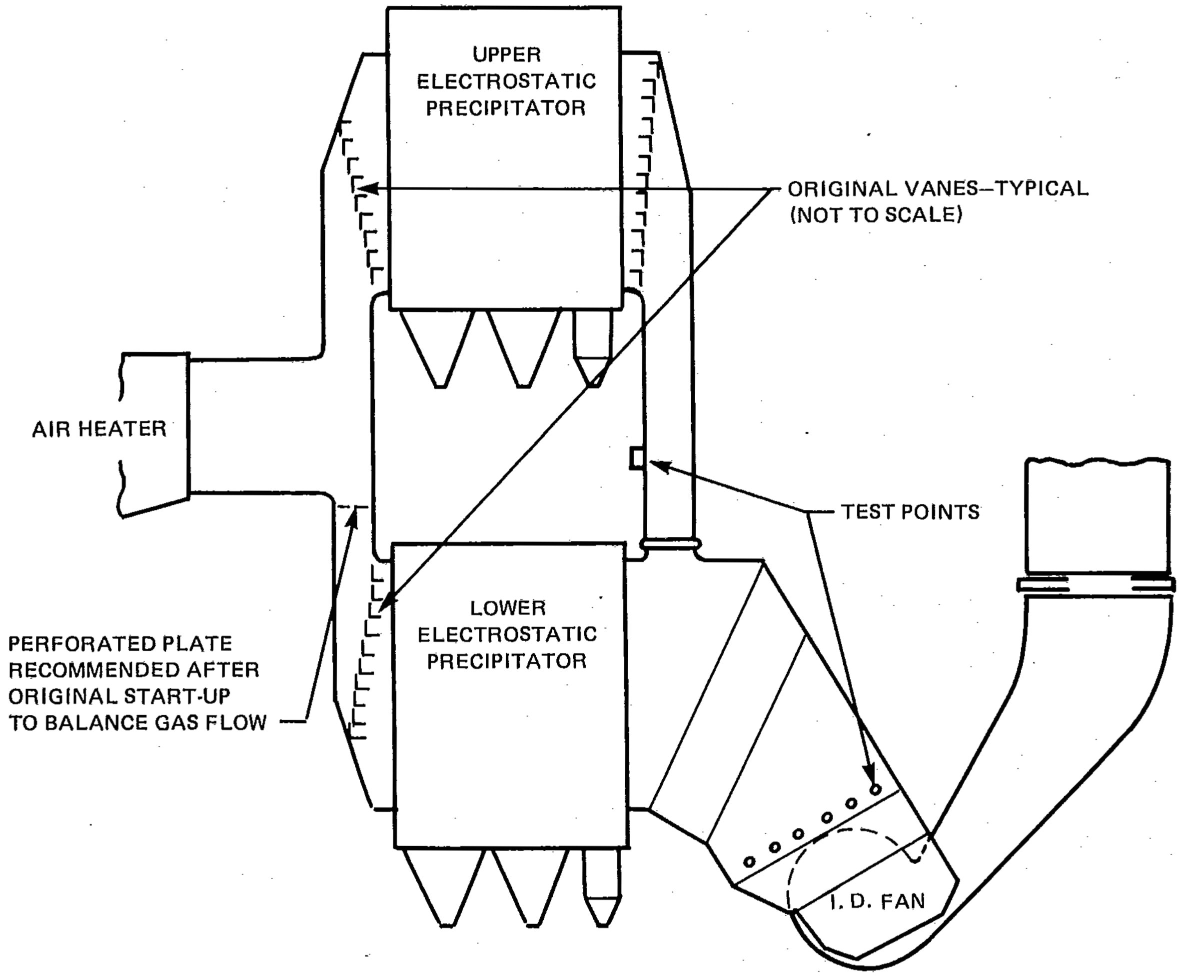

EX. 5-1 SIDE ELEVATION OF ELECTROSTATIC PRECIPITATOR

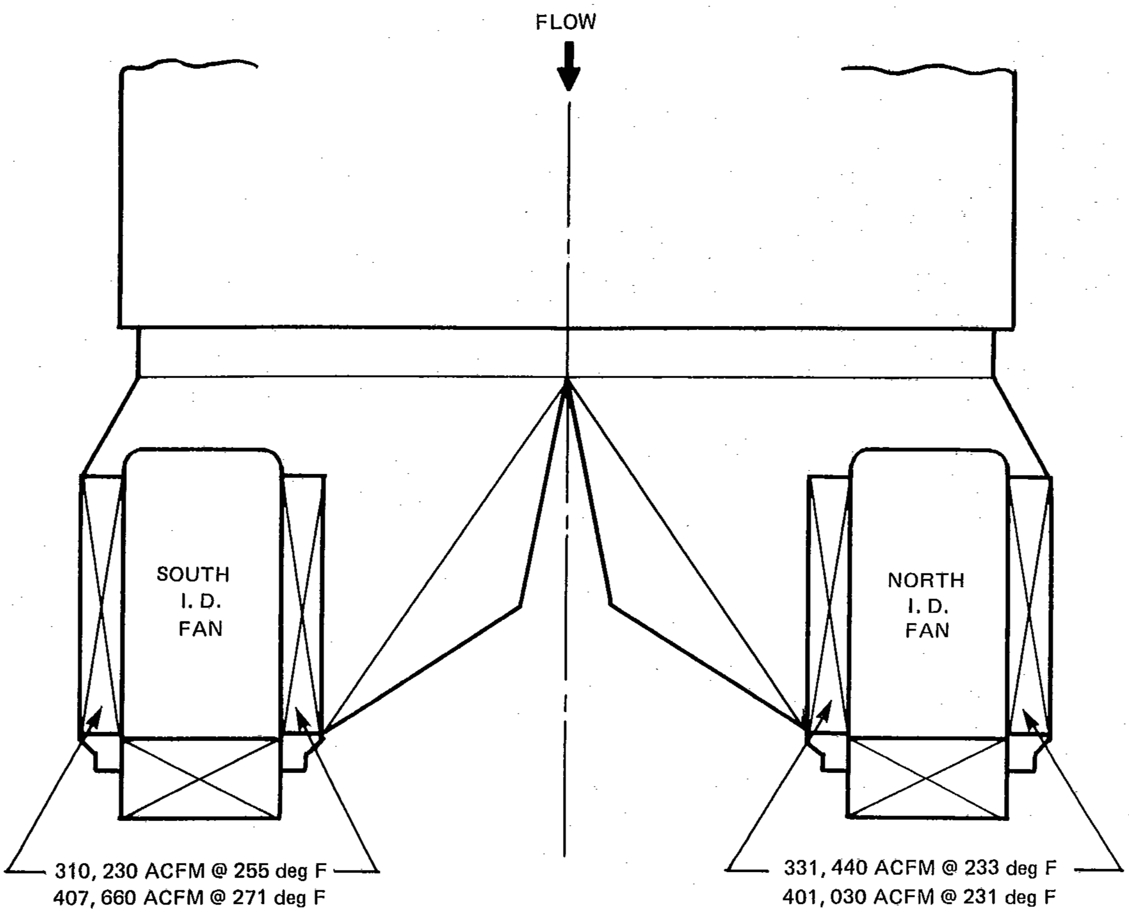

EX. 5-2 GAS FLOW IMBALANCE – OUTLET FLUES AND I.D. FANS

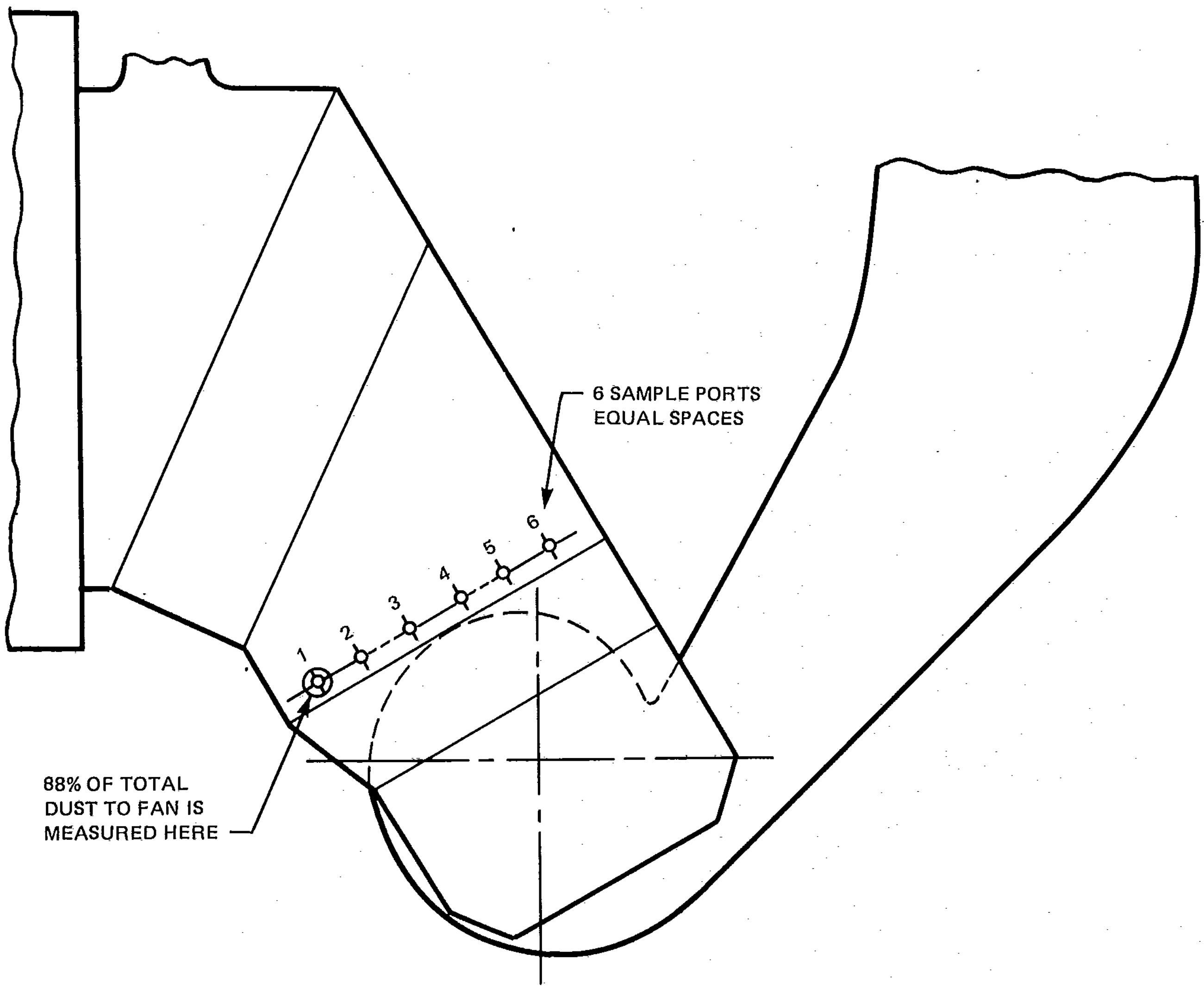

EX. 5-3 SIDE ELEVATION OF I.D. FANS

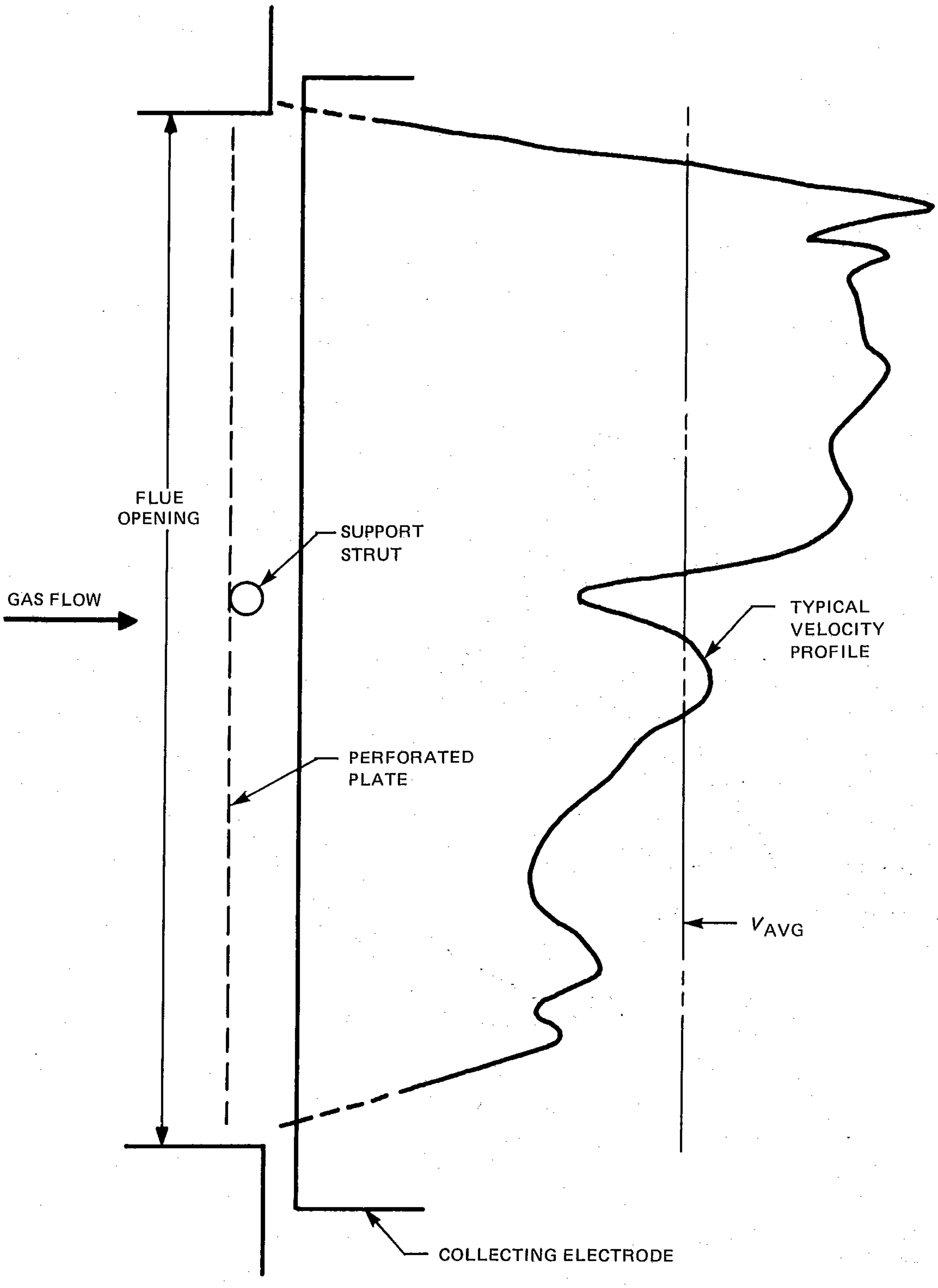

EX. 5-4 TYPICAL MEASURED VELOCITY PROFILE, AS INSTALLED LOWER PRECIPITATOR INLET

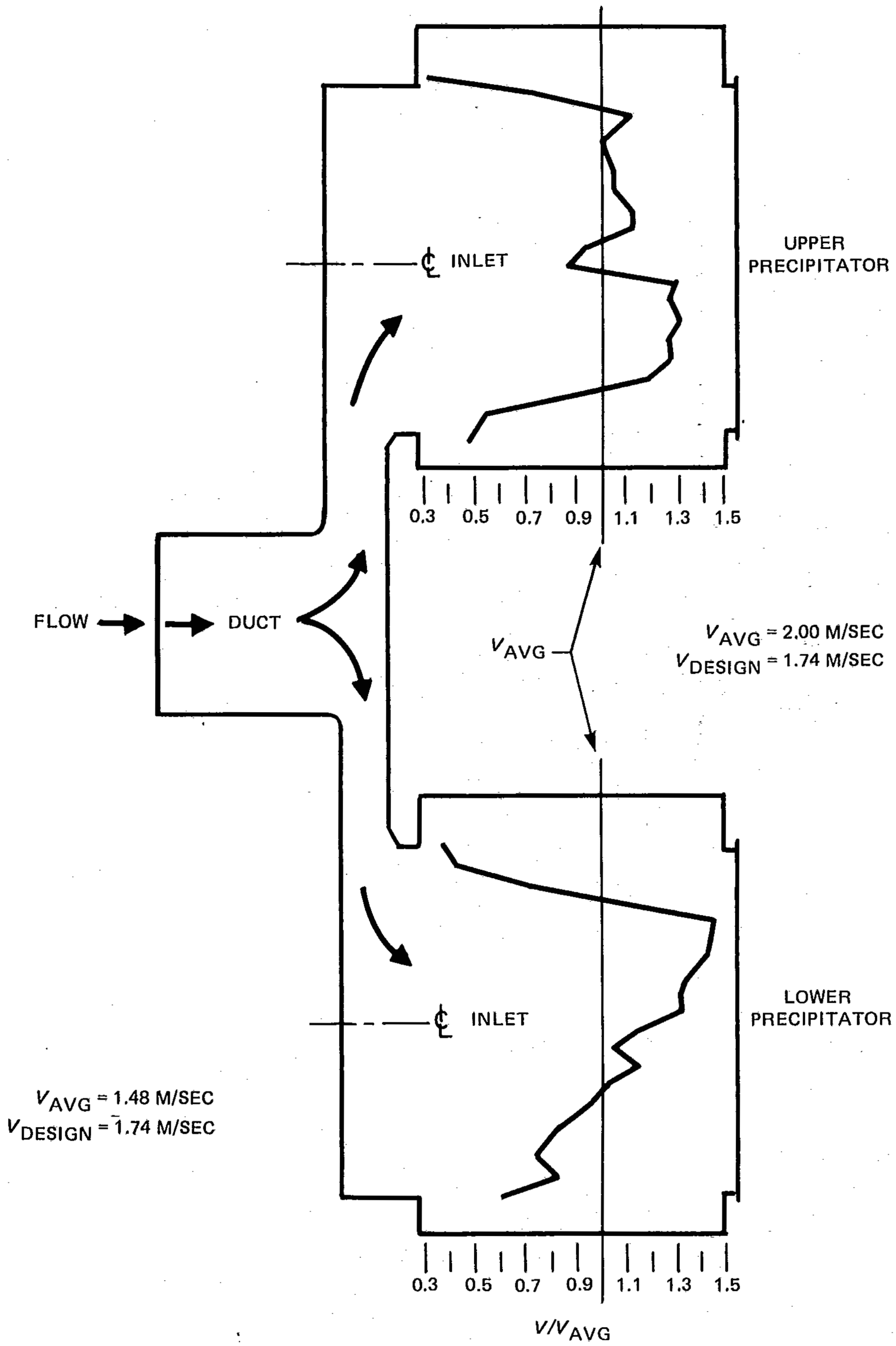

EX. 5-5 AVERAGE INLET VELOCITY SIDE ELEVATION PROFILES, AS INSTALLED

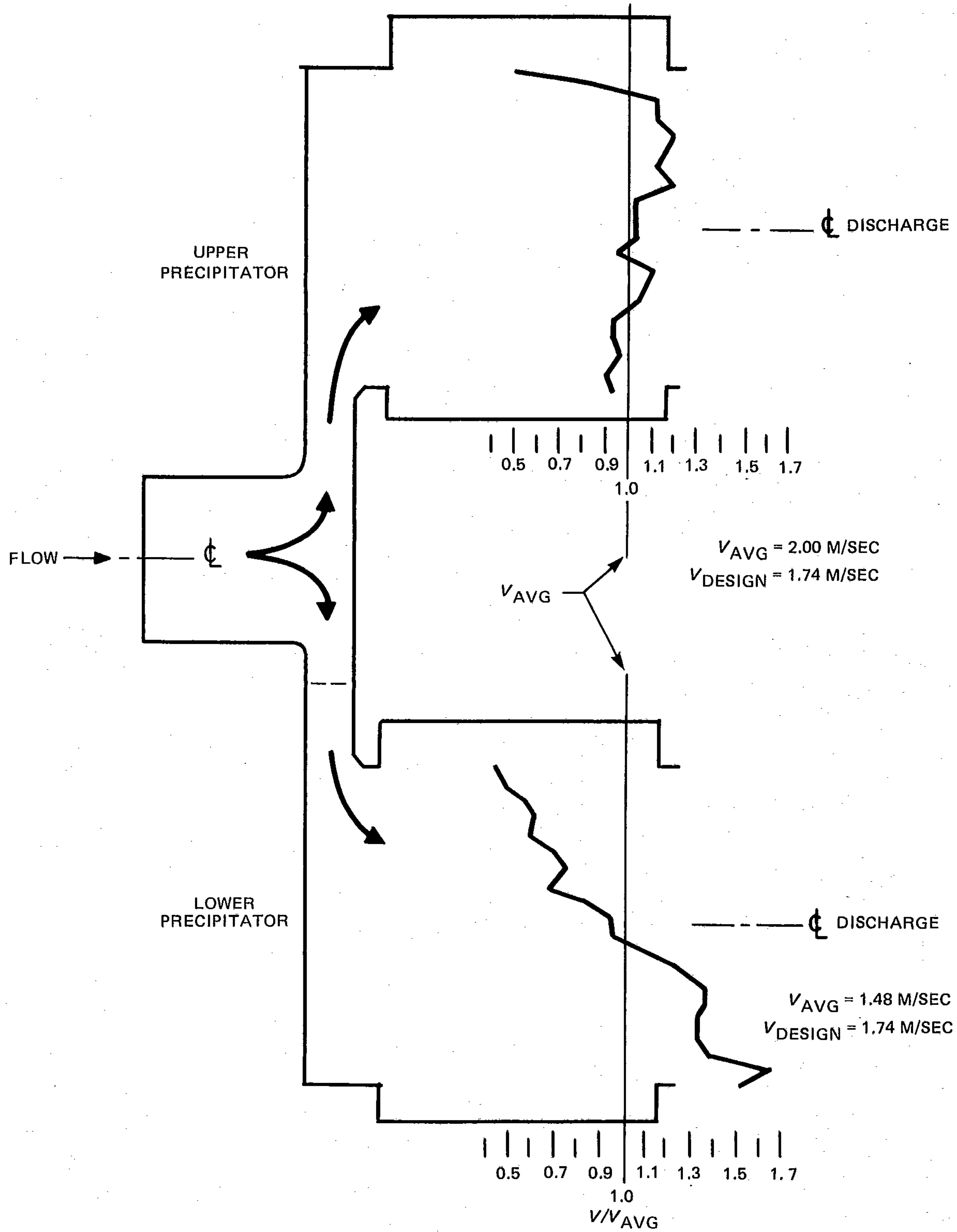

EX. 5-6 AVERAGE OUTLET VELOCITY SIDE ELEVATION PROFILES, AS INSTALLED

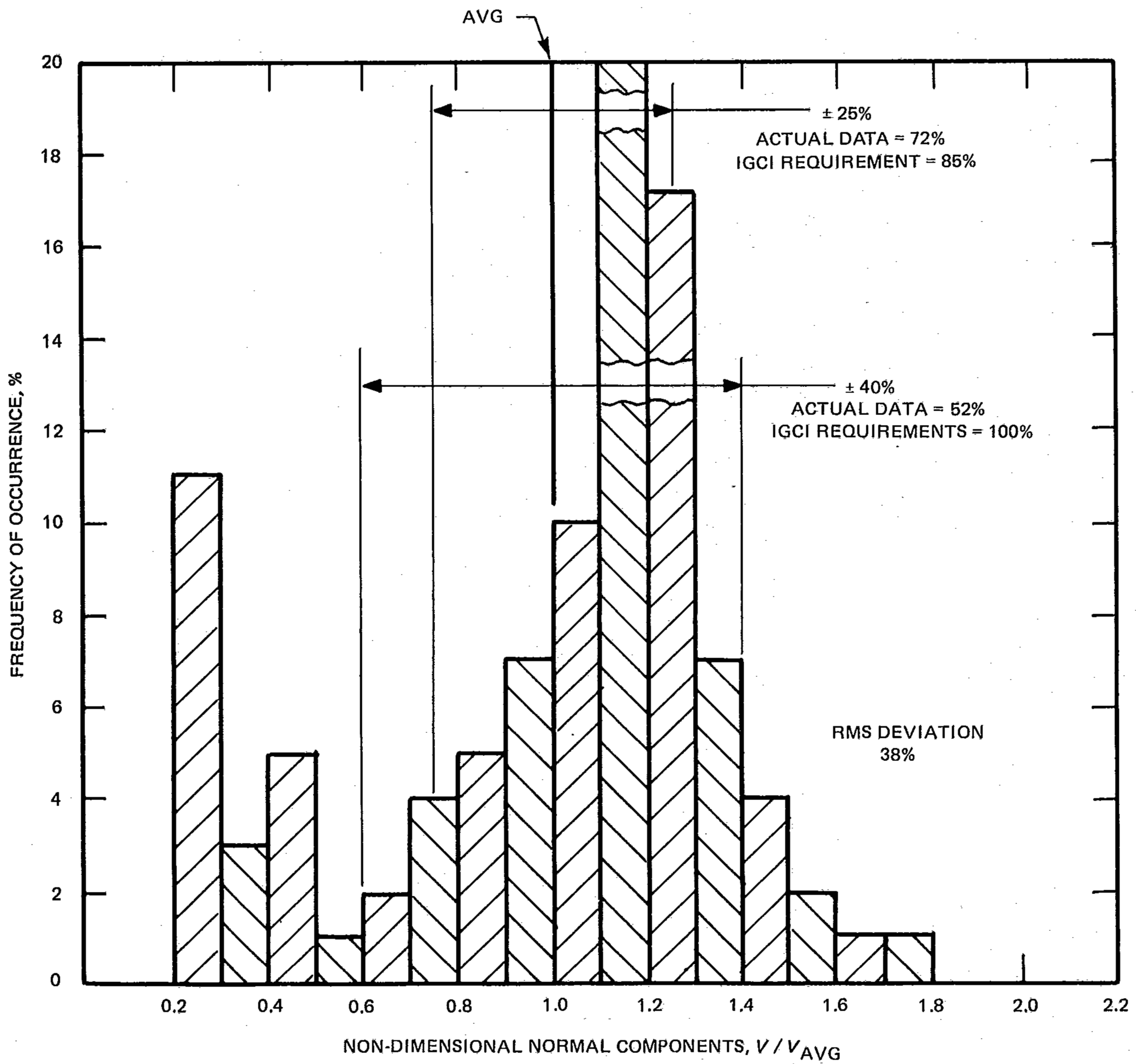

EX. 5-7 HISTOGRAM ANALYSIS OF UPPER PRECIPITATOR INLET VELOCITY MEASUREMENTS

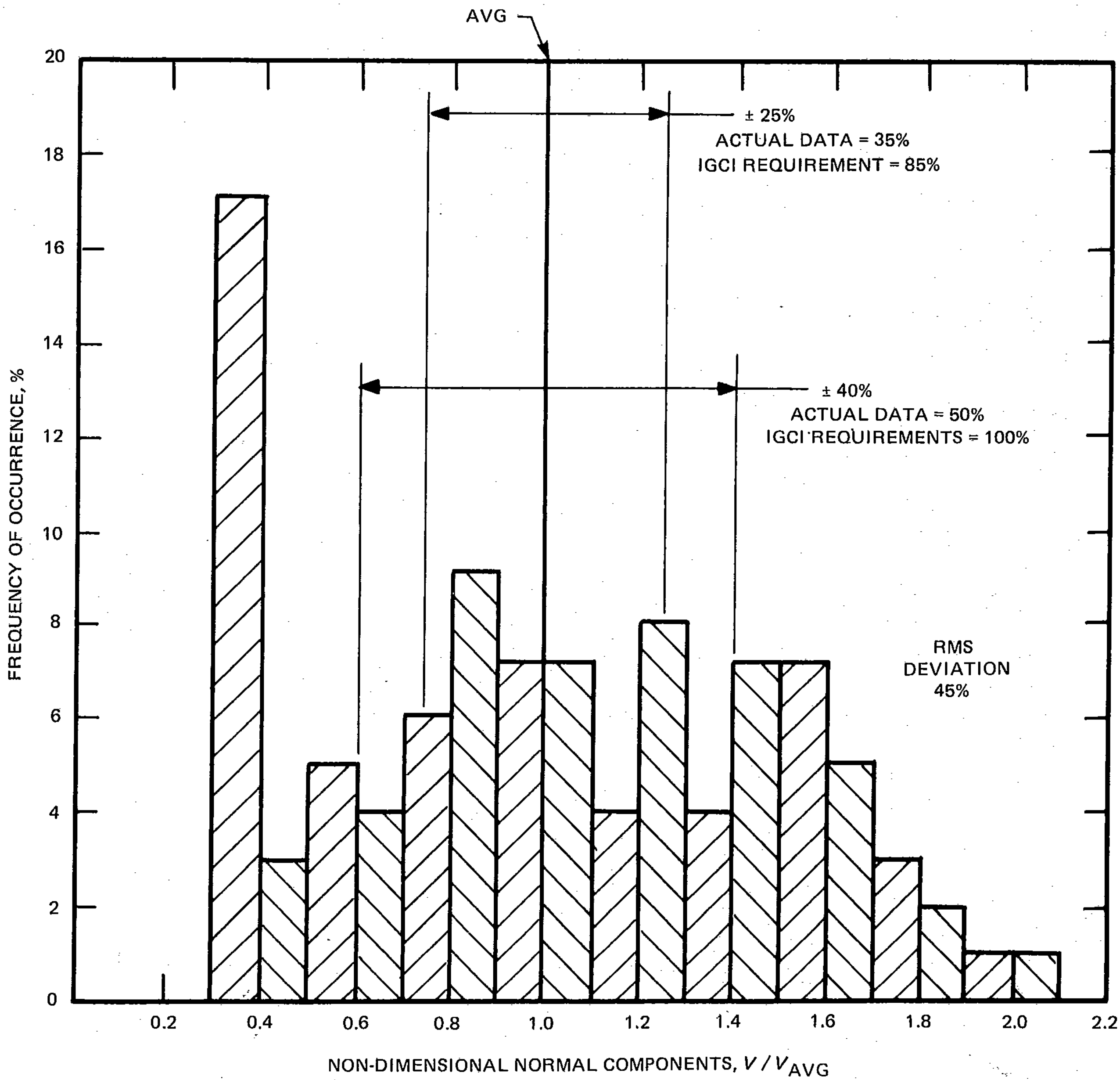

EX. 5-8 HISTOGRAM ANALYSIS OF LOWER PRECIPITATOR INLET VELOCITY MEASUREMENTS

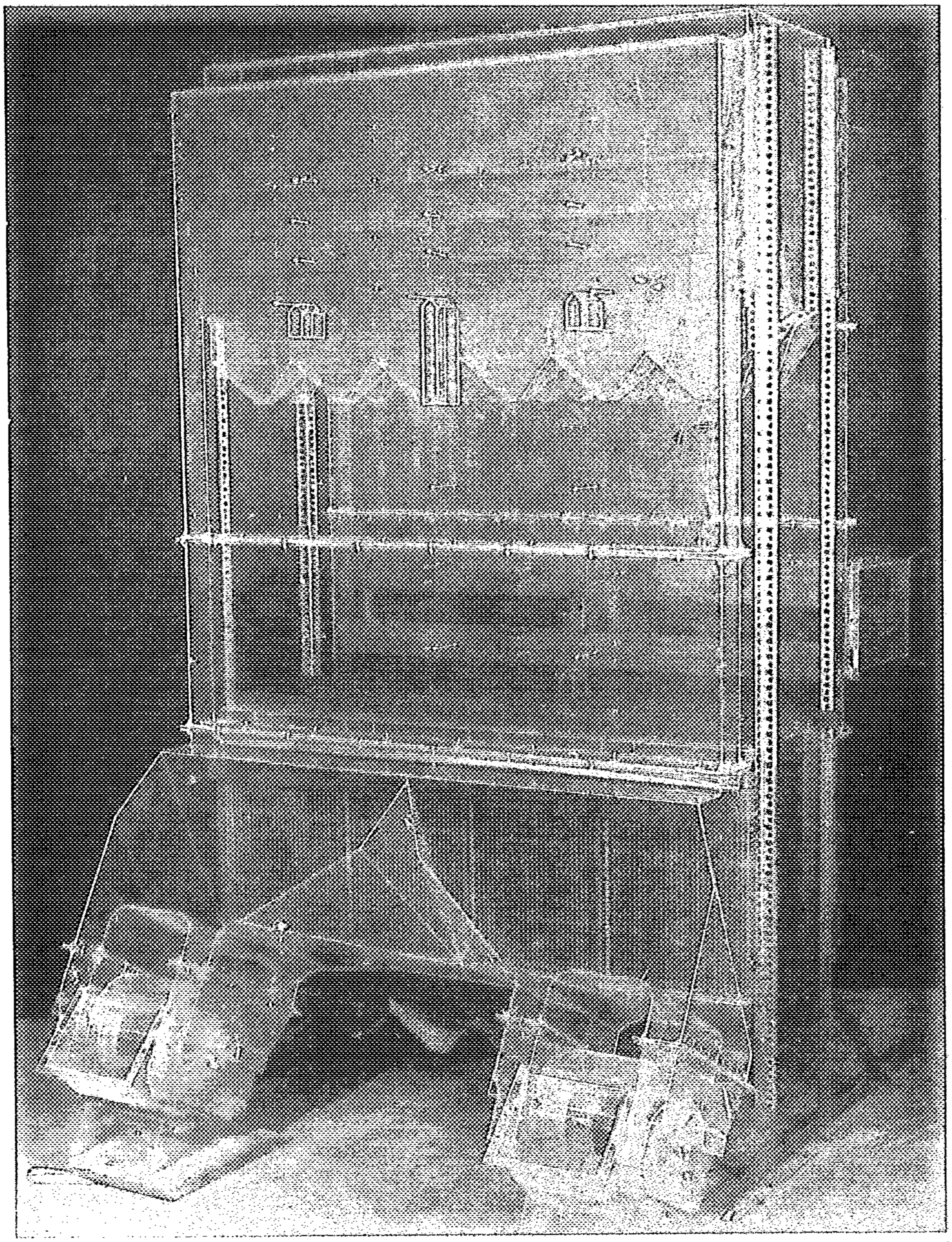

EX. 5-9 MODEL STUDY OF THE PRECIPITATOR INSTALLATION

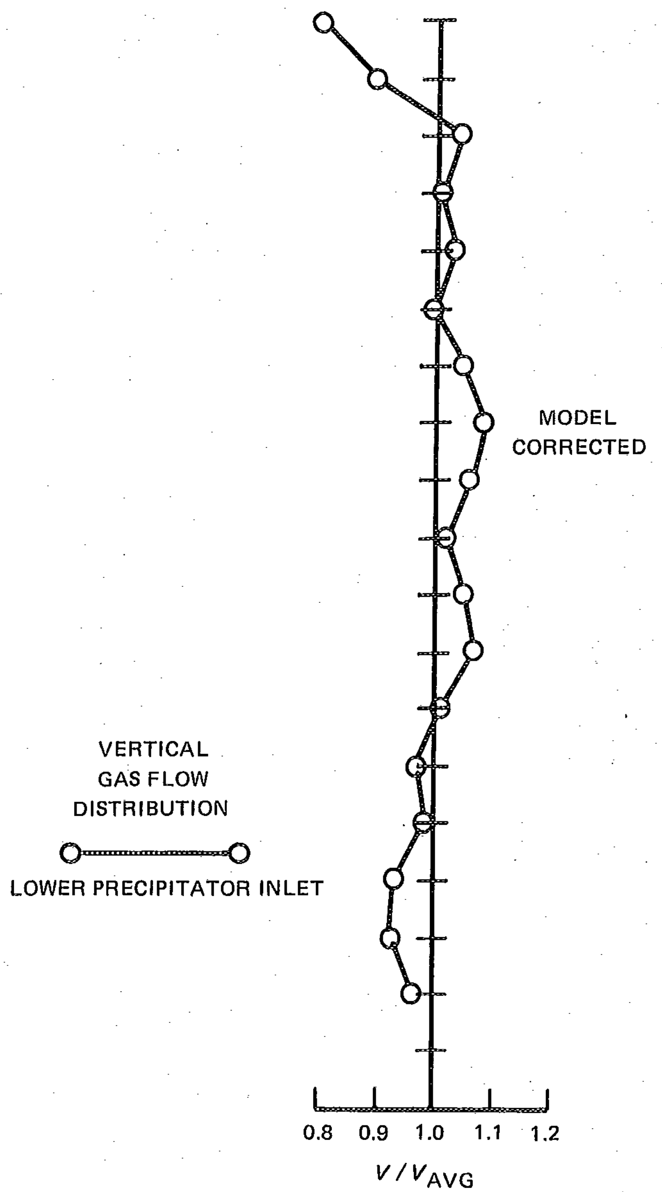

EX. 5-10 VERTICAL GAS FLOW DISTRIBUTION LOWER PRECIPITATOR INLET

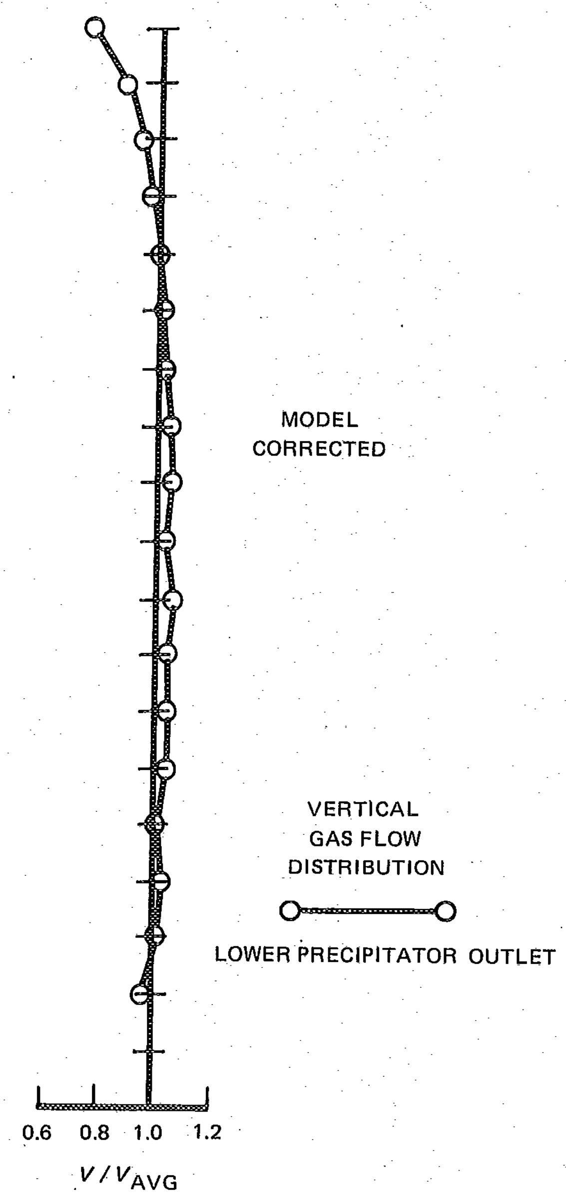

EX. 5-11 VERTICAL GAS FLOW DISTRIBUTION LOWER PRECIPITATOR OUTLET

points were then numerically averaged to establish an average vertical and horizontal velocity profile for each precipitator. Example 5-5 illustrates a simplified side elevation view of the upper and lower precipitators showing the average vertical inlet velocity profile for each as obtained from the field tests. Approximately 58 percent of the gas was found to be passing through the upper precipitator with the remainder passing through the lower. Example 5-6 demonstrates the dramatic effect that the outlet flue has on the velocity profile leaving the lower precipitator. This pointed out a condition that had to be corrected if re-entrainment and hopper sweepage in the lower precipitator were to be eliminated.

Examples 5-7 and 5-8 detail the statistical distribution of the data points taken in the upper and lower precipitators and also compare these results with the recommended criteria of the IGCI (Industrial Gas Cleaning Institute). The vertical bars of these histograms represent the percentage of the data points occurring at each velocity range. The actual velocity values have been normalized, that is, they have been divided by the average velocity following standard practice.

As can be seen, neither precipitator met the IGCI requirements with the upper precipitator being approximately two times better than the lower precipitator. It was then decided to proceed with the construction of a 1/16 scale model study to produce the necessary corrective devices and optimize the flow fields of the two precipitators. The model was made and is shown in Ex. 5-9. The internals of this model reproduced the details of Ex. 5-1. Velocity traverses in the model effectively matched the data of Ex. 5-5 through 5-8 within normal experimental accuracy. These results confirmed that the model could reproduce the problems and then be used to arrive at design solutions.

It was decided that "ladder vanes" would be used to replace the inlet radius vanes. Ladder vanes are a series of flat surfaces that are oriented perpendicular to the direction of the duct inlet gas flow. The positioning of the inlet flue ladder vanes was optimized in the model study.

The model study also indicated that the floor of the lower precipitator inlet flue would be subject to potential fly ash dropout. It was, therefore, recommended that a dust blower be installed in this area to keep the flue clean.

A major problem that still remained was the correction of the lower precipitator outlet gas flow distribution. The lower precipitator outlet of the model was still experiencing both vertical and lateral gas flow problems. It was concluded that this was the result of the close coupling of the lower precipitator to the I.D. fans.

A pressure drop device was placed at the lower precipitator outlet to provide for a decoupling between the I.D. fans and the precipitator. Standard structural shaped channels were installed in vertical orientation which formed continuous vertical slots that would not plug from the residual fly ash leaving the precipitator. This satisfactorily decoupled the I.D. fans from the precipitator. The vertical slots were lined up with the centerline of the precipitator ducts. The net free area required was found to be 15 percent open.

The net result of the above changes, i.e., the installation of the inlet ladder vanes and the installation of a 15 percent open "picket" fence at the lower precipitator outlet produced a flow distribution slightly biased to the lower precipitator. The resultant corrected flow patterns for the lower precipitator was shown in Ex. 5-10 for the inlet and Ex. 5-11 for the outlet. The gross improvement is noted when these figures are compared to Ex. 5-5 and 5-6.

Further analysis of the corrected model study data produced the following results:

Lower Precipitator
Inlet: 10.6% RMS Deviation
Outlet: 12.0% RMS Deviation

Upper Precipitator
Inlet: 11.1% RMS Deviation
Outlet: 9.2% RMS Deviation

Because of these favorable results, the full sized flues were modified in accordance with the model recommendations. Once the modifications were completed a walk-through inspection was performed with the fans running. No high velocity jets or hopper sweepage could be found. Due to system load requirements and the confidence levels established with the model study results, field follow-up velocity traverses were not performed.

The unit was permitted to operate for at least one month before performance testing. Three tests were then run. All three tests produced equal to or better than required dust collection efficiencies. The customer agreed to accept the installation as having made its contractual guarantee.

It is recommended that gas flow distribution be studied before an installation is built. The cost of a model study, during the design stages of a system, is significantly less expensive than finding and correcting the problems in the field. It has been experienced that correcting an existing installation can cause roughly ten to fifteen times the cost of performing a design stage model study. It has been shown, through the study reported here, that model studies and full-size installations produce results which correlate well within the range of experimental error. The important factors in producing a reliable model study are complete and accurate reproduction of system geometry being studied, and the proper modeling of the system flow fields and pressure gradients entering and leaving the model. Most of the time, this last requirement is easily satisfied by including major system components (heat exchangers, fans, etc.) ahead of and following the model.

ABSTRACTED FROM

C. L. Burton and D. A. Smith "Precipitator Gas flow Distribution," page 191, EPA-650/2-75-016 "Symposium on Electrostatic Precipitators for the Control of Fine Particulates" and C-E TIS-4257.

EXAMPLE 6 – FLOW IN FURNACES AND DUCTS, SMOKE AND WATER TABLE TESTS

The substantial increase in physical size of commercial furnaces and auxiliary equipment, together with increasing emphasis on high availability and minimum cost of operation, puts a distinct premium on effective equipment design. Simple extrapolation of previous designs often is not enough, since tolerable flow maldistributions of earlier designs may become intolerable from the standpoint of heat transfer, pressure loss, corrosion, wear, material selection, or overall performance. Properly applied cold flow models are a useful tool for identifying all the major pitfalls and many of the minor pitfalls which should be avoided in duct and furnace gas flow design. One of the principal areas of interest has been the simulation or representation of the flow of the products of combustion in boiler furnaces and gas passages so that the engineer can select and locate heat transfer surfaces in the most effective manner. In general, the most effective use of heat transfer surface is accomplished within uniform flow distribution of the heat transfer fluids.

It has been found that there is no single best modeling technique to use as a guide for obtaining uniform flow distribution in the gas passages of a boiler. Rather, it has been found that utilization of a variety of modeling and test techniques often leads to the quickest and most accurate solution of gas flow distribution problems. Two-dimensional smoke table models, two-dimensional water table models, three-dimensional water models, and three-dimensional air models can be adapted to virtually any significant flow distribution problem in furnaces or ductwork, despite the isothermal nature of each of these modeling techniques. None of the methods result in so-called true models, but we can call them adequate models for lack of a better term.

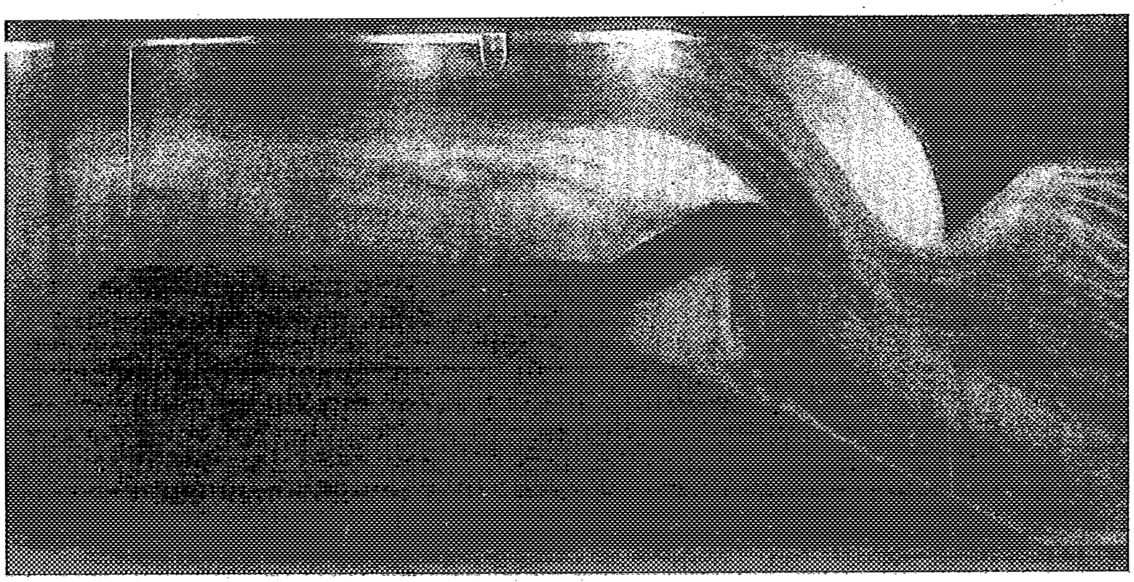

EX. 6-1 SMOKE TABLE–ECONOMIZER TO AIR HEATER – AS DESIGNED

All that is necessary for successful utilization of each of the methods is recognition of the similarity criteria which need to be maintained for each method.

One additional factor, which has been found to be of importance in flow model work, is visual impact. Several earlier authors have stressed this point. It is agreed that visual observation and photographic records are vital to the success in using the flow modeling technique. Smoke table modeling provides a quick method of making a visual assessment of the aerodynamic characteristics of fluid flow systems. This technique, shown in Ex. 6-1, lends itself to rapid screening of a series of proposed design features. The models are simple, inexpensive, easily set up, and readily modified. Modeling is limited to two-dimensional flow studies. This technique provides pertinent information as to areas in which further study, using more refined models, should be carried out. In many cases, smoke table tests, in themselves, are sufficient to provide a suitable answer as to the effectiveness of a design. Qualitative data is obtained from smoke models. Records of model flow characteristics may be made by tracing the flow streamlines on the glass top of the table, making freehand sketches of flow patterns, and by taking still photographs or movies of the operating model. Relative values may be arrived at by scaling the size of the indicated eddies, stagnant areas, or the portion of a flow channel that is being effectively used.

Exact geometrical similarity with the prototype is used in the smoke table slice models. In some instances, a component upstream or downstream of the model is not scale modeled. An example of this would be a regenerative type air heater in which the draft loss is ten or more times greater than the loss of the ductwork ahead of it. The air heater in this case tends to improve flow distribution due to the flow resistance. When modeling the ductwork, a screen or perforated plate is used to simulate the air heater resistance in the system, and approximates the effect of the complicated air heater section.

The basic smoke table apparatus consists of a support arrangement for two parallel sheets of glass plate, a smoke generator, and a fan used to induce the air flow through the model. The model is mounted between the parallel sheets of glass. Smoke is introduced through a series of jets at the model inlet, and a flow of air induced by these jets. When the inlet velocity of the induced air and the smoke are equal, streamers of smoke are carried through the model tracing out the flow pattern. Flow velocities in the model areas under study are maintained in the laminar flow range. Reynolds number range is approximately 1000. The use of laminar flow in this type of model produces conservative results. Turbulent flow separation noted in three-dimensional air models has correlated directly with the laminar flow separation observed in the smoke table. Besides producing conservative observations, the laminar flow enhances visualization. If the flow velocities are increased to the turbulent range, the smoke streamers dissipate in the air making interpretation of results more difficult.

These models are quite effective for demonstration purposes. Areas where flow separation from the boundaries occur may be readily seen. Stagnant areas and eddies are apparent to the observer. Flow disturbances may be traced

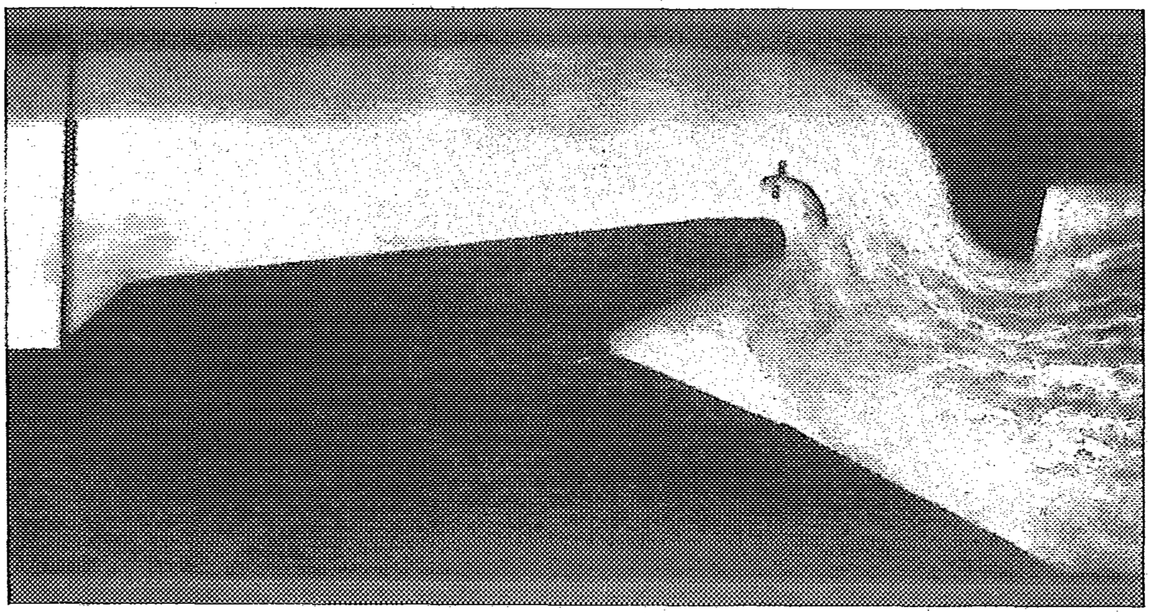

EX. 6-2 SMOKE TABLE–ECONOMIZER TO AIR HEATER – AS MODIFIED IN MODEL

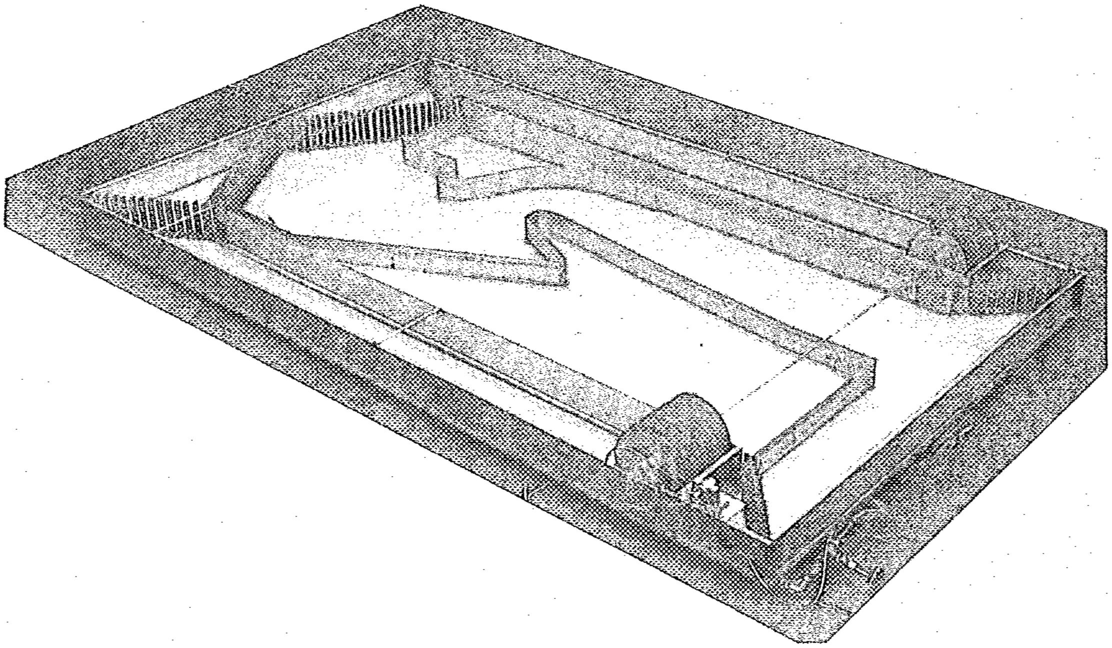

EX. 6-3 WATER TABLE – TWO-DIMENSIONAL MODEL

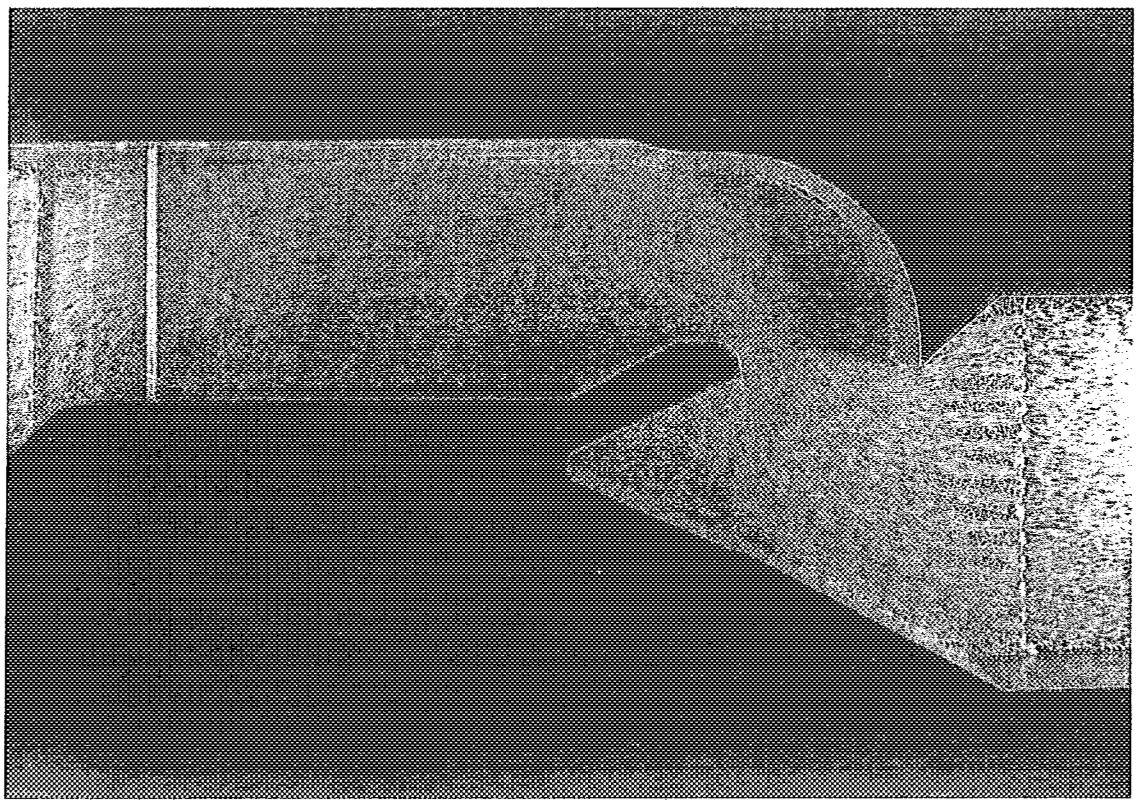

EX. 6-4 WATER TABLE – REPEAT OF EX. 6-1

to their source and their magnitude assessed. The investigator can readily illustrate the flow streamlines, trace effects of flow separation, and point out good and bad design features. The fluid motion can be clearly seen, and judged without resorting to vectors, contours, or other conventional graphical methods of presenting flow information. A series of models can be demonstrated quickly to show a sequence in development of an acceptable design. A typical before and after sequence is shown in Ex. 6-1 and 6-2, which illustrates the boundary flow separation which can occur and the correction that can be made in the flue gas ductwork between the economizer and the air heater of a large boiler. Movies and still pictures of smoke models have been quite effective in demonstrating the characteristics of a system to engineering design personnel who do not have the opportunity to view the models at first hand.

The same study of Ex. 6-1 and 6-2 was repeated in a two-dimensional water table to illustrate the effectiveness of this technique. The water table shown in Ex. 6-3 is a portable device and can be transported to various facilities to provide flow solutions to local problems. Example 6-4 is a report of the flue geometry of Ex. 6-1. It is obvious from Ex. 6-4 that the photographic record of the water table is superior to the smoke table. However, subsurface details are not readily discernible in the water table. Again, it takes engineering judgment to select the best technique for a particular problem.

ABSTRACTED FROM

R. C. Patterson, R. F. Abrahamsen, "Flow Modeling of Furnaces and Ducts," ASME, *Journal of Engineering for Power*, October 1962, page 345.

EXAMPLE 7 – COOLING TOWER, FLOW RECIRCULATION

The Problem

Cooling tower recirculation is defined as the proportion of the air entering the tower that originated from the warm, saturated exhaust air leaving it. This raises the inlet air wet bulb temperature above ambient and reduces the overall tower performance that might otherwise be expected. In power plant operation, the resultant high cold water temperature means higher condenser temperatures and increased turbine back pressure. The net effect is a loss in plant generating output and efficiency. An adequate recirculation allowance must be included in the selection of the cooling tower design inlet wet bulb if power plant performance is to be assured under adverse atmospheric conditions.

What Was Done

A cooling tower model was constructed of 3/16 inch mahogany to a scale of 1 inch equals 10 feet or 1:120. The overall length for the maximum 16 cell model configuration was 57.6 inches which corresponds to an actual tower length of 576 feet. Each model cell represents a cooling tower cell 36 feet long. The model and associated equipment were built so that a tower configuration representing 4, 8, 12 or 16 cells could be tested. This corresponds to a range of tower lengths from 144 to 576 feet.

Fundamental aerodynamic theory and related experimental observations were used to identify the major factors influencing recirculation. Because of the complexity of the recirculation phenomenon, the quantitative significance of these factors were evaluated by model studies where variables such as wind speed, direction, ambient and operating temperatures and tower configuration could be easily controlled and measured.

Discussions

In model testing, it is necessary to maintain geometric, kinematic and where applicable, dynamic similitude. Geometric similitude was satisfied by keeping linear dimensions proportional to those of an actual tower. To satisfy kinematic similitude, velocity components for tower exhaust air, incoming air, and atmospheric wind were proportioned to actual operating conditions.

Two non-dimensional terms must be considered in satisfying dynamic similitude in model tests of this kind. They are the Reynolds number and a densimetric Froude number. The Reynolds number is the ratio of the inertia forces to the viscous forces acting on the fluid. For streamlined bodies, the flow field and pressure distributions are established by geometry and boundary layer effects which are directly related to viscous and dynamic forces. For streamline flow dynamic similitude will be identical for model and prototype only if the Reynolds numbers are identical. However, in flow over blunt bodies, pressure distribution and flow patterns occur as a result of flow separation induced by discontinuities in geometry which are essentially independent of viscous forces. Previous studies concur that identical Reynolds numbers are not necessary to assure dynamic similitude for blunt structure flow as long as the Reynolds number is above 11,000. The minimum Reynolds number was 13,200 for the wind speed and model size tested. It was thus concluded that geometric shape alone controlled the air flow pattern and the pressure profiles and that the flow fields of the model did represent those of a full size tower.

A densimetric Froude number $N_{Fr'}$, is pertinent when it is desired to model the behavior of a hot exhaust plume entering a colder air stream. It is defined as:

$$N_{Fr'} = \frac{V^2}{Lg} \times \left(\frac{T_1}{T_1 - T}\right) \tag{1}$$

or

$$N_{Fr'} = N_{Fr}{}^* \times \left(\frac{T_1}{T_1 - T}\right) \tag{2}$$

Where:

$N_{Fr'}$ = densimetric Froude number, or ratio of inertial force to buoyancy force

N_{Fr} = Froude number, or ratio of inertial force to gravity force

V = velocity through the stack

L = configuration reference length (diameter of the stack in this case)

The ratio $\frac{T_1}{T_1 - T}$ is used as an approximation of the density ratio, $\frac{\rho_1 - \rho}{\rho_1}$

The magnitude of the densimetric Froude number must be considered because of the influence of buoyant forces on the near field flow behavior of the warm exhaust air from the cooling tower. The greater the density (temperature) difference between the plume and the outside air, the more influence the buoyant force has on the plume path, and the lower the $N_{Fr'}$ number. Conversely, $N_{Fr'}$ scaling becomes unimportant at very large values. The "critical" $N_{Fr'}$ number has been determined to be approximately 0.8.

*This is the square of the Froude number used in Example 2.

For a cooling tower, however, the $N_{Fr'}$ is on the order of 25, and the model is about 3100, both far in excess of the critical value. This implies that the plume momentum forces far outweigh the buoyant and gravitational forces in determining the plume path near the model. Thus, $N_{Fr'}$ scaling or modeling of the buoyant forces, is not necessary in the present model test to assure accurate near-field plume simulation.

Hence, for the model size, velocities, and operating temperatures chosen, it is only necessary to satisfy geometric and kinematic similitude to simulate full size pressure profiles, flow fields and plume behavior.

Conclusions

Recirculation occurs primarily because of the atmospheric winds blowing over and around a cooling tower. These winds influence the exhaust plume behavior and cause low pressure zones on the leeward side of the tower. These phenomena cause a portion of the exhaust air to be recirculated back into the tower, thus raising the inlet air wet bulb above ambient. The major factors influencing the magnitude of recirculation are:

(1) Tower orientation relative to the wind.
(2) Wind speed.
(3) Tower length.
(4) Exhaust plume behavior and temperature.

The results of the model tests conducted to simulate actual tower behavior indicate, in general:

(1) For wind, parallel to the tower axis, recirculation is at a minimum, averaging 1½ percent. It is fairly constant for all lengths and wind velocities.

For all other wind directions:

(2) As tower length increases, recirculation increases.
(3) As wind velocity increases, recirculation increases.
(4) As wind direction approaches 90 deg to the tower axis, recirculation increases. However, recirculation tends to diminish for orientations of 67½ deg and 90 deg when winds exceed 8 mph.

The model test is believed to accurately simulate actual tower behavior since the model plume behavior is consistent with actual observed cooling tower plume behavior and magnitudes of recirculation determined by the model test correlate generally with field test experience.

EXAMPLE 8 – LARGE COMPRESSOR FOR THE TULLAHOMA WINDTUNNEL

Definition of the Problem

The problem was one of predicting the performance of a huge 216,000 horsepower, 30 foot diameter, 600 rpm axial flow compressor to be used in the transonic leg of the windtunnel at the Arnold Engineering Development Center (AEDC) at Tullahoma, Tennessee.

This three stage compressor (Ex. 8-1) was an addition to four other compressors used in series-parallel combination in the main leg of the windtunnel.

What Was Done

Model testing was the means available to obtain the required performance data prior to design and manufacturing of the compressor. Two models were tested. The first, was a 1/18 size low speed (2500 rpm), 100 horsepower model, Ex. 8-2. For similarity of Mach number (tip speed), a 1/18 size model should be tested at 18 x 600 = 10,800 rpm instead of 2500 rpm as limited by the mechanical design of the model. Due to the low speed, the pressure developed by the compressor was, of course, low and the proper incidence to the latter blade rows was obtained by adjusting (distorting) the rotor and stator blade heights and angle settings. The test results for different rotor blade angles are shown on Ex. 8-3.

The second (more expensive) model was a 1/16 size high speed (9600 rpm) model tested at full scale Mach number (Ex. 8-4).

Limitation of the Method

The low speed distorted model, of course, would be expected to give a lower pressure rise and lower efficiency due to the lower Mach and Reynolds numbers of the test. The high speed 1/16 size undistorted model matched the full size Mach number but had 1/16th the full size Reynolds number. It therefore would be expected to give a poorer performance than the full size compressor.

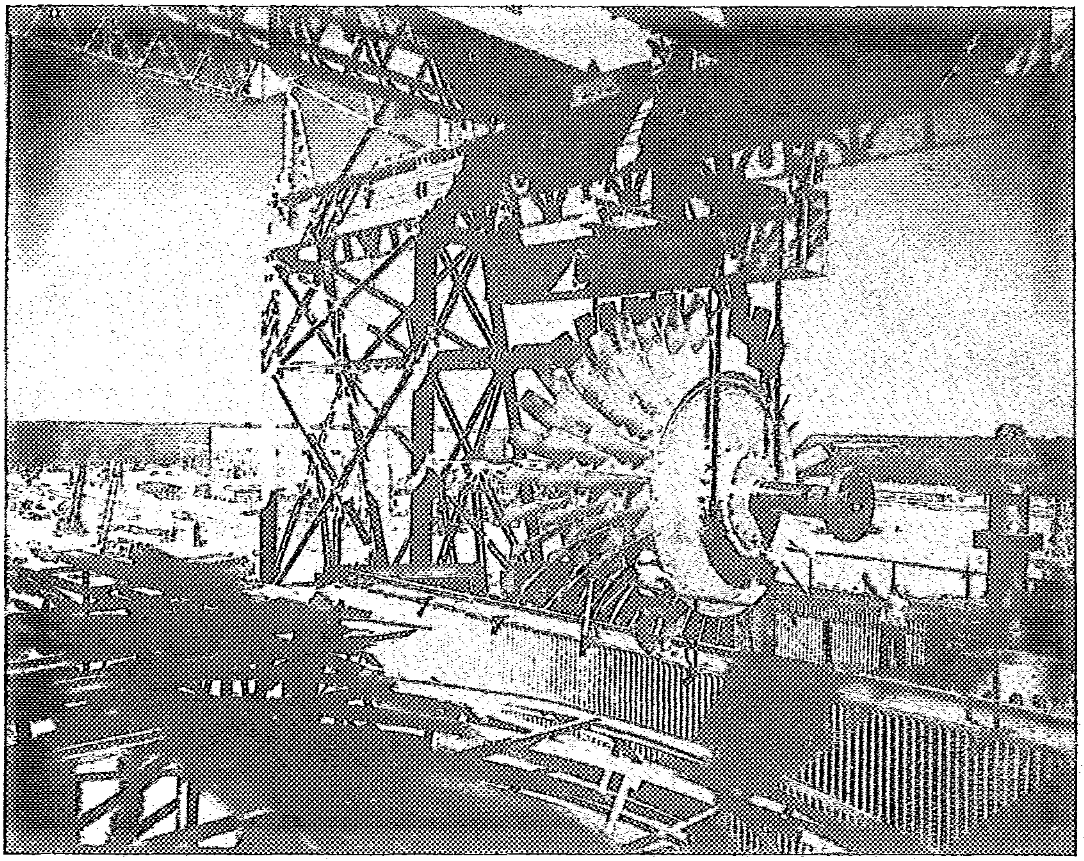

EX. 8-1 ONE OF FOUR SECTIONS OF THE 400,000 HP TULLAHOMA WINDTUNNEL COMPRESSOR. THIS COMPRESSOR WAS DEVELOPED USING 1/8 AND 1/16 SCALED MODELS.

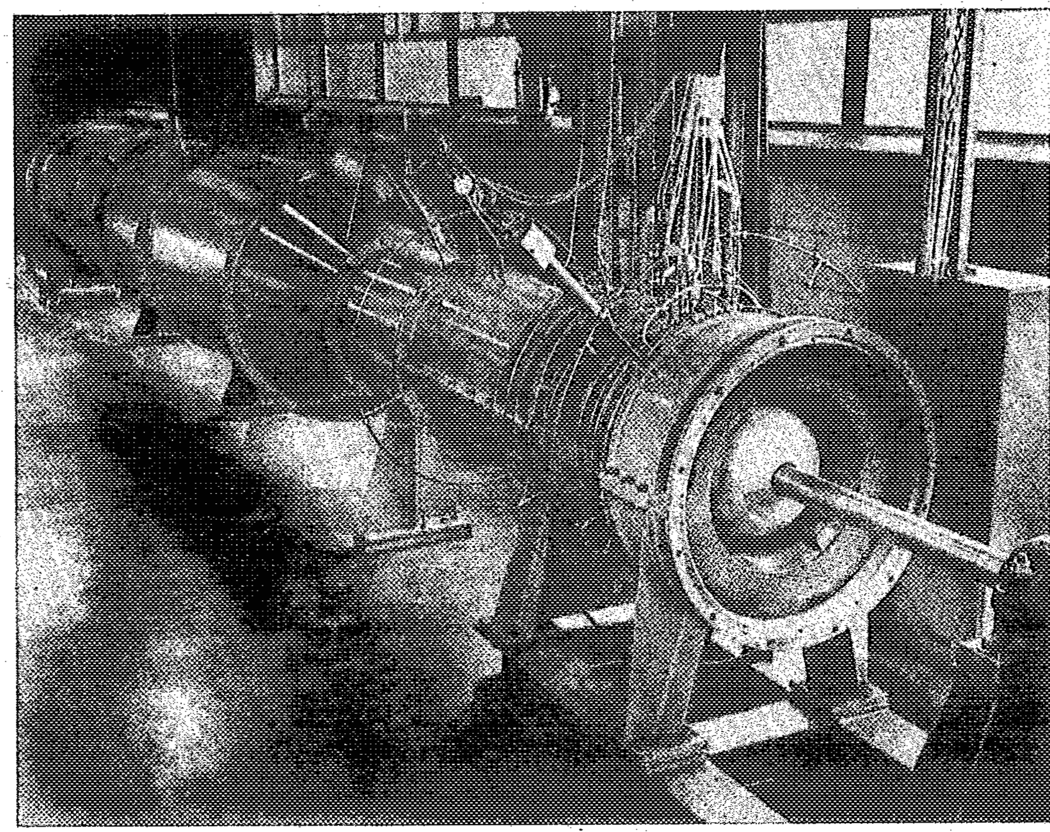

EX. 8-2 1/18 SIZE LOW SPEED MODEL (100 HP) (74.6 kW)

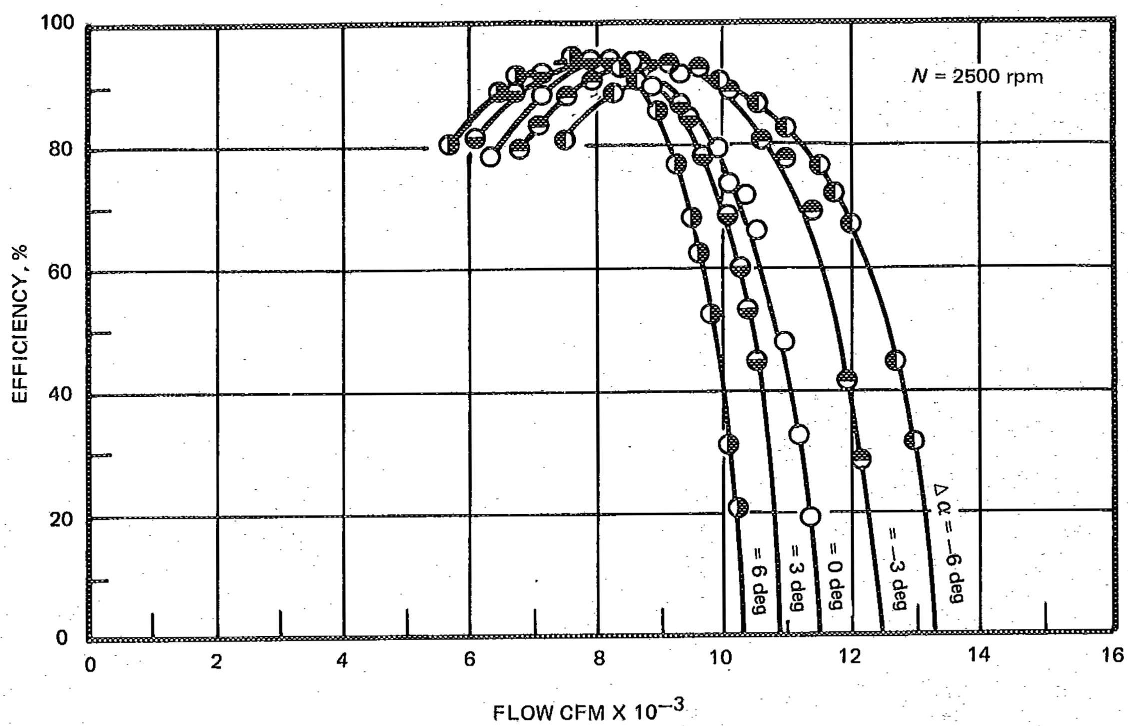

EX. 8-3

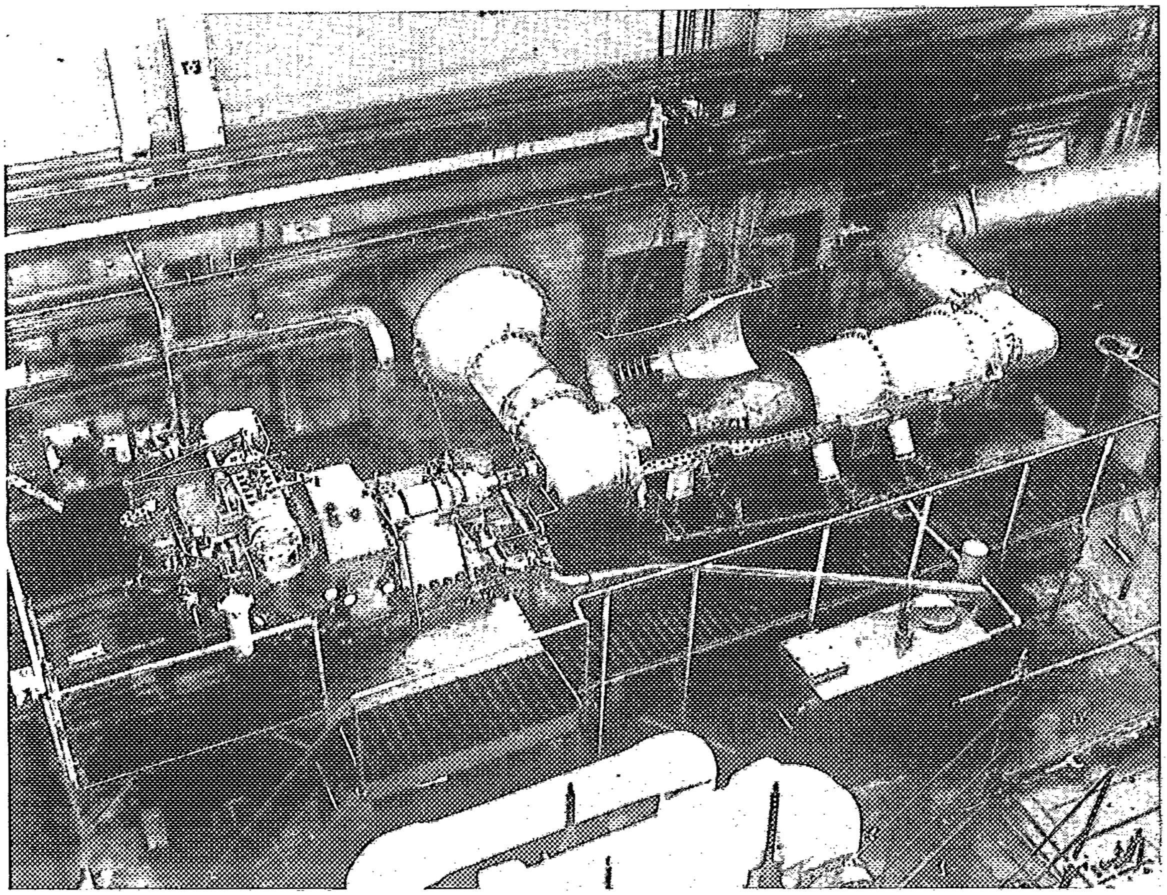

EX. 8-4 1/16 SIZE MODEL OF ONE SECTION OF THE TULLAHOMA COMPRESSOR (216,000 HP) (161,194 kW)

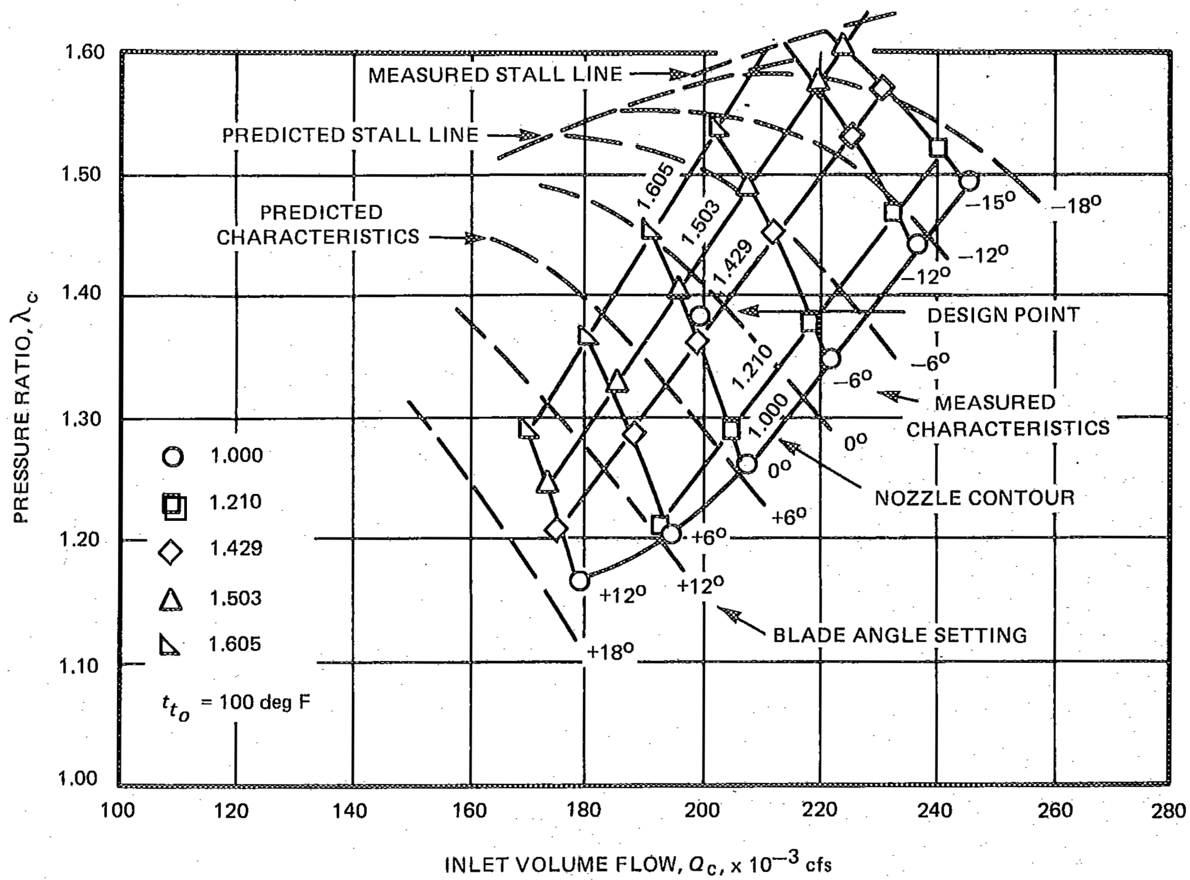

EX. 8-5 COMPARISON OF THE PREDICTED AND MEASURED PERFORMANCE CHARACTERISTICS OF THE COMPRESSOR

Results

A comparison of the test results of the low speed model and the full scale compressor is shown on Ex. 8-5[1]. The model test predicted stall line matches closely the full scale tests. The different blade angle setting curves are steeper for the prototype than for the model, due to its higher speed.

The tested efficiency of the low speed model was 87 percent, the tested efficiency of the high speed model was 86 percent and the tested efficiency of the prototype was 90 percent.

Conclusions

The use of an inexpensive low speed model and later a more expensive high speed model enabled the prediction of the performance of the compressor as follows:

DESIGN	FULL SCALE TEST
Pressure ratio 1.385	1.07-1.385-1.595
Flow cfm 200,000	247000 195000* 128000
Efficiency 0.85	0.90
Stall pressure ratio 1.585	1.590

REFERENCE

[1] B. B. Estabrooks and J. R. Milillo, AEDC TR-57-15, Oct. 1957.

*The flow at design point pressure ratio was 2.5 percent low but could be adjusted by changing the blade settings.

EXAMPLE 9 – RIVER MODEL HEATING STUDIES

It is generally accepted that "river modeling" includes studies with physical models of any free surface flow through a body of water contained and encompassed by a geometrically modeled configuration such as a reservoir, harbor, ocean, estuary or river. The purposes are numerous and include definition of flow patterns, density currents, forces on structures, bed movement, erosion of shoreline and mixing characteristics.

In considering problems in the river model context, the advantages include the capabilities usually associated with models such as facility of change or modification, accessibility, control of test conditions and ability to reproduce unusual natural phenomena. In addition synoptic data, improved precision, and accuracy of readings are possible.

The scaling laws or relationships are based on Froude scaling since dynamic similitude for free surface flows involve the ratio of gravitational forces and the dynamic or inertia forces. It should be pointed out that for certain model studies involving density effects (thermal problem or esturine problem), the densimetric Froude number is applied. This means simply modifying the acceleration of gravity (g) by the ratio of density difference and the fluid density.

A particular example could be the Yorktown Steam Power Station of the Virginia Electric Power Company and the proposed addition of an 845 MW unit. The State of Virginia had imposed strict limits on the allowed temperature rise in the area of the plant discharge. A model study at the Alden Research Laboratory of Worcester Polytechnic Institute was commissioned to aid in developing and documenting a system to disperse the effluent and satisfy the state requirements. Since the plant site is in the York River estuary, tidal conditions were involved, reverse flow, salt water intrusion and navigation as well as aquatic biology.

The model was designed as a distorted model having a horizontal ratio of 1/465 and a vertical ratio of 1/60 in order to avoid viscosity problems associated with small models and corresponding small depth of water. The resulting scale ratios are listed in Table 9-1 below:

TABLE 9-1

Horizontal distance	1/465
Vertical distance	1/60
Area (vertical)	1/27,900
Velocity	1/7.75
Time	1/60
Flow rate	1/216,225
K (heat transfer coeff.)	1/1
Temperature	1/1

The lower 11 miles of the York River Estuary, starting from the Chesapeake Bay were modeled in concrete with pertinent structures fabricated from steel, plastics and wood. In addition the additional 22 miles of estuary were reproduced as a labyrinth in order to fully model the tidal-wedge (Ex. 9-1). An automated inflow control and a water level gate were both programmed to produce the tidal flow effects while a small pump and electric immersion heaters modeled the plant intake flow and heated outflow.

Instrumentation comprised 240 copper constantan thermocouples linked to a computer in order to provide simultaneous temperatures printed by the computer center on a plan view of the modeled area.

On the basis of the studies, an underwater multiport diffuser was developed and installed as the heated water outfall. The resulting surface temperature rises through the condensers was 2°F or less. (Ex. 9-2). Subsequent field tests of the installed manifold have confirmed the results indicated by the model.

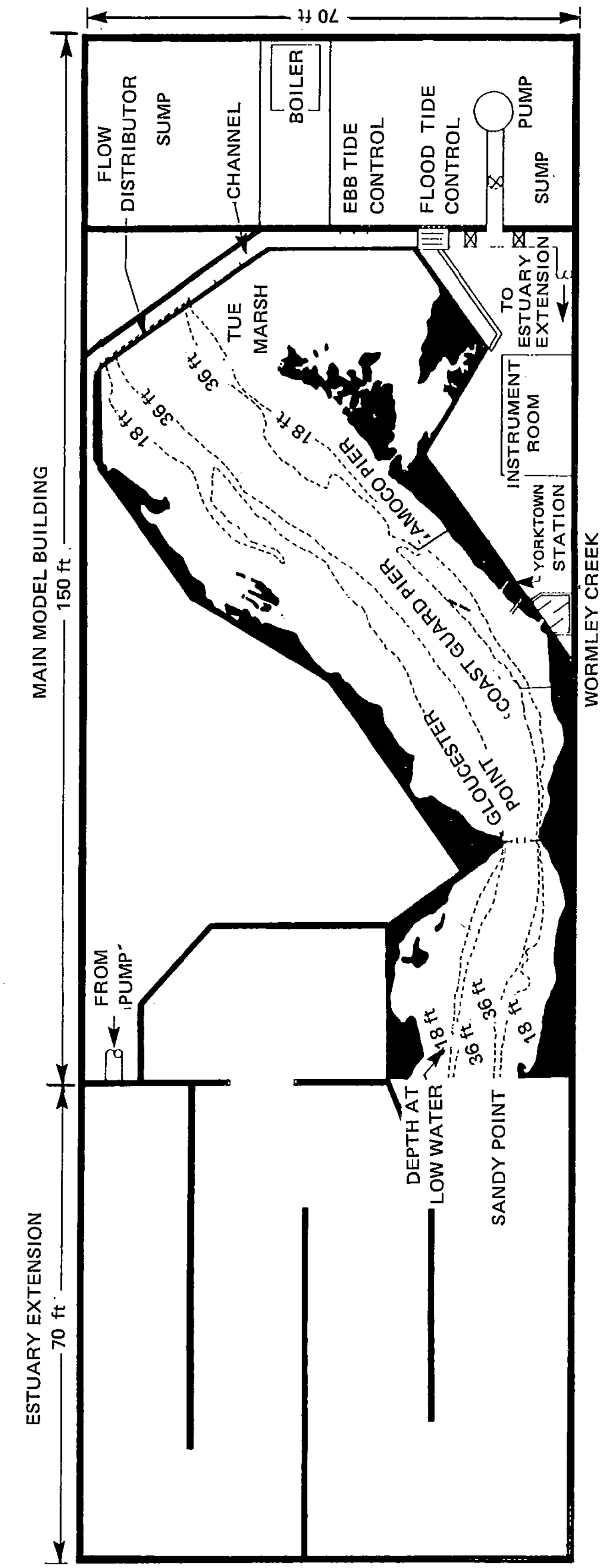

EX. 9-1 GENERAL ARRANGEMENT OF YORKTOWN ESTUARY MODEL

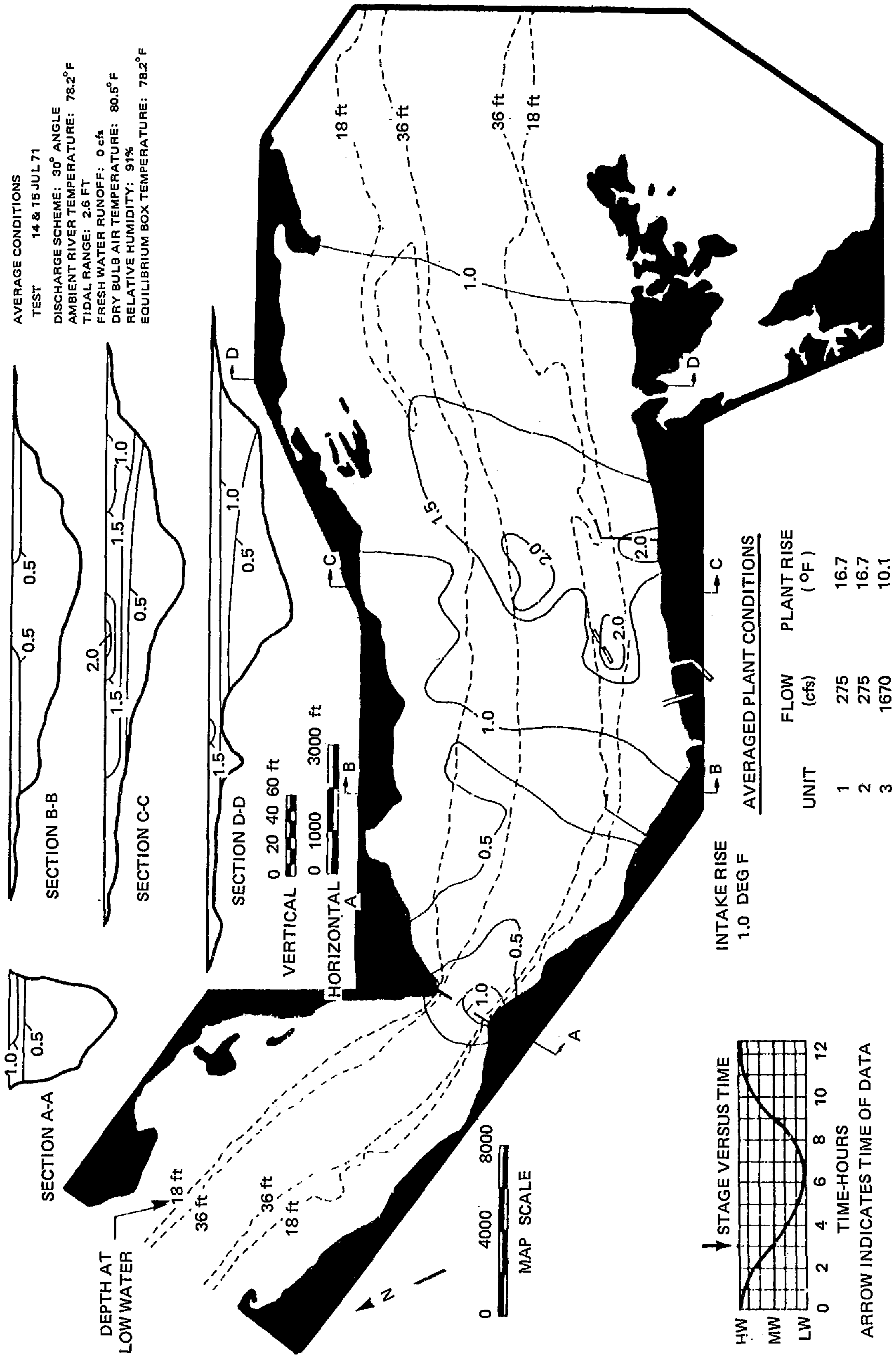

EX. 9-2 TEMPERATURE RISE ABOVE RIVER AMBIENT SURFACES/PROFILES

EXAMPLE 10 – MODEL TESTING OF LARGE FANS

Definition

Model testing of large fans would be conducted only when it is not possible to test the full-sized fan other than in its field installation. The objective of the model test would be to obtain preliminary performance information with the model fan tested in a scale model of the prototype installation.

Some fans required by industry today are very large in size and require large amounts of power to operate. Examples of applications of large fans are large wind tunnels, mechanical draft cooling towers, mine and tunnel ventilation fans, etc. Some of these fans may be as large as 60 feet in diameter and require thousands of horsepower to operate. The manufacturer of these large fans probably would not have the facilities required to test such fans because of its size and power requirements.

Method of Modeling Large Fans

Dimensionless Performance Parameters

The performance of a family of fans is described by the volume flow rate (Q), the developed head (H), and the input shaft power (P) or efficiency. The performance is also a function of the speed (n), a characteristic dimension (D), the fluid density (ρ), the viscosity (μ) and the speed of sound (a). These eight variables with three primary dimensions (mass, length, time) can be combined into five dimensionless groups that completely describe the performance of a family of geometrically similar fans by using the Buckingham Pi Theorem.*

The combination of five dimensionless groups that has proved to be the most meaningful for fans is the following:

Flow coefficient $= \dfrac{Q}{nD^3}$

Head rise coefficient $= \dfrac{gH}{n^2D^2}$

Power coefficient $= \dfrac{P}{\rho n^3 D^5}$

Reynolds number $= \dfrac{\pi \rho nD}{\mu}$

Mach number $= \dfrac{\pi nD}{a}$

If the model scale factor, model speed, and model fluid properties were properly selected so that all of the five dimensionless parameters were the same for the model and the prototype, then the prototype performance could be accurately predicted from the measured model performance. However, it is usually not possible to do this without an elaborate and expensive model test rig that would permit the use of different fluids and possibly the use of operating pressures and temperatures different from ambient conditions.

The applications mentioned above are primarily air fans. If a 1/10 size model were operated with the same air conditions, the following model operating conditions would occur if Mach number were held constant:

(1) The speed (n) would be increased 10 times.
(2) The flow rate (Q) would be decreased 100 times.
(3) The head rise (H) would remain the same.
(4) The power (P) would decrease 100 times.
(5) The Reynolds number would be reduced 10 times.

The change in Reynolds number would be a deviation from exact similarity that would cause the prototype performance results, scaled from the model test results to be in error. The error would generally be in the conservative direction by predicting lower generated head and larger power because of increased losses in the model fan blades and attached ducts due to reduced model Reynolds number.

A different set of assumptions for size scale, model fluid properties and what group of variables should be held constant will lead to different conclusions and different sources of error between predicted prototype results and actual field results.

Model Testing

The choice of model parameters would be governed by the testing facilities available for flow rate and power as well as the desire to obtain conservative model results. The previous discussion assumes that all aspects of the fan and duct geometry are scaled including clearances, blade thicknesses, roughness and blade shapes. The effect of any variation from geometric similarity must be considered along with any non-similarity between the model and prototype dimensionless ratios when evaluating the model results.

The model fan should be tested according to the Performance Test Code for Fans.

*The Pi Theorem states that a functional relation involving Q dimensional variables, whose dimensions can be expressed in terms of N fundamental units (like M, L and T), can be reduced to a relation involving only $(Q - N)$ dimensionless variables. Example: (5 quantities – 3 units) = 2 dimensionless variables.

SECTION 3

THEORETICAL BACKGROUND

1 DIMENSIONS

Scientific reasoning is based on concepts of various entities, such as force, mass, length, time, acceleration, velocity, temperature, specific heat, electric charge, electric current, etc. All these things possess a common characteristic, called *magnitude.* The magnitudes of an entity are an ordered set; for instance, one force is larger than another or one temperature is lower than another. Because of natural order, the magnitudes of an entity may be placed in one-to-one correspondence with the real numbers (or a subset of them); that is, each magnitude corresponds to a number, and each number corresponds to a magnitude. The larger the magnitude the larger the number that represents it. A system of measurement is a specific method for establishing such a correspondence. The way in which a system of measurement is set up depends, to a large extent, on conventions. The customary procedure is to designate a few entities as "fundamental," and to assign arbitrary units of measurement of the magnitudes of these entities. For example, length is regarded as a fundamental entity, and an arbitrary unit of length is specified; e.g., the inch, the meter, or the wavelength of a particular kind of light. The unit of length customarily determines the units of area and volume. However, this condition is not essential. For example, the inch might be designated as the unit of length, and the unit of volume might be taken as the volume of some object that is preserved in a bureau of standards. Then length and volume would both be fundamental entities, but this convention would lead to cumbersome formulas in geometry.

According to one widely used convention, deceptively called the "absolute system," the fundamental entities are mass, length, time, temperature and electric charge. Frequently, in engineering practice, force is regarded as a fundamental entity rather than mass; this convention characterizes the so-called "gravitational system." The fundamental entities of the absolute system are designated by the symbols (M), (L), (T), (θ), (Q). These symbols are called *dimensions.*

Dimensions were devised by the French mathematician J. Fourier (1768-1830) as a means for clarifying units of measurement. For example, the velocity of a particle that moves on the x-axis is $v = dx/dt$. Since dx is an increment of length and dt is an increment of time, the dimension of velocity is (L/T) or $(L\ T^{-1})$. Similarly, since acceleration is represented by a derivative dv/dt, the dimension of acceleration is (L/T^2) or $(L\ T^{-2})$. These dimensions show that velocities may be expressed in feet per second (ft/sec), miles per hour (mi/hr), meters per second (m/sec), etc., and that accelerations may be expressed in feet per second squared (ft/sec^2), miles per hour squared (mi/hr^2), etc. The dimensions of a given entity are not fixed but depend upon the arbitrary fundamental units chosen to measure it. For example, the dimensions of velocity can be (length/time), (acceleration × time), (volume/time × area).

Since force and acceleration have the respective dimensions (F) and $(L\ T^{-2})$, Newton's equation when written in the form, $F = m(a)$ shows that mass has the dimension $(M) = (F\ T^2\ L^{-1})$ in the gravitational system. Conversely, in the absolute system, force has the dimension $(F) = (M\ L\ T^{-2})$.

It may happen that certain distinct physical quantities have the same dimension. For example, work and torque each have the dimension $(F\ L)$. This situation results from the choice of the fundamental entities; it should be regarded as a coincidence rather than an inconsistency. It may be noted that work is a scalar and torque a vector quantity.

The dimension of an arbitrary variable ϕ is denoted by $[\phi]$. If ϕ is dimensionless, this fact may be denoted by $[\phi] = [M^0 - L^0 - T^0 - \theta^0 - Q^0]$. As a number raised to the zero power is unity, this relationship is denoted conventionally by $[\phi] = [1]$. The dimension of an integral $y\ dx$ is $[y]\ [x]$ or $[y\,x]$.

Dimensions may be regarded as a device for determining how the numerical value of a quantity changes when the fundamental units of measurement* are subjected to pre-

*The fundamental units might be kilograms, meters and seconds, or, alternatively pounds, inches, and minutes.

scribed changes. This is the only characteristic of dimensions having significance in the development of dimensional analysis.

For example, since 1 ft = 0.3048m and 1 min = 60 sec, an acceleration of 1000 ft/min^2 is transformed to the metric system as follows:

$$\left(\frac{\text{ft}}{\text{min}^2}\right)\times\left(\frac{\text{m}}{\text{ft}}\right)\times\left(\frac{\text{min}}{\text{sec}}\right)^2=\left(\frac{\text{m}}{\text{sec}^2}\right)$$

$$1000 \times 0.3048 \times \frac{1}{60^2} = 0.0847$$

The method illustrated by this example is perfectly general.

2 DIMENSIONAL ANALYSIS

Fourier observed that the laws of nature are independent of man-made systems of measurement. Therefore, the equations that represent natural phenomena should be independent of the units assigned to the fundamental entities; for example, they should be the same for the metric system as for the English system. If an equation possesses this property, it is said to be dimensionally homogeneous. For example, a continuity equation $V = Q/A$ is equally valid in all systems of measurement. Many empirical equations are not *dimensionally homogeneous*; hence they are applicable only for particular systems of measurement.

The concept of dimensional homogeneity leads to a general theory, called *dimensional analysis.* It may be regarded as the algebraic theory of equations that are invariant under arbitrary transformations of the size of the fundamental units of measurement. One conclusion from dimensional analysis is that an equation of the type $x = a + b + c + ...$ is dimensionally homogeneous if, and only if, the variables $x, a, b, c, ...$ all have the same dimension. This theorem is useful for checking algebraic derivations. If a derived equation contains a sum or difference of two terms that have different dimensions, a mistake has been made.

Dimensional analysis is concerned primarily with dimensionless products. Certain dimensionless products arise so frequently that they have received special names. A few of them are:

Reynolds number	$N_{Re} = VL\rho/\mu = VL/\upsilon$	(1)
Euler number	$N_{Eu} = p/\rho V^2$ or $F/\rho V^2 L^2$	(2)
Froude number	$N_{Fr} = V/\sqrt{gL}$ or V^2/gL	(3)
Mach number	$N_{Ma} = V/a$	(4)
Weber number	$N_{We} = V^2 \rho L/\sigma$	(5)

in which $F, p, L, V, \rho, \mu, g, a, \sigma$ denote force, pressure, length, velocity, mass density, dynamic coefficient of viscosity, acceleration of gravity, speed of sound, and surface tension, respectively.

Innumerable dimensionless products can be formed from the variables $F, L, V, \rho, \mu, g, a, \sigma$. However, it is shown in dimensional analysis that any dimensionless product of these variables is of the form $(N_{Re})^{a_1}$ $(N_{Eu})^{a_2}$ $(N_{Fr})^{a_3}$ $(N_{Ma})^{a_4}$ $(N_{We})^{a_5}$, in which a_1, a_2, a_3, a_4, a_5 are constant exponents. On the other hand, the products (N_{Re}), (N_{Eu}), (N_{Fr}), (N_{Ma}) and (N_{We}) are independent of each other, in the sense that no one of these products is identically a product of powers of the others. Examples of other dimensionless products that can be formed from the given variables are $V^3\rho/\mu g$ and $\rho F/\mu^2$. However, these are not new products, as they are expressible in terms of the preceding ones as follows:

$$\frac{V^3\rho}{\mu g} = N_{Re} N_{Fr} \qquad (6)$$

$$\frac{\rho F}{\mu^2} = N_{Re}^2 \; N_{Eu} \qquad (7)$$

In general, *a set of dimensionless products of given variables is said to be complete, if each product in the set is independent of the others, and every other dimensionless product of the variables is a product of powers of dimensionless products in the set.* Accordingly, $(N_{Re}, N_{Eu}, N_{Fr}, N_{Ma}, N_{We})$ is a complete set of dimensionless products of the variables $(F, L, V, \rho, \mu, g, a, \sigma)$. Dimensional analysis provides routine methods for composing complete sets of dimensionless products of any given variables.*

The most significant property of a dimensionless product is that its numerical value does not depend on the units of the fundamental entities. For example, the critical value of Reynolds number for flow in a pipe is stated to be about 2000, without regard for the system of measurement.

Conversely, if an equation is dimensionally homogeneous, it can be reduced to a relationship among a complete set of dimensionless products.

This theorem, which is generally attributed to E. Buckingham, is the foundation of dimensional analysis.

The result of a dimensional analysis of a problem is a reduction of the number of variables in the problem, since the number of dimensionless products in a complete set is generally less than the number of initial variables. For example, the eight variables $(F, L, V, \rho, \mu, g, a, \sigma)$ provide only five independent dimensionless products $(N_{Re}, N_{Eu}, N_{Fr}, N_{Ma}, N_{We})$. In general, if there are n initial variables, there are $n-r$ dimensionless products in a complete set,

*Notice (according to Meyer) that the five dimensionless numbers given above are simply the viscosity, force, gravity, sonic velocity and surface tension, measured in terms of L, V and ρ taken as fundamental units themselves, to replace M, L and T.

where r is a positive number. Formerly, it was thought that r is equal to the number of fundamental entities involved, but this is not invariably true. Van Driest [9] stated the rule that r is equal to the maximum number of initial variables that will not form a dimensionless product. This rule can be proved rigorously. For instance, from the set of variables (F, L, V, ρ, μ, g, a, σ), we can choose three of the variables (e.g., V, L, ρ) that will not form a dimensionless product. However, any four of the variables will form a dimensional product. Consequently, $r = 3$. Van Driest's rule is awkward to apply if there are many variables. A more convenient rule that is derived in dimensional analysis is based on matrix algebra.

It is noteworthy that r generally depends on the set of fundamental entities that is chosen. Occasionally, r may be increased by augmenting the set of fundamental entities. In particular, if there is not appreciable conversion of energy from work to heat or vice versa, as often happens in heat transfer processes, heat may be regarded as a fundamental thermal entity, in addition to temperature, and the factor representing the mechanical equivalent of heat is not involved. Examples may be cited in which this circumstance enhances the information that is gained by dimensional analysis.

3 REFERRED QUANTITIES AND SPECIFIC SPEED

(a) Referred Quantities

It is sometimes advantageous to replace dimensionless numbers by *referred quantities* in certain types of turbomachinery. When analyzing the performance data for jet engines[14] referred quantities have considerable convenience. Examining one frame size at a time it is possible to eliminate the size factor, and with it the inconvenience of defining a "characteristic length."

Refer all pressures (p) and temperatures (T) to the static sea level values (p_0) and (T_0), then:*

TABLE 3 REFERRED QUANTITIES

Quantity	Dimensionless Number	Referred Quantity	Units
Air Flow w_a	$w_a a/pAg$	$w_a\sqrt{\theta}/\delta$	lbm/sec or kg/sec
Rotational n frequency**	nD/a	$n/\sqrt{\theta}$	rpm or rps or hertz
Any force (F)	F/pA	F/δ	lbf or newtons
Fuel flow w_f	$w_f Q/pAa$	$w_f/\delta\sqrt{\theta}$	lbm/sec or kg/sec

*See PTC 2 and other codes as applicable.
**Formerly called rotational speed.

Where:

a = acoustic velocity
g = 32.2 ft/sec^2
D = size
A = area
Q = heating value, energy/unit mass
$\delta = p/p_0$
$\theta = T/T_0$

$$\frac{a}{a_0} \cong \sqrt{\theta}$$

The referred quantity:

(1) has been arrived at by assuming that the acoustic velocity varies as the square root of the temperature. This is not too serious as we generally neglect the effect of the variation of the ratio of specific heats γ and gas constant R. This could be partially corrected by redefining θ as the ratio of acoustic velocities.

(2) has dimension, for instance, the referred flow can be measured in pounds mass per second, whereas the value of the dimensionless flow does not give one an idea of the machine size.

(3) does not involve the question of which dimension was used as the characteristic size in the dimensionless quantity, which is the case, for instance, when one uses the Reynolds number.

(4) is somewhat less general than the dimensionless number as the size factor has been eliminated.

(5) represents the value of the particular variable while under standard pressure and temperature conditions.

Referred quantities are often used to record the performance of compressors, blowers and gas turbines under standard sea level atmospheric conditions.

(b) Specific Speed

In testing a turbine, compressor or pump of any fixed geometry, one can choose arbitrarily, as independent variables, the rotational frequency or speed (n) and the pressure drop (or rise). Selecting values of these two independent variables completely determines the performance of the fixed geometry device. That is, the volumetric (or mass) flow and power (or efficiency) are set. Any other desired quantity such as the maximum efficiency or bending stress or end thrust will depend on these two variables (rotational frequency and pressure drop, or head (H)).

One can non-dimensionalize these two independent variables in terms of size (such as D = diameter) and a fluid property (such as a = acoustic velocity). Table 4 shows typical non-dimensional forms of the independent variables speed and pressure head and also of the dependent variables volumetric flow, power and bending stress.

TABLE 4 TURBOMACHINERY DIMENSIONLESS* VARIABLES

$$\left.\begin{array}{l}\text{Speed } \bar{n} = \dfrac{nD}{a} \\ \text{Head } \bar{H} = \dfrac{gH}{a^2}\end{array}\right\} \text{Independent Variables}$$

$$\left.\begin{array}{ll}\text{Volumetric flow} & = \bar{Q} = (Q/aD^2); \text{mass flow} = \bar{\Gamma} = (W/\rho a D^2) \\ \text{Fluid power } (\bar{\Gamma}\bar{H}) & = \bar{P} = (\rho QgH/\rho a^3 D^2) = (P_f/\rho a^3 D^2); P_f = \rho QgH \\ \text{Stress} & = \bar{S} = \sigma/\rho g D \\ \text{Pump efficiency } \eta_P & = P_f/P = QgH/P_s\end{array}\right\} \text{Dependent Variables}$$

For a given turbomachine:

$\bar{Q}$ = a function of $(\bar{n}, \bar{H})$ and (N_{Re}), (γ) (N_{Pr})

$\bar{P}$ = a function of $(\bar{n}, \bar{H})$ and (N_{Re}), (γ) (N_{Pr})

$\bar{S}$ = a function of $(\bar{n}, \bar{H})$ and (N_{Re}), (γ) (N_{Pr})

η_p = a function of $(\bar{n}, \bar{H})$ and (N_{Re}), (γ) (N_{Pr})

where P_s is shaft power and σ is stress and N_{Pr} is Prandtl Number. If one specifies the two independent dimensionless variables, speed $\bar{n}$ and head $\bar{H}$ together with *one other* dependent variable say the volumetric flow $\bar{Q}$; one can eliminate the size (D) and fluid property (a) from the three dimensionless variables and obtain a new dimensionless variable, the specific speed.

$$n_s = \frac{(\bar{n})\sqrt{\bar{Q}}}{\bar{H}^{3/4}}$$

Thus, the specific speed can be imagined as a dimensionless variable involving only the design conditions n, Q and H, after eliminating the size and fluid property.** For some turbomachines, specific speed could be expressed in terms of shaft power (P_s) rather than volumetric flow Q.

$$n_s = \frac{n\sqrt{P_s/\rho}}{(gH)^{5/4}}$$

Other specific speeds may be obtained by eliminating the size (D) and fluid property (a) from any three design condition variables. For example, rather than specifying n, Q and H if we prefer to specify n, Q and bending stress (σ), we obtain $(n/Q)\,(\sigma/\rho g)^3$ as a design number.

*Ignoring variations in the fluid properties, such as viscosity, compressibility, and thermal conductivity, which are covered later by introducing Reynolds number, γ (isentropic exponent) and Prandtl number, respectively.

**In past American practice[15] the specific speed of pumps has usually been calculated using n in rpm, Q in gpm, H in ft and ignoring g. This gives a dimensional number having mixed units.

Another stress form could be obtained by specifying H and σ, to obtain $(gH\rho/\sigma)$ as a design number.

Balje[17] has defined a specific diameter $(D_s) = (DH^{1/4}/Q^{1/2})$ by eliminating the fluid property (a) and the speed (n). It is interesting to note that:

$$n_s D_s = \frac{2}{\pi}\left(\frac{u}{c}\right) \quad \text{where } \left(\frac{u}{c}\right) = \text{velocity ratio}$$

Some observations, with regard to specific speed (n_s), may be of interest.

Consider as design possibilities:

(1) Driving through a gear of ratio (r)
(2) Dividing the head among (z) stages
(3) Dividing the flow through (f) parallel turbines (pump inlets), (compressors), then the specific speed formula becomes more generally

$$n_s = \frac{Nr\sqrt{Q/f}}{\left(g\frac{H}{z}\right)^{3/4}} \tag{10}$$

Thus, the concept of specific speed can be extended to cases which involve changes in speed due to gearing, number of stages and multiple flow turbines. The designer of steam turbines for power generation usually has a choice of 1800 or 3600 rpm***, number of stages, and multiflow low pressure turbines.

Summarizing

The specific speed is a number, which is calculated using the design requirements of speed, flow rate, and head. The numerical value of the specific speed is an indication of the type of pump (or turbine) best suited to the given design requirements. For example, Figs. 11 and 12 show[16] the variation of efficiency and the type of pump impeller selected by expert designers to satisfy the design requirements expressed in terms of the single variable specific speed.

4 SIMILARITY AND MODEL LAWS

For experimental studies, reference frames must be established. Rectangular coordinates (x,y,z) may be set up on the reference frame of the prototype, and rectangular coordinates (x', y', z') on the reference frame of the model. Usually the geometric relation between corresponding points of the model and the prototype is represented by simple proportions between the coordinates; that is, $x' = x\,K_x$, $y' = y\,K_y$, $z' = z\,K_z$, where (K_x, K_y, K_z) are

***For 60 hertz generators.

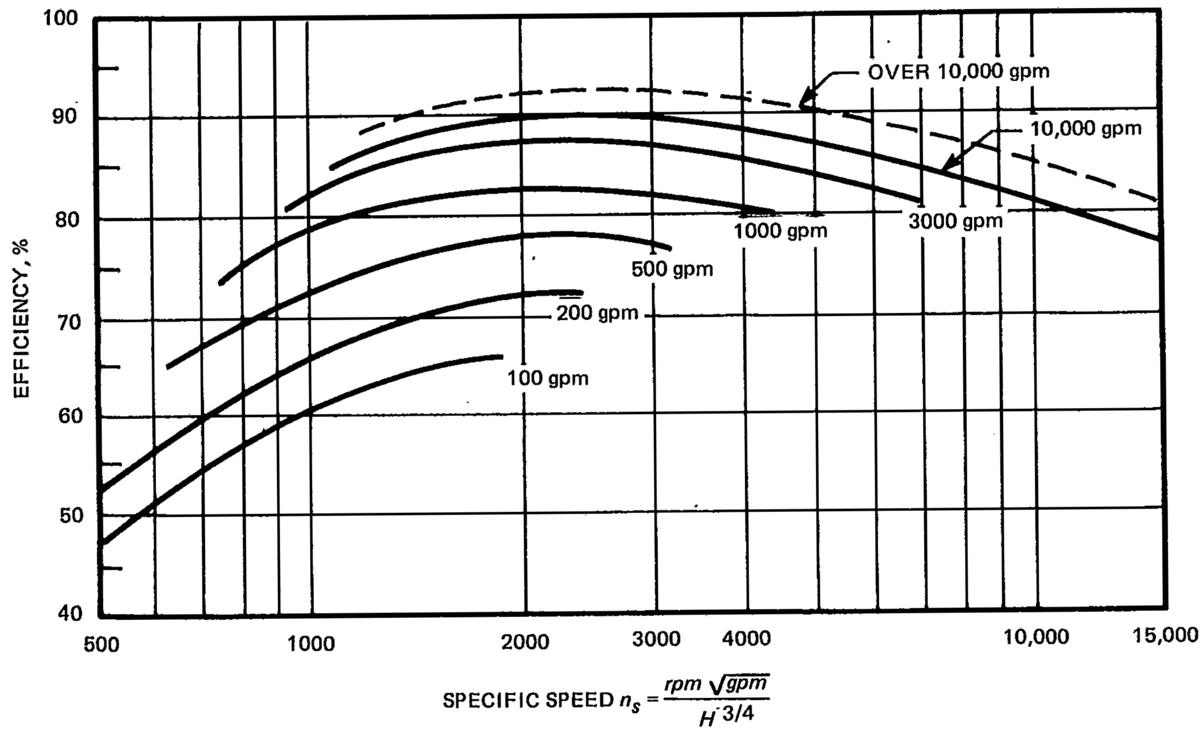

FIG. 11 CENTRIFUGAL AND AXIAL FLOW PUMPS

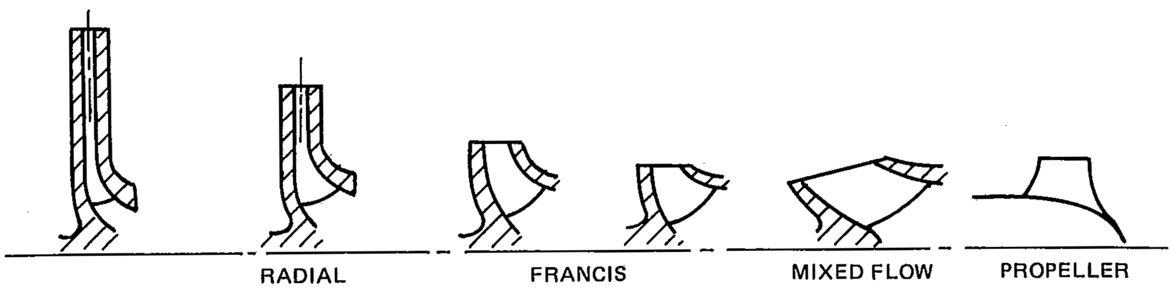

FIG. 12 PUMP EFFICIENCY VERSUS SPECIFIC SPEED AND PUMP SIZE

positive constants called similarity ratios or scale factors. If $K_x = K_y = K_z = K_L$; the model is geometrically similar to the prototype, that is, the prototype is a uniform enlargement or contraction of the model with magnification factor $1/K_L$. If the factors K_x, K_y, K_z are not all equal, the model is said to be distorted. A model of a moving system is meaningful only if a time scale factor K_t is also established, so that corresponding times for the model and the prototype are determined by $t' = t\,K_t$. A moving model is said to be kinematically similar to the prototype if the factors K_x, K_y, K_z, K_t exist. When ideal kinematic similarity exists, all ancillary effects must be scaled by these same factors, such as approach conditions, turbulence levels, etc.

If a particle of the model experiences the infinitesimal displacement dx', dy', dz' in time dt', its velocity is $v_x' = dx'/dt'$, ... where dots indicate that similar relationships apply for v_y' and v_z'. The corresponding particle of the prototype undergoes the displacement dx, dy, dz in time dt; hence, its velocity is $v_x = dx/dt$ . . . . , and $dt' = K_t dt$. Consequently, $K_{vx} = K_x/K_t$, ... Thus, the velocity scale factors are determined by the similarity ratios K_x, K_y, K_z, K_t. Likewise, the second derivatives provide the acceleration scale factors, $K_{ax} = K_x/K_t^2$, ... If the model is geometrically similar to the prototype, there is a single velocity factor, $K_v = K_L/K_t$, and a single acceleration scale factor, $K_a = K_L/K_t^2$.

Two systems are said to be dynamically similar if they are kinematically similar, and, in addition, corresponding parts of the two systems have a constant mass ratio, $K_m = m'/m$. For dynamically similar systems, Newton's law, $F_x = m_{ax}'$ . . . . yields the force scale factors, $K_{Fx} = K_m K_{ax'}$ . . . or $K_{Fx} = K_m K_x/K_t^2$. If the model is geometrically similar to the prototype, there is a single force scale factor, $K_F = K_m K_L/K_t^2 = K_\rho K_L^4/K_t^2$, where K_ρ is the scale factor for mass density.

The scale factors for a model and its prototype are said to express the *model law*. In cases of geometrical similarity, model laws may be derived by dimensional analysis. In general, dimensional analysis reduces a relationship of the form $y = f(x_1, x_2, ..., x_n)$ to the form $\pi = \phi(\pi_1, \pi_2, ..., \pi_p)$, in which $(\pi, \pi_1, ..., \pi_p)$ are a complete set of dimensionless products of $(y, x_1, ... , x_n)$. If the independent dimensionless variables $\pi_1, \pi_2, ..., \pi_p$ are adjusted to have the same value for a model as for the prototype, the dependent dimensionless variable obviously has the same value for the model and prototype. The two systems are then said to be completely similar. If these are fluid systems, then they will have geometrically similar flow patterns.

5 EXAMPLES

5.1 Efficiency of a Centrifugal Pump

A part of the shaft power of a pump is spent in overcoming friction of the packing, but this is disregarded in this discussion. For purposes of dimensional analysis, a centrifugal pump, or any other machine, is conveniently specified by a characteristic length (e.g., the diameter D of the impeller), and the ratio of all other lengths to the characteristic length. These length ratios fix the shape of the machine.

If there is no cavitation and if the liquid is a Newtonian fluid, the efficiency η of a centrifugal pump depends on the design of the pump, the diameter D of the impeller, the volumetric rate of discharge Q, the mass density ρ of the liquid, the kinematic viscosity ν of the liquid, and the rotational frequency n of the shaft. More concisely,

$$\eta = f(D, Q, n, \rho, \nu, \text{shape}) \tag{11}$$

where, as usual, the symbol f denotes a correspondence from the independent variables to the dependent variable. The word "shape" could be replaced by numerous ratios of lengths, L_1/D, L_2/D, ... Since $\mu = \rho\nu$, the dynamic viscosity coefficient μ could be introduced instead of ν, inasmuch as ρ is included among the independent variables. The delivered head does not appear in equation (11) because it is a dependent variable; i.e., it also is determined by the variables $(D, Q, n, \rho, \nu$, shape).

A complete set of dimensionless products of the preceding variables is

$$\eta, \left(\frac{Q}{nD^3}\right), \left(\frac{nD^2}{\nu}\right), \text{ shape}$$

Consequently, by Buckingham's theorem,

$$\eta = \phi\left\{\left(\frac{Q}{nD^3}\right), \left(\frac{n\,D^2}{\nu}\right), \text{ shape}\right\} \tag{12}$$

in which ϕ denotes an unknown function. Equation (12) signifies that, if two pumps of the same design but different sizes operate at the same values of (Q/nD^3) and $(n\,D^2/\nu)$, each has the same efficiency. This conclusion holds even though different* fluids are being pumped by the two machines. Reynolds number $(n\,D^2/\nu)$ represents the effect of viscosity.

If viscosity effects are neglected, an analysis like the preceding one shows that the shaft power P is given by an equation of the form

$$\eta = \left(\frac{P_s}{\rho n^3\,D^5}\right) = \phi\left\{\left(\frac{Q}{nD^3}\right), \text{ shape}\right\} \tag{13}$$

Consequently, if pumps of the same design but different sizes operate at the same value of (Q/nD^3), (which implies the same efficiency), their shaft powers vary directly as the density of the fluid, as the cube of their rotational frequencies and as the fifth power of the impeller diameter. An alternative statement is: For a given tip speed $(u^3 \sim n^3 D^3)$ the power varies as ρD^2 which is proportional to the mass flow. Similarly, it may be shown that their delivered heads (h) vary as the squares of their rotational frequencies and as the squares of the impeller diameters $(h \sim u^2 \sim (nD)^2)$.

5.2 Film-Type Condensation in a Vertical Pipe

Vapor at the saturation temperature θ flows through a smooth vertical pipe with a wall temperature $\theta - \Delta\theta$. The condensate forms a film on the wall that is an insulating layer. Consequently, the rate of condensation is influenced by the coefficient of thermal conductivity k of the condensate. The rate of condensation is determined directly by the average surface film heat-transfer coefficient, h, as the heat that is extracted from the vapor per unit time is $h\,A\,\Delta\,\theta$, where A is the area of the wall of the pipe.

The main geometrical variable is the thickness of the film of condensate. This depends on the rate of condensation and the nature of the flow of the condensate. The rate of condensation depends on the enthalpy of vaporization h_{fg}, of the fluid. Since the volume rather than the mass of condensate is significant, h_{fg} should be expressed as enthalpy per unit volume of condensate. This is represented by $\lambda = (h_{fg}/v_f)$.

The flow of condensate from the wall is influenced mainly by viscosity μ and the specific weight ρg. Since the laminar flow of the condensate is presumed, inertial forces are neglected, and the mass density of the condensate consequently enters only in the product ρg. Since the thickness

*Incompressible.

of the film is not constant along the pipe, the length L of the pipe affects the coefficient of heat transfer. The diameter of the pipe does not affect the thickness of the film (and consequently it does not affect h), if it is large compared to the thickness of the film. The velocity of the vapor in the pipe influences the thickness of the film to some extent, but this effect is small if the velocity is not large. If the interaction between the flow of vapor and the flow of condensate is neglected, the density of the vapor is irrelevant. Since the process under consideration involves no appreciable conversion of energy from work to heat, the mechanical equivalent of heat is not involved.

On the basis of the preceding discussion, we infer that there is a relationship of the form

$$f(h, \Delta, \theta, L, \lambda, k, \rho, g, \mu) = 0 \tag{14}$$

in which f denotes an undetermined function. The establishment of an undetermined relationship, such as equation (14), is always the first step in dimensional analysis. The identification of the significant variables, and the exclusion of the inconsequential ones, is the hardest part of dimensional analysis. It usually requires a good insight into the phenomenon under consideration. Heat (H) may be taken as a fifth dimension; the other four being F, L, T and θ. The dimensions of the variables are then $(h) = (L^{-2}\ T^{-1}\ \theta^{-1}\ H)$, $(\theta) = (\theta)$, $(L) = (L)$, $(\lambda) = (H\ L^{-3})$, $(k) = (H\ L^{-1}\ T^{-1}\ \theta^{-1})$, $(\rho g) = (FL^{-3})$, $(\mu) = (F\,T\,L^{-2})$. Seven variables are involved, and five dimensions. Consequently, two dimensionless products may be expected to form a complete set. This may be confirmed by Van Driest's rule, or by verifying that the rank of the dimensional matrix is 5. One standard dimensionless product, $N_{Nu} = (h\ L/k)$, called Nusselt's number, may be seen immediately. Another dimensionless product that is obviously independent of N_{Nu} can be found by inspection. Following the custom of denoting dimensionless products by *pi*, we write it as $\pi_1 = \dfrac{k\mu\Delta\theta}{\rho g\lambda L^3}$. The result of the dimensional analysis is, according to Buckingham's theorem,

$$\left(\frac{h\,L}{k}\right) = \phi\left[\frac{k\mu\Delta\theta}{\rho g\lambda L^3}\right] \text{ or } N_{Nu} = \phi\,(\pi_1) \tag{15}$$

where ϕ denotes an undetermined function.

Although the function ϕ is unknown, equation (15) is much more amenable to experimental plotting than equation (14). On the basis of a complete mathematical analysis of the problem, Nusselt arrived at the equation, $N_{Nu} = 0.943\,(\pi_1)^{-1/4}$.

It is noteworthy that, in this example, an advantage is gained by taking (H) as an independent dimension. If, on the basis of the mechanical equivalent of heat, we had written $(H) = (F\,L)$, three independent dimensionless products would have been obtained instead of two.

5.3 Dimensional Analysis of a Time Dependent Radiative Model

The intensity of external radiation incident upon the surface of a wall from one side only is denoted by q (e.g., Btu per second incident upon a square foot of the surface; Fig. 13). The dimension of q is $(H\,L^{-2}T^{-1})$ where (H) denoted heat. The initial condition is specified to be $\theta\ (x, 0)$ by θ_0 = constant. The heat conduction within the wall is governed by the differential equation.

$$a\frac{\partial^2\theta}{\partial x^2} = \frac{\partial\theta}{\partial t} \tag{16}$$

in which $a = k/C$, with k being the coefficient of thermal conductivity and C the volumetric specific heat (heat to raise a unit *volume* one degree). The wall absorbs heat at the rate $\alpha_1\ q$, where α_1 is the coefficient of absorption of the surface $x = 0$. Also, the wall reradiates heat at the rate $\epsilon_1\sigma\theta^4$ where ϵ_1 is the emissivity, σ is the Boltzmann constant, and θ_1 is the absolute temperature at surface $x = 0$. Accordingly, the boundary condition at $x = 0$ is

$$\alpha_1\ q - \epsilon_1\ \sigma\,\theta^4 = -k\frac{\partial\theta}{\partial x} \text{ at } x = 0 \tag{17}$$

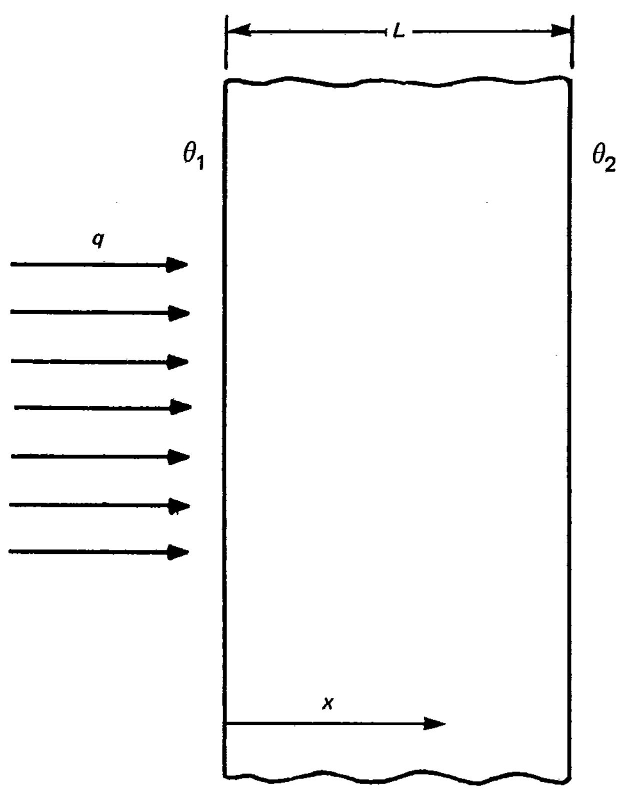

FIG. 13

Since the surface $x = L$ is not subjected to incident radiation, the boundary condition at the surface is

$$\epsilon_2 \, \sigma \, \theta^4 = -k \frac{\partial \theta}{\partial x} \text{ at } x = L \tag{18}$$

With the initial condition, equations (16), (17) and (18) present a purely mathematical problem, provided that ϵ_1, ϵ_2, α_1 are constants. The problem is quite difficult, because of the nonlinear θ^4 appearing in the boundary conditions.

Even though the mathematical problem is difficult, the equations serve to identify the significant variables. Consequently, dimensional analysis can be applied. Evidently, the solution is of the form,

$$\theta = f(\theta_0, x, t, L, a, \sigma, q, k/\epsilon_1, k/\epsilon_2, \alpha_1/\epsilon_1),$$

since equations (17) and (18) may be divided through by ϵ_1 and ϵ_2, respectively. Dimensional analysis of this relationship yields

$$\frac{\theta}{\theta_0} = f\left(\frac{q}{\sigma \theta_0^4}, \frac{x}{L}, \frac{L^2}{a t}, \frac{\sigma \theta_0^3 L \epsilon_1}{k}, \frac{\epsilon_1}{\epsilon_2}, \frac{\alpha_1}{\epsilon_1}\right) \tag{19}$$

It is known that $\alpha = \epsilon$ if equilibrium prevails (12). Usually the condition is satisfactory for gray bodies, even for non-equilibrium conditions. Consequently, the ratio α_1/ϵ_1 is practically unity. Equation (19) yields the model law for radiative heat transfer.

Although a wall was considered, equation (19) applies for a body of any given shape. If the model is made of the same material as the prototype, $K_a = 1$ and $K_k = 1$. Also, since σ is a basic physical Boltzmann constant, $K_\sigma = 1$. If the model and the prototype operate at the same temperature, $K_\theta = 1$. Then the product $\sigma \, \theta_0^3 \, L\epsilon_1/k$ in equation (19) yields $K_\epsilon = 1/K_L$, and the product $g/\sigma \, \theta_0^4$ yields $K_q = 1$.

These conclusions signify that a small model of a radiative system should have greater surface emissivity than the prototype, and the intensity of incident radiation should be the same as for the prototype. Unfortunately, the condition $K_\epsilon = 1/K_L$ cannot be realized in most cases, since surface finishes for providing the required emissivity are unavailable. In fact, for a small model the condition $K_\epsilon = 1/K_L$ may require that $\epsilon > 1$, and this is impossible. Consequently, models of radiative systems are not very satisfactory. Commenting on this situation, Chao and Wedekind[13] state: "When the model and the prototype are made of the same materials, the model operates at temperatures higher than those of the prototype. The smaller the scaled model, the higher the temperatures will be. One thus encounters all the adverse effects inherently associated with such operation: namely, dimensional instability and warpage, changes in surface and bulk properties, deterioration of surface paints, variations in joint conductances, etc." These conditions occur because the emissivity of the surface of the model being equal to that of the prototype is too low for the model to operate at equal temperature and the model consequently does not reradiate as much heat as it should.

This example illustrates the danger in a naive approach to dimensional analysis, in which the significant variables are not carefully identified.

Failure to recognize that ϵ_1 and ϵ_2 occur only in the ratios k/ϵ_1 and k/ϵ_2, and substituting k, ϵ_1, ϵ_2 separately in the dimensional analysis, would have resulted in the dimensionless product $qL/k\theta_0$. As $K_\theta = 1$, this yields $K_q = 1/K_L$, which indicates that a small model should receive much higher radiation intensity than the prototype. Actually, the radiation intensity imposed by $K_q = 1/K_L$ might be disastrous for a small model. As the preceding dimensional analysis shows, the dimensionless product $qL/K\theta_0$ really does not arise; rather, the product $\epsilon_1 qL/k\theta_0$ occurs. It can be obtained by multiplying the two products $q/\sigma\theta_0^4$ and $\sigma \, \theta_0^3 \, L\epsilon_1/k$ which occur in equation (19).

The product L^2/at in equation (19) yields $K_T = K_L^2$. This signifies that the time required to bring a body of given shape up to a given temperature varies as the surface area of the body – not as the volume of the body.

In all of the above examples – systematic, boundary and material properties have all been suitably defined or assumed. However, there are problems where physical or thermodynamic properties are incompletely defined. Attempts to model plows, road scrapers and other earth moving machines have had only marginal success because the properties of soils are obscure. Also, models of highly loaded mechanical structures, where the material is subject to creep, will tend to be inconclusive because the creep phenomenon is still being studied and is as yet ill-defined. To some extent, the same problem arises in the modeling of steam water flow systems operating under transient conditions. Here the properties of steam are documented for conditions of thermodynamic equilibrium. The enthalpy of "superheated" water* and "subcooled" steam* cannot be characterized for analysis using the usual mechanical measurements. Because of the limited understanding of all of the prerequisite information similar to those described above, the user of model studies is cautioned that engineering judgment will be required to interpret and correlate the results of a model study in terms of the prototype system. This judgment is only gained through practice and experience.

6 THE SIMILARITY LAWS OF REYNOLDS AND FROUDE

If two flow systems are geometrically and dynamically similar, there is a length scale factor K_L, a time scale factor

*These phenomena can be demonstrated in the laboratory under carefully controlled steady-state conditions.

K_T, and a mass scale factor K_m. The scale factor K_ρ for mass density is determined by $K_m = K_\rho K_L^3$. By the definitions of velocity and acceleration, $K_V = K_L/K_T$ and $K_a = K_L/K_T^2$. Equivalence of Reynolds number yields $K_\mu = K_\rho K_V K_L$. Consequently, Newton's equation for viscous shearing stress, $\tau = \mu d V/dy$, yields $K_\tau = K_\mu K_V/K_L = K_\rho K_V^2$. Therefore, $K_{Ff} = K_\tau K_L^2 = K_\rho K_V^2 K_L^2$, in which F_f denotes the external frictional force on any part of the fluid.

The inertial force F_i; on any part of the fluid is the negative time rate of change of its momentum, hence, $K_{F_i} = K_m K_V/K_T$.

$$\text{Therefore,} \quad K_{F_i} = \frac{K_\rho K_L^3 K_V}{K_L/K_V} = K_\rho K_L^2 K_V^2 \tag{20}$$

$$\text{Accordingly,} \quad K_{F_f} = K_{F_i} \ : \text{ i.e.,} \quad \frac{(F_f/F_i)'}{(F_f/F_i)} = 1 \tag{21}$$

where the prime denotes the model.

This conclusion may be stated as follows:

In geometrically and dynamically similar systems, the ratios of inertial force to frictional force are identical for corresponding masses of fluid if the Reynolds numbers of the two flows are equal. This principle is known as Reynolds' law of similarity. By a similar analysis, Froude's law of similarity is obtained.*

Namely:

In geometrically and dynamically similar systems, the ratios of inertial force to weight are identical for corresponding masses of fluid if the Froude numbers of the two flows are equal.

(It is implied above that geometrical and dynamic similarity leads to similarity in streamline pattern.)

7 DERIVATION OF MODEL LAWS FROM BASIC PHYSICAL LAWS

Dimensional analysis is only one of several methods that can be used to derive model laws. A widely used method rests on underlying physical laws which may be expressed in algebraic form or as differential equations.

As an example, the modeling of a derailment of a train is considered. The objective is to obtain realistic motion pictures of the tumbling and sliding of the cars in a derailment. Separation of the wheel trucks might also be observed in the pictures. Simulation of mangling and rupture of the cars requires consideration of properties of the material.

For a model study of a derailment, the cars need be only crude reproductions of the prototype, although mass distributions must be proportioned so that centers of gravity are preserved and moments of inertia are scaled properly. We suppose however, that geometric similarity is preserved, except for minor details. Then if L is a length of the prototype car and L' is the corresponding length in the model, $L'/L = K_L$ is a constant, irrespective of the particular length that is measured. The mass m of the prototype is proportional to ρL^3, where ρ is the mass density of the material. The factor of proportionality depends on the design of the car. Hence, $K_m = K_\rho K_L^3$ where $K_m = m'/m$ and $K_\rho = \rho'/\rho$.

Gravity has a significant effect upon the behavior of the parts in a derailment. Consequently, the equation $W = mg$ is essential. Hence, $K_W = K_m K_g$. Since g is generally unalterable, $K_g = 1$ and $K_W = K_m$. True modeling requires that there be a single force scale factor K_F, and, since weight is a force,

$$K_F = K_m = K_\rho K_L^3 \tag{22}$$

When the present approach to model analysis is used, one must be careful to introduce only relevant laws, and to include all laws that are relevant. For example, if weight were negligible, $W = mg$ should not have been used. Newton's law, $F = ma$, certainly would enter into any rational analysis of the motions of the parts of a derailed train. Consequently, $K_F = K_m K_a$. With equation (22), this yields $K_a = 1$; i.e., corresponding parts of the model and the prototype experience the same accelerations. As, by definition, $a = d^2x/dt^2$, $K_a = K_L/K_T^2$, where K_T is the time scale factor. Hence,

$$K_T = \sqrt{K_L} \tag{23}$$

For example, if $K_L = 1/25$, $K_T = 1/5$; i.e., the whole process or any particular movement (e.g., a gyration of a car) occurs in only one-fifth the time in which it occurs in the prototype. Consequently, high speed photography might be needed to get all the details of the behavior of the model.

Since velocity is defined by $V = dx/dt$, $K_V = K_L/K_T$. Therefore by equation (23), $K_V = \sqrt{K_L}$. For example, if $K_L = 1/25$, the model should run at only one-fifth the speed of the prototype.

Motions of the cars and the wheels in a derailment might be studied with a model of different material than the prototype. Then $K_\rho \neq 1$. If $K_\rho = 1$, equation (22) yields $K_F = K_L^3$. The relationships $K_F = K_L^3$ and $K_V = \sqrt{K_L}$ are known as Froude's law in hydrodynamics; in fact, with a slight change of wording, the preceding argument applies for a ship model instead of a train.

Bibliography

[1] "A Modern Approach to Dimensions," Parry Moon, *Jour. Franklin Inst.*, Dec., 1969.

[2] "Dimensional Analysis," P. Bridgman, Yale University Press, 2nd ed., 1931.

*This assumes, of course, that viscous forces are important. At large Reynolds numbers the friction loss coefficient is independent of viscosity and Reynolds number.

[3] "On Physically Similar Systems: Illustrations of the Use of Dimensional Equations," E. Buckingham, *Phys. Rev.*, vol. IV, p. 345, 1914.

[4] "Thermodynamics, Fluid Flow, and Heat Transmission," H. W. Croft, McGraw-Hill, New York, 1938.

[5] "Dimensionless Groups," J. P. Catchpole and G. Fulford, Ind. and Engrg. Chem., vol. 58, no. 3, Mar., 1966.

[6] "Handbook of the Engineering Sciences," vol. 1, J. H. Potter, D. Van Nostrand, Princeton, N.J., 1967.

[7] "Dimensional Analysis," Special Issue, *Jour. Franklin Inst.*, Dec., 1971.

[8] "Dimensional Analysis and Theory of Models," H. L. Langhaar, John Wiley & Sons, New York, 1951.

[9] "On Dimensional Analysis and the Presentation of Data in Fluid Flow Problems," E. R. van Driest, *Jour. Appl. Mech.*, vol. 13, no. 1, p. A-34, Mar. 1946.

[10] "Heat Transmission," W. H. McAdams, 3rd ed., McGraw-Hill, New York, 1954.

[11] "Centrifugal Pumps, Turbines, and Propellers," W. Spannhake, Technology Press, MIT Press, Cambridge, Mass., 1934.

[12] "Radiative Transfer," H. C. Hottel and A. F. Sarofim, McGraw-Hill, New York, 1967.

[13] "Similarity Criteria for Thermal Modeling of Spacecraft," B. Chao and G. Wedekind, *Jour. of Spacecraft and Rockets*, vol. 2, no. 2, Mar. 1965.

[14] "Jet Propulsion Engines," Princeton University Press, p. 99, 1959.

[15] "Dissimilarity Laws in Centrifugal Pumps and Blowers," A. J. Stepanoff and H. A. S. Hahl, *Jour. of Engrg. for Power*, Oct. 1961.

[16] "Centrifugal and Axial Flow Pumps," A. F. Stepanoff, 2nd ed., John Wiley & Sons, New York, p. 67, 1957.

[17] "A Study on Design Criteria and Matching of Turbomachines," O. E. Balje, *Jour. of Engrg. for Power*, pp. 83-114, Jan. 1962.

APPENDIX

The Land Chart of Dimensionless Numbers

by Permission of Alliance Electric Co.

(A-Cl)

ACCELERATION $\frac{E_l^3}{\rho g^2 \mu^2}$	**AEROELASTIC** $\frac{2E}{\rho V^2}$ stiffness / aerodynamic force	**ALFVEN** $\frac{V(\rho\mu_o)^{1/2}}{B}$ flow speed / Alfven wave speed	**ARCHIMEDES** $\frac{gl^3\Delta\rho_o\rho^2}{\rho\mu^2}$ buoyant force / viscous force
ARRHENIUS $\frac{\epsilon_a}{RT}$ activation energy / potential energy	**BAGNOLD** $\frac{3\phi\rho_a V^2}{4d_p\rho_p g}$ drag on particle / particle weight	**BANSEN** $\frac{h_r A_r}{Q_m c}$ heat radiated / heat capacity	**BINGHAM** $\frac{\sigma_y l}{\mu_p V}$ yield stress / viscous stress
BIOT HEAT XFER $\frac{h_t l}{h_c}$ heat Xfer to fluid / heat Xfer within body	**BIOT MASS XFER** $\frac{m_c\theta_w}{D_i}$ mass Xfer rate at interface / mass Xfer rate at interior of wall	**BLAKE** $\frac{\rho V}{\mu(1-I)S}$ inertia force / viscous force	**BODENSTEIN** $\frac{Vl_r}{D_a'}$ bulk mass Xfer / diffusive mass Xfer
BOLTZMANN $\frac{\rho c_p V}{e_s\eta_s T^3}$ bulk heat Xport / radiative heat Xport	**BOND** $\frac{pl^2 g}{\sigma_t}$ gravity force / surf. tens. force	**BOUGUER** $\frac{3C_d L_r}{2\rho_d d_m}$	**BOUSSINESQ** $\frac{V}{(2gr_h)^{1/2}}$ inertia force / gravity force
BRINKMAN $\frac{\mu V^2}{h_c T}$ heat from viscous dissipation / heat Xport by molec. conduction	**BUBBLE NUSSELT** $\frac{Q_f d_b}{h_c \Delta T_s}$	**BUBBLE REYNOLDS** $\frac{d_b}{\mu}\left(\frac{\pi}{6} d_b^3 \rho_v fn\right)$	**BUOYANCY** $\frac{l^2 W\beta\Delta T}{\mu XV}$ buoyant force / viscous force
CAPILLARITY-1 $\frac{\sigma_i k^{1/2}}{\mu Vl}$ capillary force / filtration force	**CAPILLARITY-2** $\left(\frac{\mu a}{\sigma_t}\right)^2$	**CAPILLARITY-BUOYANCY** $\frac{g\mu^4}{\rho\sigma_t^3}$	**CAPILLARY** $\frac{\mu V}{\sigma_t}$ viscous force / surf. tens. force
CARNOT $\frac{T_H - T_c}{T_H}$	**CAVITATION** $\frac{p - p_v}{p_d}$; $\frac{2(p - p_v)}{\rho V^2}$ pressure margin / dynamic pressure	**CENTRIFUGE** $\frac{\rho r_t^2 z\omega^2}{\sigma_t}$ centrifugal force / capillary force	**CLAUSIUS** $\frac{V^3 l\rho}{h_c \Delta T}$

(Co-Fe)

CONDENSATION-1 $\frac{h_t}{h_c}\left(\frac{\mu^2}{\rho^2 g}\right)^{1/3}$	**CONDENSATION-2** $\frac{l^3\rho^2 g\lambda_c}{h_c\mu\Delta T_f}$	**CRISPATION** $\frac{\mu D_t}{\sigma_t z}$	**CROCCO** $\frac{V}{V_{max}}$; $\frac{V}{[(2\gamma RT_t)/(\gamma-1)]^{1/2}}$ $\left(\frac{2a^2}{(\gamma-1)V^2}+1\right)^{-1}$ $\frac{\text{velocity}}{\text{max. velocity}}$
DAMKÖHLER'S FIRST $\frac{Ul}{Vc_o}$; $\frac{t_t}{t_r}$ $\frac{\text{reaction or relaxation rate}}{\text{flow rate}}$	**DAMKÖHLER'S SECOND** $\frac{Ul^2}{Dc_o}$ $\frac{\text{reaction rate}}{\text{diffusion rate}}$	**DAMKÖHLER'S THIRD** $\frac{QUl}{c_p\rho VT}$ $\frac{\text{heat liberated}}{\text{heat Xported}}$	**DAMKÖHLER'S FOURTH** $\frac{QUl^2}{h_c T}$ $\frac{\text{heat liberated}}{\text{heat conducted}}$
DARCY $\frac{2gHd}{V^2 l}$ $\left(\frac{\text{head loss}}{\text{vel. head}}\right)\left(\frac{\text{diameter}}{\text{length}}\right)$	**DEAN** $\frac{\rho Vl}{\mu}\left(\frac{l}{2r_c}\right)^{1/2}$	**DEBYE** $\frac{L_d}{r_p}$; $\frac{\left(\frac{\eta e_{ps} T}{q_e^2 n_e}\right)^{1/2}}{r_p}$ $\frac{\text{Debye length}}{\text{probe radius}}$	**DERYAGIN** $\theta_f\left(\frac{\rho g}{2\sigma_t}\right)^{1/2}$ $\frac{\text{film thickness}}{\text{capillary length}}$
DULONG $\frac{V^2}{c_p\Delta T_r}$ $\frac{\text{kinetic energy}}{\text{thermal energy}}$	**EKMAN** $\left(\frac{\mu}{2\rho\omega l^2}\right)^{1/2}$ $\frac{\text{viscous force}}{\text{coriolis force}}$	**ELASTICITY-1** $\frac{4t_r\mu}{\rho d^2}$; $\frac{t_1\mu_x}{\rho d_j^2}$ $\frac{\text{elastic force}}{\text{inertia force}}$ see note 1	**ELASTICITY-2** $\frac{c_p}{\beta a^2}$
ELASTICITY-3 $\frac{\rho c_p}{\beta_b E}$	**ELECTRIC REYNOLDS** $\frac{e_b V}{q_s b l}$	**ELECTROVISCOUS** $\left(\frac{\rho_e}{2\pi e_{ps}}\right)^{1/2}\frac{\rho l^2}{\mu}\frac{q}{m_p}$	**ELLIS** $\frac{2\mu_z V}{\tau_h d}$
ELSASSER $\frac{\rho}{\mu G\mu_o}$	**EULER** $\frac{p_s}{\rho V^2}$; $\frac{F_i}{\rho V^2 l^2}$ $\frac{\text{pressure force}}{\text{inertia force}}$	**EVAPORATION-1** $\frac{V^2}{\lambda_v}$	**EVAPORATION-2** $\frac{c_p}{\lambda_v\beta}$
EVAPORATION-ELASTICITY $\frac{a^2}{\lambda_v}$	**EXPLOSION** $\frac{r_b}{\left(\frac{\epsilon_c}{\rho}\right)^{1/5} t^{2/5}}$	**FANNING** $\frac{2\tau}{\rho V^2}$ $\frac{\text{shear stress}}{\text{dynamic pressure}}$	**FEDEROV** $d_p\left[\frac{4g\rho^2}{3\mu^2}\left(\frac{\Gamma_p}{\Gamma_f}-1\right)\right]^{1/3}$

Note 1 — t_1 is the solution to: $\tau + t_1\dot{\tau} = -\mu_Z\Delta$

(Fl-Kn)

FLIEGNER $\frac{Q_m(c_pT)^{1/2}}{A(p_s+\rho V^2)}$	**FLOW** $\frac{Q_v}{\omega d_i}$	**FOURIER HEAT XFER** $\frac{h_c t}{c_p \rho l^2}$	**FOURIER MASS XFER** $\frac{Dt}{l^2}$
FROUDE $\frac{V^2}{gl}$; $\frac{V}{\sqrt{gl}}$ $\frac{\text{inertia force}}{\text{gravity force}}$	**FRUEH** $\frac{K\omega_a}{a}\left(\frac{m_w}{C_L\rho_a K^2}\right)^{1/2}$	**GALLILEO** $\frac{gl^3\rho^2}{\mu^2}$ $\frac{\text{gravity force}}{\text{viscous force}}$	**GOUCHER** $r_w\left(\frac{\rho g}{2\sigma_t}\right)^2$ $\frac{\text{gravity force}}{\text{sur. tens. force}}$
GRAETZ $\frac{Q_m c_p}{h_c l}$ $\frac{\text{fluid thermal capacity}}{\text{conductive heat Xfer}}$	**GRASHOF** $\frac{\rho^2 g l^3 \beta \Delta T}{\mu^2}$ $\frac{\text{(inertia force) (buoyant force)}}{\text{(viscous force)}^2}$	**GRAVITY** $\frac{kg\Delta\rho_f}{\mu V_r}$ $\frac{\text{gravity force}}{\text{filtration force}}$	**GUKHMAN** $\frac{T_\kappa - T_m}{T_\kappa}$
HALL $\omega_c t_r$	**HARTMANN** $\frac{BG^{1/2}l}{\mu^{1/2}}$ $\frac{\text{magnetic force}}{\text{viscous force}}$	**HEAT XFER** $\frac{Q_h}{\rho V^3 l^2}$	**HEDSTROM-1** $\frac{\sigma_y \rho l^2}{\mu_p^2}$
HERSEY $\frac{F_h}{\mu V_L l_h}$ $\frac{\text{load force}}{\text{viscous force}}$	**HODGSON** $\frac{x f_p \Delta p}{Q_v p_a}$ $\frac{\text{time constant}}{\text{pulsation period}}$	**J-FACTOR HEAT XFER** $\frac{h_t}{c_p M}\left(\frac{c_p\mu}{h_c}\right)^{2/3}$	**J-FACTOR MASS XFER** $\frac{m_c\rho}{M}\left(\frac{\mu}{\rho D}\right)^{2/3}$
JACOB $\frac{\lambda_v}{c_p\Delta T}$	**JAKOB** $\frac{(T_l - T_{sat})\rho_l c_p}{\lambda_v \rho_v}$	**JOULE** $\frac{2\rho c_p \Delta T}{\mu_o H_m^2}$ $\frac{\text{joule heating energy}}{\text{magnetic field energy}}$	**KARMAN-1** $\frac{\rho\Delta p d^3}{\mu^2 l}$
KIRPICHEV HEAT XFER $\frac{Q_f l}{h_c\Delta T}$ $\frac{\text{external heat Xfer intensity}}{\text{internal heat Xfer intensity}}$	**KIRPICHEV MASS XFER** $\frac{M_e l}{D_m\rho R_m}$ $\frac{\text{external mass Xfer intensity}}{\text{internal mass Xfer intensity}}$	**KIRPITCHEFF** $\left(\frac{\rho F_r}{\mu^2}\right)^{1/3}$	**KNUDSEN** $\frac{L}{l}$; $\frac{1.28\gamma^{1/2}\mu}{a\rho l}$ $\frac{\text{molec. mean free path}}{\text{characteristic body length}}$

(Ko-Pe)

KOSSOVICH $\frac{\lambda_v R_m}{c \Delta T_b}$ heat to evaporate moisture / heat to raise body temp.	**LAGRANGE-1** $\frac{\Delta p l}{\mu V}$ pressure force / viscous force	**LAGRANGE-2** $\frac{P}{\mu l^3 \omega_{ag}^2}$	**LEVERETT** $\left(\frac{k}{I}\right)^{1/2} \frac{p_c}{\sigma_t}$ char. dim. of interface curvature / char. dim. of pores
LEWIS $\frac{D \rho c_p}{h_c}$ mass diffusivity / thermal diffusivity	**LUNDQUIST** $\frac{G H_m l \mu_o^{3/2}}{\rho^{1/2}}$	**LYKOUDIS** $\frac{G}{\rho}(\mu_o H_m)^2 \left(\frac{l}{g \beta \Delta T}\right)^{1/2}$	**MACH** $\frac{V}{a}$ inertia force / elastic force
MAGNETIC-DYNAMIC $\frac{G V B^2 l}{\rho V^2}$ magnetic pressure / dynamic pressure	**MAGNETIC FORCE** $\frac{\mu_o^2 H_m^2 G l}{\rho V}$ magnetic force / dynamic force	**MAGNETIC INTERACTION** $\frac{\mu_o H_m^2 r_t}{2 \sigma_t}$	**MAGNETIC PRANDTL** $\mu_o G \nu$
MAGNETIC PRESSURE $\frac{\mu_o H_m^2}{\rho V^2}$ magnetic pressure / dynamic pressure	**MAGNETIC REYNOLDS** $G V l \mu_o$ motion induced mag. field / applied mag. field	**MARANGONI** $\frac{\delta \sigma_t}{\delta T} \frac{\delta T}{\delta l} \frac{z^2}{\mu D_t}$ see note 2	**MASS RATIO** $\frac{m_b}{\pi \rho l^3}$ mass of immersed body / mass of surrounding fluid
McADAMS $\frac{h_t^4 l \mu \Delta T}{h_c^3 \rho^2 g \lambda_c}$	**MERKEL** $\frac{M A_c x_t}{Q_m}$ $\left(\frac{\text{mass of } H_2O \text{ Xferred}}{\text{unit of humidity diff.}}\right)$ / mass of dry gas	**MOMENTUM** $\frac{M_v \theta_l \rho}{\mu \Delta V}$	**MORTON** $\frac{g \mu^4}{\rho \sigma_t^3}$
NUSSELT HEAT XFER $\frac{Q_f l}{h_g \Delta T_w}$ total heat Xfer / conductive heat Xfer	**NUSSELT MASS XFER** $\frac{m_c l}{D_{mol}}$; $\frac{\tau_w l}{\rho V D_{mol}}$ mass diffusivity / molec. diffusivity	**NUSSELT FILM THICKNESS** $\left(\frac{\rho^2 g}{\mu^2}\right)^{1/3} \theta_f$	**OCVIRK** $\frac{F_L}{\mu V_b}\left(\frac{w}{r_s} \frac{2 r_s}{l_b}\right)^2$ bearing load / viscous force
OHNESORGE $\frac{\mu}{(l \rho \sigma_t)^{1/2}}$ viscous force / surf. tens. force	**PARTICLE** $\frac{V_f V}{g l}$	**PECLET HEAT XFER** $\frac{\rho c_p V l}{h_c}$ heat convection / heat conduction	**PECLET MASS XFER** $\frac{l V}{D}$ bulk mass Xfer / diffusive mass Xfer

(Pi-St)

PIPELINE $\frac{a_p V}{2gH_s}$ max. H_2O hammer pressure rise / static pressure	**POISEUILLE** $\frac{d^2}{\mu V}\frac{\delta p}{\delta l}$ pressure force / viscous force see note 2	**POISSON** $\frac{E_t}{2E_K} - 1$ lateral contraction / longitudinal extension	**POMERANTSEV** $\frac{Q_L l^2}{h_c \Delta T}$
POROUS FLOW $\frac{V\mu l}{k^{1/2}\sigma_t \cos\theta}$ viscous pressure / capillary pressure	**POSNOV** $\frac{\sigma_\theta \Delta T}{R_c}$	**POWER** $\frac{P}{l^5 \rho \omega_{ag}^3}$ paddle drag / inertia force	**PRANDTL HEAT XFER** $\frac{c_p \mu}{h_c}$ momentum diffusivity / thermal diffusivity
PRANDTL MASS XFER $\frac{\mu}{\rho D}$ momentum diffusivity / mass diffusivity	**PRANDTL VEL. RATIO** $V\left(\frac{\rho}{\tau_w}\right)^{1/2}$ $\left(\frac{\text{inertia force}}{\text{wall shear force}}\right)^{1/2}$	**PREDVADITLEV** $\frac{\delta T}{\delta t}\frac{l^2}{D_t T_i}$ medium temp. change rate / body temp. change rate see note 2	**RADIATION PRESSURE** $\frac{\eta_{SB} T^4}{3p}$ radiation pressure / gas pressure
RAYLEIGH $\frac{c_p \rho^2 g l^3 \beta \Delta T}{\mu h_c}$ gravity / thermal diffusivity	**REGIER** $\frac{K\omega}{a}\left(\frac{m_w}{\pi \rho K^2}\right)^{1/2}$	**REYNOLDS** $\frac{\rho V l}{\mu}$ inertia force / viscous force	**RICHARDSON** $\frac{g l \Delta \rho}{\rho V^2}$ buoyant force / turbulent force
ROSSBY $\frac{V}{2\omega l}$ inertia force / coriolis force	**RUSSELL** $\frac{V_w}{NY}$; $\frac{V_w}{Y\left(-\frac{g}{\rho}\frac{\delta \rho}{\delta y}\right)^{1/2}}$ inertia force / buoyancy force see note 2	**SACHS** $\frac{r p_o^{1/3}}{\epsilon_o^{1/3}}$	**SCHILLER** $Vl\left(\frac{\rho^2}{2\mu F_i}\right)^{1/3}$
SLOSH TIME $\left(\frac{\sigma_t}{\rho r_t^3}\right)^{1/3} t$	**SOMMERFELD** $\frac{F_n \psi^2}{\mu \omega}$ viscous force / load force	**SPECIFIC HEAT RATIO** $\frac{c_p}{c_v}$ spec. heat at const. pressure / spec. heat at const. volume	**SPECIFIC SPEED** $\frac{\omega (Q_v)^{1/2}}{(gH_{st})^{3/4}}$
SQUEEZE $\frac{12\mu\omega}{p_a}\left(\frac{r_B}{\theta\mu}\right)^2$	**STANTON** $\frac{h_t}{\rho c_p V}$ heat Xferred to fluid / heat Xported by fluid	**STEFAN** $\frac{\eta_s A_r T^4}{h_c A_K \frac{\delta T}{\delta l}}$ heat radiated / heat conducted see note 2	**STOKES** $\frac{\mu V}{\rho g l^2}$ viscous force / gravity force

Note 2 — $\delta y/\delta x$ indicates a gradient or rate of change coefficient between variables y and x.

(St-We)

STROUHAL $\frac{l\omega_v}{V_T}$ $\frac{\text{vibration speed}}{\text{Xlation speed}}$	**STRUCTURAL MERIT** $\frac{\gamma_w l}{E}$ $\frac{\text{weight}}{\text{stiffness}}$	**SURATMAN** $\frac{\rho l \sigma_t}{\mu^2}$	**SURFACE VISCOSITY** $\frac{\mu_s}{\mu_z}$
TAYLOR $\frac{\omega^2\theta_c{}^4\rho^2}{\mu^2}$ $\frac{\text{centrifugal force}}{\text{viscous force}}$	**THOMA** $\frac{p_{in}-p_v}{p_{out}-p_{in}}$ $\frac{\text{pressure margin above cavitation}}{\text{pressure rise in pump}}$	**THOMSON** $\frac{tV}{l}$	**TOMS** $\frac{Q_w}{\rho V^3 l}$ $\frac{\text{fuel weight}}{\text{air drag}}$
TRUNCATION $\frac{\mu\alpha}{p}$ $\frac{\text{shear stress}}{\text{normal stress}}$	**TWO-PHASE FLOW** $\frac{\mu d_b V}{\sigma_i l}$ $\frac{\text{viscous force}}{\text{surf. tens. force}}$	**TWO-PHASE POROUS FLOW** $\frac{V\mu}{(k_L k_H)^{1/2} g\Delta\rho_f}$ $\frac{\text{viscous pressure}}{\text{gravity pressure}}$	**VISCOELASTIC** $\frac{E_s}{\mu\omega}$ $\frac{\text{elastic force}}{\text{viscous force}}$
WEBER $\frac{\rho V^2 l}{\sigma_t}$ $\frac{\text{viscous force}}{\text{surf. tens. force}}$	**WEISSENBERG** $\frac{(t_2-t_3)\,V}{d_j}$ see note 3		

Note 3 — t_2 and t_3 are solutions to: $\tau + t_2\dot{\tau} = -\mu_Z\,(\Delta + t_3\dot{\Delta})$

NOMENCLATURE

a	sonic speed (l/t)
a_p	pressure wave velocity (l/t)
A	area (l^2)
A_c	cooling surface area per unit volume (l^{-1})
A_g	conducting area (l^2)
A_r	radiating area (l^2)
b	carrier mobility, speed/voltage gradient (Qt/m)
B	magnetic induction (m/Qt)
c	specific heat (l^2/t^2T)
c_o	concentration (m/l^3)
c_p	specific heat at constant pressure (l^2/t^2T)
c_v	specific heat at constant volume (l^2/t^2T)
C_d	ratio of dust mass to bed volume (m/l^3)
C_L	slope of wing lift curve (dimensionless)
d	pipe or tube diameter (l)
d_b	bubble or droplet diameter (l)
d_i	impeller diameter (l)
d_j	jet diameter (l)
d_m	mean particle diameter (l)
d_p	particle diameter (l)
D	mass diffusivity (l^2/t)
D_a	axial mass diffusivity (l^2/t)
D_i	mass diffusivity at interface (l^2/t)
D_m	mass diffusivity of moisture in body (l^2/t)
D_{mol}	molecular diffusivity (l^2/t)
D_t	thermal diffusivity (l^2/t)
e_p	permittivity (Q^2t^2/ml^3)
e_{ps}	permittivity of free space (Q^2t^2/ml^3)
e_s	surface emissivity (dimensionless)
E	modulus of elasticity (m/lt^2)
E_b	fluid bulk modulus (m/lt^2)
E_g	torsion modulus of elasticity (m/lt^2)
E_s	shear modulus of elasticity (m/lt^2)
E_t	tension modulus of elasticity (m/lt^2)
f	frequency of formation (t^{-1})
f_p	pulsation frequency (t^{-1})
F_a	bearing load per unit area (m/lt^2)
F_b	bearing load (ml/t^2)
F_i	force on immersed body (ml/t^2)
F_L	bearing load/length (m/t^2)
F_r	resistance force on immersed body (ml/t^2)
g	gravitational acceleration (l/t^2)
G	electrical conductivity (Q^2t/ml^3)
h_c	thermal conduction coefficient or thermal conductivity (ml/t^3T)
h_g	thermal conductivity of gas (ml/t^3T)
h_r	radiant heat transfer coefficient (m/t^3T)
h_t	heat transfer coefficient (m/t^3T)
H	head loss (l)
H_m	magnetizing force (Q/lt)
H_s	static head (l)
H_{st}	head produced per stage (l)
I	porosity, ratio of void to solid volume (dimensionless)
k	permeability (l^2)
k_H	horizontal permeability (l^2)
k_L	longitudinal permeability (l^2)
K	wing half-chord (l)
l	characteristic length or dimension (l)
l_b	bearing length (l)
l_r	reactor length (l)
L	mean free path of molecules (l)
L_d	Debye length (l)
L_r	mean radiation path length (l)
m_b	mass of body (m)
m_c	mass transfer rate or mass transfer coefficient (l/t)
m_p	particle mass (m)
m_w	wing mass per unit length (m/l)
M	mass transfer per unit area per unit time (m/l^2t)
M_e	mass of moisture evaporated per unit area per unit time (m/l^2t)
M_v	momemtum flux (l^2/t^2)
n	number of nucleation centers per unit area (l^{-2})
n_e	number of electrons per unit volume (l^{-3})
N	natural vertical frequency of fluid element about its equilibrium altitude in a density-stratified atmosphere (t^{-1})
p	pressure (m/lt^2)
p_a	average static pressure (m/lt^2)
p_c	capillary pressure (m/lt^2)
p_d	dynamic pressure (m/lt^2)
p_{in}	total pressure at pump inlet (m/lt^2)
p_o	atmosphere pressure (m/lt^2)
p_{out}	total pressure at pump outlet (m/lt^2)
p_s	local static pressure or pressure drop (m/lt^2)
p_v	fluid vapor pressure (m/lt^2)
Δp	pressure drop (m/lt^2)
P	power input to agitator (ml^2/t^3)
q	charge (q)
q_e	electron charge (q)
q_s	space charge density (q/l^3)
Q	liberated heat per unit mass (l^2/t^2)
Q_f	heat flux per unit area per unit time (m/t^3)
Q_h	heat flow per unit time or heat flow rate (ml^2/t^3)
Q_L	heat liberated per unit volume per unit time (m/lt^3)
Q_m	mass flow rate (m/t)
Q_v	volume flow rate (l^3/t)
Q_w	fuel weight flow per unit time (ml/t^3)
r	radius from explosive to reference point (l)
r_b	blast wave radius (l)
r_B	bearing radius (l)
r_c	bend radius of curvature (l)
r_h	hydraulic radius, ratio of wetted cross sectional area to perimeter (l)
r_p	probe radius (l)
r_s	shaft radius (l)
r_t	tank radius (l)
r_w	wire radius (l)
R	gas constant (l^2/t^2T)
R_c	fractional difference in moisture content of bodies (dimensionless)
R_m	fractional change in moisture content of body (dimensionless)
S	ratio of particle area to volume (l^{-1})
t	time (t)
t_f	ratio of average free path to average velocity (t)
t_r	reaction or relaxation time (t)
t_t	translation time (t)
t_1	time constant (t)
t_2	time constant (t)
t_3	time constant (t)
T	temperature (T)
T_c	sink temperature (T)
T_g	ambient gas temperature (T)
T_H	source temperature (T)
T_i	initial temperature of body (T)
T_l	bulk liquid temperature (T)
T_m	wet bulb temperature at moist surface (T)
T_{sat}	saturation temperature (T)
T_t	total stagnation temperature (T)
ΔT	temperature differential (T)

NOMENCLATURE (Cont'd)

ΔT_b body temperature change (T)
ΔT_f temperature difference across liquid film (T)
ΔT_r temperature range of interest (T)
ΔT_s surface temperature minus saturation temperature (T)
ΔT_w temperature difference between wall and gas stream (T)

U reaction rate (m/l^3t)
V velocity or flow speed (l/t)
V_b bearing surface speed (l/t)
V_f terminal free fall particle velocity (l/t)
V_{max} maximum gas velocity when expanded to zero temperature (l/t)
V_r reference velocity (l/t)
V_T translational speed (l/t)
V_w wind speed (l/t)
ΔV velocity difference (l/t)

w clearance width (l)
W weight (ml/t^2)
X volume (l^3)
X_t total volume (l^3)

y vertical coordinate (l)
Y height of obstacle (l)
z liquid depth (l)

α shear strain rate (t^{-1})
β temperature coefficient of volumetric expansion (T^{-1})
β_b coefficient of bulk expansion (T^{-1})
γ specific heat ratio (dimensionless)
γ_w weight density (m/l^2t^2)
Γ_f specific gravity of fluid (dimensionless)
Γ_p specific gravity of particles (dimensionless)
ϵ_a activation energy (l^2/t^2)
ϵ_e explosive energy (ml^2/t^2)
Δ rate of deformation (l/t)
η Boltzmann constant (ml^2/t^2T)
η_s Stefan-Boltzmann constant (m/t^3T^4)
η_{SB} Stefan-Boltzmann constant (m/lt^2T^4)
θ contact angle (dimensionless)
θ_c clearance between cylinders (l)

θ_f film thickness (l)
θ_l fluid layer thickness (l)
θ_u unloaded film thickness (l)
θ_w wall thickness (l)
λ_c heat of condensation (l^2/t^2)
λ_v heat of vaporization per unit mass or heat of evaporation (l^2/t^2)

μ absolute viscosity (m/lt)
μ_l permeability of free space (ml/q^2)
μ_o magnetic permeability (ml/q^2)
μ_p absolute viscosity in plastic state (m/lt)
μ_s surface viscosity (m/t)
μ_z zero shear viscosity (m/lt)
ν kinematic viscosity (l^2/t)
ρ mass density (m/l^3)
ρ_a mass density of air (m/l^3)
ρ_c mass density of particle cloud (m/l^3)
ρ_d mass density of dust (m/l^3)
ρ_l mass density of liquid (m/l^3)
ρ_p particle mass density (m/l^3)
ρ_v vapor mass density (m/l^3)
$\Delta\rho$ mass density difference (m/l^3)
$\Delta\rho_f$ mass density difference between fluids (m/l^3)
$\Delta\rho_o$ mass density difference between objects and fluid (m/l^3)

σ_i interfacial tension (m/t^2)
σ_t surface tension (m/t^2)
σ_y stress at elastic yield (m/lt^2)
σ_θ thermal gradient (T^{-1})
τ shear or friction stress (m/lt^2)
τ_s fluid shear stress at surface (m/lt^2)
τ_w wall shear stress (m/lt^2)
τ_λ shear stress when $\mu = \mu_z/2$ (m/lt^2)
ϕ air drag coefficient of particle (dimensionless)
ψ ratio of radial clearance to diameter (dimensionless)
ω angular velocity or rotational speed (t^{-1})
ω_a first torsional natural frequency of wing (t^{-1})
ω_{ag} rotational speed of agitator (t^{-1})
ω_c cyclotron frequency (t^{-1})
ω_v vibrational frequency (t^{-1})
• indicates time derivative (t^{-1})

VARIABLES WHOSE RATIOS FORM NONDIMENSIONAL NUMBERS

DIFFUSIVITY
- Lewis
- Nusselt Mass Transfer
- Peclet Mass Transfer
- Prandtl Heat Transfer
- Prandtl Mass Transfer
- Rayleigh

ENERGIES
- Arrhenius
- Dulong
- Joule

FORCES
- Aeroelastic
- Archimedes
- Bagnold
- Blake
- Bond
- Boussinesq
- Buoyancy
- Capillarity 1
- Capillary
- Centrifuge
- Ekman
- Elasticity-1
- Euler
- Froude
- Galileo
- Goucher
- Grashof
- Gravity
- Hartman
- Hersey
- Hooke
- Lagrange-1
- Mach
- Magnetic Force
- Ocvirk
- Ohnesorge
- Poiseuille
- Power
- Prandtl velocity ratio
- Rayleigh
- Reynolds
- Richardson
- Rossby
- Russell
- Sommerfeld
- Stokes
- Structural Merit
- Taylor
- Toms
- Two-Phase Flow
- Viscoelastic
- Weber

HEAT AND SPECIFIC HEAT
- Bansen
- Biot Heat Transfer
- Boltzmann
- Brinkman
- Carnot
- Damköhler's Third
- Damköhler's Fourth
- Graetz
- Kirpichev Heat Transfer
- Kossovich
- Lewis
- Nusselt Heat Transfer
- Peclet Heat Transfer
- Prandtl Heat Transfer
- Rayleigh
- Specific Heat Ratio
- Stanton
- Stefan

LENGTHS
- Debye
- Deryagin
- Knudsen
- Leverett
- Poisson

MAGNETIC FIELDS
- Magnetic Reynolds

MASS AND MOMENTUM
- Biot Mass Transfer
- Bodenstein
- Kirpichev Mass Transfer
- Lewis
- Mass Ratio
- Merkel
- Nusselt Mass Transfer
- Peclet Mass Transfer
- Prandtl Heat Transfer
- Prandtl Mass Transfer
- Structural Merit

PRESSURE
- Cavitation
- Fanning
- Magnetic-Dynamic
- Magnetic Pressure
- Pipeline
- Porous Flow
- Radiation Pressure
- Thoma
- Two-Phase Porous Flow

RATES
- Damköhler's First
- Damköhler's Second
- Predvaditlev

STIFFNESS
- Aeroelastic
- Structural Merit

STRESS
- Bingham
- Fanning
- Truncation

TEMPERATURE
- Carnot
- Gukhman

TIME
- Damköhler's First
- Hodgson

VELOCITY
- Alfven
- Cowling
- Crocco
- Mach
- Strouhal

DUPLICATE NONDIMENSIONAL NUMBERS

Cauchy ≡ $(\text{Mach})^2$
Colburn ≡ Prandtl Mass Transfer
Cowing ≡ 1/Alfven
Damköhler's fifth ≡ Reynolds
Eckert ≡ Dulong
Eotvos ≡ Bond
Hedstrom 2 ≡ Bingham
Hooke ≡ $(\text{Mach})^2$
Jeffrey ≡ 1/Stokes
Karman 2 ≡ Alfven
Laval ≡ Crocco
Leroux ≡ Cavitation
Magnetic Mach ≡ Alfven
Newton ≡ Euler
Plasticity ≡ Bingham
Reech ≡ 1/Froude
Sarrau ≡ Mach
Schmidt ≡ Prandtl Mass Transfer
Semenov ≡ 1/Lewis
Sherwood ≡ Nusselt Mass Transfer
Smoluckowski ≡ 1/Knudsen
Thring ≡ Boltzmann

PHENOMENA IN WHICH NONDIMENSIONAL PARAMETERS ARE APPLICABLE

AEROELASTICITY
- Aeroelastic
- Frueh
- Mass Ratio
- Regier
- Strouhal

BEARINGS AND LUBRICATION
- Hersey
- Ocvirk
- Reynolds
- Sommerfeld
- Squeeze

BOILING AND BUBBLES
- Bubble Nusselt
- Bubble Reynolds
- Jakob
- Morton

BUOYANCY
- Archimedes
- Buoyancy
- Capillarity-Buoyancy
- Richardson
- Russell

CAPILLARY FLOW
- Blake
- Bond
- Capillarity 1
- Capillarity 2
- Capillarity-Buoyancy
- Capillary
- Deryagin
- Gravity
- Kirpichev Mass Transfer
- Kossovich
- Leverett
- Ohnesorge
- Porous Flow
- Posnov
- Two-Phase Flow
- Two-Phase Porous Flow
- Weber

CAPILLARY JETS
- Bingham
- Elasticity 1
- Ellis
- Hedstrom 1
- Ohnesorge
- Weissenberg

CAVITATION
- Cavitation
- Thoma

CENTRIFUGAL FORCE
- Centrifuge
- Ekman
- Lagrange 2
- Taylor

CHEMICAL REACTIONS
- Arrhenius
- Damköhler's First
- Damköhler's Second
- Damköhler's Third
- Damköhler's Fourth

COATINGS AND FILMS
- Deryagin
- Goucher
- Nusselt Film Thickness

COMPRESSIBLE FLOW
- Acceleration
- Crocco
- Dulong
- Fliegner
- Knudsen
- Mach
- Radiation Pressure
- Specific Heat Ratio

CONDENSATION
- Condensation 1
- Condensation 2
- McAdams

CONDUCTION
- Brinkman
- Clausius
- Damköhler's Fourth
- Graetz
- Nusselt Heat Transfer
- Peclet Heat Transfer
- Stefan

CONVECTION
- Buoyancy
- Crispation
- Grashof
- Marangoni
- Momentum
- Nusselt Heat Transfer
- Peclet Heat Transfer
- Prandtl Heat Transfer
- Rayleigh
- Stanton
- Surface Viscosity

CURVED FLOW
- Centrifuge
- Dean
- Ekman
- Rossby
- Taylor

DIFFUSION
- Damköhler's Second
- Fourier Mass Transfer
- J Factor Mass Transfer
- Kirpichev Mass Transfer
- Lewis
- Nusselt Mass Transfer
- Peclet Mass Transfer
- Prandtl Mass Transfer
- Rayleigh

ENERGY
- Arrhenius
- Dulong
- Explosion

ENTRAINMENT
- Archimedes
- Bagnold
- Blake
- Bubble Nusselt
- Bubble Reynolds
- Buoyancy
- Froude
- Particle

EVAPORATION
- Evaporation 1
- Evaporation 2
- Evaporation-Elasticity
- Gukhman
- Jacob
- Kirpichev Mass Transfer
- Kossovich
- Merkel

EXPLOSIONS
- Explosion
- Sachs

FANS, PUMPS, AND TURBINES
- Cavitation
- Flow
- Lagrange 2
- Power
- Specific Speed
- Thoma

FLUID AND MATERIAL PROPERTY
- Capillarity 2
- Elasticity 2
- Elasticity 3
- Lewis
- Poisson
- Prandtl Mass Transfer
- Specific Heat Ratio

FLUIDIZATION
- Archimedes
- Blake
- Federov

GRAVITY
- Bond
- Boussinesq
- Froude
- Galileo
- Goucher
- Gravity
- Rayleigh
- Russell
- Stokes
- Two-Phase Porous Flow

HEAT TRANSFER
- Bansen
- Biot Heat Transfer
- Boltzmann
- Bouguer
- Brinkman
- Carnot
- Condensation 1
- Condensation 2
- Damköhler's Third
- Damköhler's Fourth
- Evaporation 1
- Evaporation 2
- Evaporation-Elasticity
- Fourier Heat Transfer
- Graetz
- Grashof
- Heat Transfer
- J Factor Heat Transfer
- Jacob
- Jakob
- Joule
- Kirpichev Heat Transfer
- Kossovich
- Lewis
- Merkel

PHENOMENA IN WHICH NONDIMENSIONAL PARAMETERS ARE APPLICABLE (Cont'd)

- Nusselt Heat Transfer
- Peclet Heat Transfer
- Pomerantsev
- Prandtl Heat Transfer
- Predvaditlev
- Rayleigh
- Stanton
- Stefan

IMMERSED BODIES
- Bagnold
- Biot Heat Transfer
- Bond
- Cavitation
- Crocco
- Euler
- Fliegner
- Kirpitcheff
- Knudsen
- Mach
- Mass Ratio
- Morton
- Predvoditlev
- Reynolds
- Schiller
- Stokes
- Suratman
- Toms

IONIZED GASES
- Debye

MAGNETOHYDRODYNAMICS
- Alfven
- Ekman
- Electric Reynolds
- Elsasser
- Hall
- Hartmann
- Joule
- Lundquist
- Lykoudis
- Magnetic-Dynamics
- Magnetic Force
- Magnetic Interaction
- Magnetic Prandtl
- Magnetic Pressure
- Magnetic Reynolds

MASS AND MOMENTUM TRANSFER
- Biot Mass Transfer
- Bodenstein
- Damköhler's Second
- Fourier Mass Transfer
- J Factor Mass Transfer
- Kirpichev Mass Transfer
- Lewis
- Merkel
- Nusselt Mass Transfer
- Peclet Mass Transfer
- Prandtl Mass Transfer

PARTICLE FLOW
- Bagnold
- Bouguer
- Electroviscous
- Particle

PIPE FLOW
- Darcy
- Fanning
- Karman 1
- Pipeline

PLASTIC AND NON-NEWTONIAN FLOW
- Bingham
- Elastocity 1
- Ellis
- Hedstrom 1
- Truncation
- Viscoelastic

POROUS BODIES
- Blake
- Bond
- Capillarity 1
- Capillarity 2
- Capillary
- Gravity
- Kirpichev Mass Transfer
- Kossovich
- Leverett
- Porous Flow
- Posnov
- Two-Phase Flow
- Two-Phase Porous Flow
- Weber

PRESSURE
- Cavitation
- Darcy
- Euler
- Fanning
- Lagrange
- Magnetic-Dynamic
- Magnetic-Pressure
- Pipeline
- Poiseulle
- Thoma

PULSATING FLOW
- Hodgson
- Pipeline
- Strouhal
- Taylor

RADIATION
- Bansen
- Boltzmann
- Bouguer
- Radiation Pressure
- Stefan

SLOSH AND SURFACE WAVES
- Bond
- Bossinesq
- Centrifuge
- Froude
- Galileo
- Ohnesorge
- Russell
- Slosh Time
- Weber

STRESS
- Bingham
- Fanning
- Poisson
- Truncation

STRUCTURES
- Structural Merit

SURFACE TENSION
- Bond
- Capillarity 1
- Capillarity 2
- Capillarity-Buoyancy
- Capillary
- Centrifuge
- Goucher
- Marangoni
- Ohnesorge
- Two-Phase Flow
- Weber

TIME
- Damköhler's First
- Hodgson
- Slosh Time
- Thomson

TWO MEDIUM FLOW
- Archimedes
- Bagnold
- Blake
- Capillarity 1
- Capillarity-Buoyancy
- Capillary
- Gravity
- Leverett
- Russell
- Two-Phase Flow
- Two-Phase Porous Flow

VELOCITY
- Alfven
- Crocco
- Damköhler's First
- Strouhal
- Thomson

VISCOELASTICS
- Bingham
- Elasticity 1
- Ellis
- Hedstrom 1
- Richardson
- Truncation
- Viscoelastic
- Weissenberg

VISCOUS FLOW
- Brinkman
- Darcy
- Fanning
- Frueh
- Hodgson
- Karman 1
- Lagrange 1
- Pipeline
- Poiseuille
- Prandtl Velocity Ratio
- Reynolds
- Stokes
- Taylor
- Truncation

INSTRUMENTS

AND

APPARATUS

These supplementary documents give descriptions of, and directions for, the use and calibration of measuring devices likely to be required.

SUPPLEMENTS ON INSTRUMENTS AND APPARATUS NOW AVAILABLE